GEOLOGICA ULTRAIECTINA

Mededelingen van de
Faculteit Aardwetenschappen
Universiteit Utecht

No. 164

Self-sealing/healing isolation and immobilization caused by chemical discontinuities in porous media

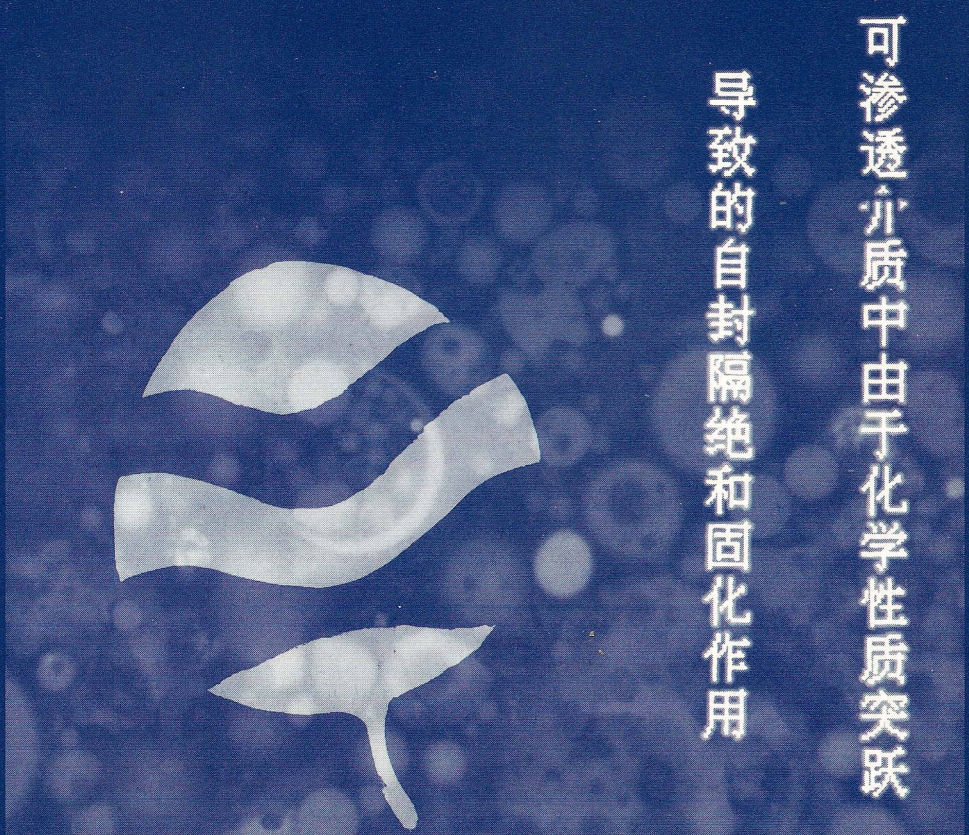

Mei Ding

GEOLOGICA ULTRAIECTINA

Mededelingen van de
Faculteit Aardwetenschappen
Universiteit Utecht

No. 164

Self-sealing/healing isolation and immobilization caused by chemical discontinuities in porous media

Mei Ding

Cover: Illustration Hylke de Jong - Computer artwork Paul van Oudenallen

ISBN : 90-5744-022-9

Self-sealing/healing isolation and immobilization caused by chemical discontinuities in porous media

Zelf-afsluitende/helende isolatie en immobilisatie veroorzaakt door chemische discontinuiteiten in poreuze media

(met een samenvatting in het Nederlands en Chinees)

PROEFSCHRIFT

TER VERKRIJGING VAN DE GRAAD VAN DOCTOR AAN DE UNIVERSITEIT TE UTRECHT, OP GEZAG VAN DE RECTOR MAGNIFICUS, PROF. DR. H.O. VOORMA, INGEVOLGE HET BESLUIT VAN HET COLLEGE VOOR PROMOTIES IN HET OPENBAAR TE VERDEDIGEN OP WOENSDAG 2 SEPTEMBER 1998 DES OCHTENDS TE 10.30 UUR

DOOR

Mei Ding

Geboren op 15 Januari 1963 te Beijing, China

PROMOTOR:	PROF. DR. R.D. SCHUILING
CO-PROMOTOR:	DR. H.A. VAN DER SLOOT

Examining Commitee:

Prof. Dr. B.H.W.S. de Jong	Utrecht University, the Netherlands
Prof. Dr. M.E. Hochella	Virginia Polytech Institute, USA
Prof. Dr. W.E. Seyfried	University Minnesota, USA
Prof. Dr. H.A. Das	Netherlands Energy reseach Foundation (ECN), Utrecht University, University of Amsterdam, the Netherlands
Prof. Dr. Ph. van Cappellen	Georgia Tech, USA
Prof. Dr. I. Neretnieks	Royal Institute of Technology, Sweden
Dr. J. Stegemann	Imperial College, UK
Ir. J. Taat	Delft Geotechnics, the Netherlands

Publications and reports related to this thesis

Ding, M. (1994) Immobilization of contaminants at the interface between jarosite and alkaline fly ash, MSc Thesis, International Institute for Hydraulic and Environmental Engineering, Delft, the Netherlands, pp 55.

Ding, M. (1995) Leaching tests NEN 7341, NEN 7349, and NEN 7349 performed on Budelco jarosite, Progress Report, Utrecht University, the Netherlands. Pp 15.

Ding, M., (1996) Effect of interface precipitation on the bulk diffusivity in jarosite and alkaline coal fly ash , Progress Report, ECN&Utrecht University, the Netherlands, pp85.

Ding, M., van der Sloot, H.A., Geusebroek, M. (1996) Interface reaction affects Fe^{3+} mobility in jarosite and alkaline coal fly ash, Ceramic Transactions, Vol. 72, Environmental Issues and Waste Management Technologies in Ceramic and Nuclear Industries II, edited by Vijay Jain and David Peeler, pp475-484.

Ding, M., van der Sloot, H.A., Geusebroek, M. (1997) Interaction of Fe^{3+}, Ca^{2+}, and SO_4^{2-} at the jarosite/alkaline coal fly ash interface, Geochemistry, edited by Xie, X. J. Proceedings 30th International Geological Congress, Vol. 19, pp207-222, VSP.

Ding, M., Geusebroek, M., and van der Sloot, H.A (1998) Interface precipitation affects the resistance to transport in layered jarosite/fly ash, J. of Geochemical Exploration (in press)

Ding, M., de Jong, B.H.W.S., Niessen, B., van der Meer, J.P.M., and van Hinsberg, V.J. Characterization of amorphous black ferric oxyhydroxide: X-ray photoelectron spectroscopy, conversion electron mössbaur spectroscopy, and chemical adsorption, Geochim. Cosmochim. Acta (submitted)

Ding, M., de Jong, B.H.W.S., Roosendaal, S.J., Vredenberg, A. XPS studies on the electronic structure of bonding between solid and solutes: adsorption of arsenate, phosphate, chromate, Pb^{2+} and Zn^{2+} ions on amorphous black ferric oxyhydroxide, Geochim. Cosmochim. Acta (submitted)

Ding, M. and H..F.P. Dorren Discontinuities in porous media affect the transport and mobility of chemical constituents, Water Resource Research (to be submitted).

Contents

Summary

Self-forming layers are formed naturally or artificially as a result of reactive transport through porous media. Such layers can be hard with low permeability, and commonly accumulate a large variety of inorganic and organic chemicals. Their development involves a transport stage in which constituents migrate along chemical gradients, followed by a concentration stage in which precipitates are formed at locations where contrasts in redox state or acid-base character prevail. These precipitates fill pores forming a layer which differs in physical and chemical characteristics from the parent materials.

Discontinuities in chemical properties at the interface of materials is the driving force behind spontaneous layer formation. Conversely, such self-forming layer can have a substantial impact on the transport and mobility of chemical constituents, forming completely impermeable seals as occur for instance below peat bogs. It is for this reason that self-sealing layers can be a viable option to isolate industrial waste from its surroundings. Besides self-sealing such a barrier is also self-healing in that it will regenerate itself after rupture. Thus any mechanical damage to a sealing layer will cause further migration and precipitation as long as the concentration of reacting constituents suffices. Commonly, immobilization of a large variety of components including organic matter occurs simultaneously during the process of sealing layer formation by co-precipitation or surface adsorption.

In this thesis the mechanism of formation of self-sealing/healing isolation and immobilization in layered materials is investigated, with particular emphasis on the impact of such self-forming layer on the transport and mobility of chemical constituents. As principal example the layered acidic jarosite/alkaline coal fly ash system is considered. The approach to this program starts with investigating the formation potential of self-sealing layer in the layered jarosite/fly ash system. Next, characteristics of the sealing layer and its impact on transport and mobility of chemical constituents are examined experimentally, followed by a mathematical description of sealing layer development. Finally, chemically reactivity of self-sealing layer in the jarosite/fly ash is explored. For application purposes self-sealing isolation and immobilization, rather than neutralization, is recommended. Placing a layer of acidic jarosite adjacent to a layer of alkaline coal fly ash offers the optimal solution to the waste acidic jarosite environmental problem.

In Chapter 1 self-forming layer formation in nature and previous studies on this issue are summarized and the practical implication of self-forming layers is discussed. Aspects of self-sealing isolation and immobilization in layered materials with particular emphasis on jarosite/fly ash are identified and the purposes and actions of the present study are defined.

In Chapter 2 the nature of each of the two parent materials, acid jarosite and alkaline

fly ash, are described including their chemical composition, mineral phases, acid-base, and leaching properties. These preliminary experiments not only provide the necessary background knowledge of the materials but, more importantly, provide information about their environmental behavior and possible consequences from a waste management point of view.

In Chapter 3 the character of the self-forming layer at the interface of the layered jarosite/fly ash system is investigated and its effect on the bulk resistance to transport and chemical retention. It will be shown by standard characterization techniques that ferric oxyhydroxide and gypsum are the principal precipitates in the layer. The transport properties and the mobility of their constituents in layered materials are determined *via* radio tracer, such as $^{3}H^{+}$, $^{22}Na^{+}$, and $^{59}Fe^{3+}$, diffusion experiments and hydraulic conductivity measurements using flow through columns. It will be shown that such self forming layer dramatically alters transport processes through a layered system.

Chapter 4 focuses on modelling the effect of discontinuities in porous media on transport and mobility of chemical constituents in general. Particular emphasis is put on the model used to simulate reactive transport in layered materials including the generation of a interfacial self-forming layer. The numerical solution and the two computer programs, DNLM (**D**iffusion **N**eutralization in **L**ayered **M**aterials) and DPLM (**D**iffusion **P**recipitation in **L**ayered **M**aterials) are described. The model calibration and verification are carried out using radio tracer $^{3}H^{+}$, $^{22}Na^{+}$ and $^{59}Fe^{3+}$ diffusion tube experiments on layered jarosite/fly ash samples. The model simulations indicate that existing differences in tortuosity at the interface of layered materials will barely affect material transport. However existing chemical gradients, such as pH and redox state, will not only affect transport processes significantly but also the mobility of chemical constituents.

Chapter 5 explores the chemical reactivity of self-sealing layer in the layered jarosite/fly ash system. To this purpose amorphous ferric oxyhydroxide FeOOH, one of the two precipitates which composes the sealing layer, has been synthesized and its adsorption capacity for arsenate, phosphate, and chromate anions, and zinc and lead cations studied. Classical bonding arguments from a solution chemical perspective are combined with quantum mechanical arguments relating the electronic structure of the FeOOH substrate and its adducts, using frontier orbital concepts as theoretical frame. X-ray photoelectron spectroscopy of the FeOOH substrate and its complexes with aforementioned cations and anions is used for verification. This study presents a state of the art approach to discuss solid-water interaction in the aquatic surface chemical realm.

In chapter 6 general conclusions are drawn based on the findings presented in Chapter 2 to 5. These conclusions in summary are that self-sealing/healing isolation is a relatively cheap, reliable, safe environmental option and may have significant use in waste jarosite management. Formation of such an isolation layer requires migration of con-

stituents from two chemically different adjacent parent materials, causing reaction and precipitation at their interface. The self-forming layer in the layered acidic jarosite/alkaline coal fly ash consists of amorphous ferric oxyhydroxide FeOOH and gypsum $CaSO_4 \cdot 2H_2O$ caused by precipitation reactions among the principal constituents from jarosite (Fe^{3+}, SO_4^{2-}) and fly ash (Ca^{2+}, OH^-). Such layer affects the resistance to transport and chemical retention of constituents significantly. The mathematical model established to describe transport characteristics in layered materials, includes porosity changes due to precipitation. Its numerical solution has been successfully implemented in two newly developed computer programs, DNLM and DPLM, and applied to the layered jarosite/fly ash system. Chemical reactivity of the self-forming layer in the layered jarosite/fly ash system is primarily due to amorphous ferric oxyhydroxide, which possesses a strong adsorption capacity for a large variety of cations and anions. XPS, as a surface technique, has been applied to study adsorption between solid and solutes, providing detailed chemical bonding information from core level and valence band shifts. It enables close to first principle rationalizations concerning the nature of chemical bonding between solid and solutes from a frontier orbital perspective.

Pertinent questions for future research include: simulating the behavior of other principal consituents such as Al^{3+}, Zn^{2+}, Pb^{2+}, Ca^{2+}, and SO_4^{2-} on the transport and reaction in layered systems and that of a single constituent involved in multireactions; and the adsorbtion of organic compounds such as pesticides on FeOOH substrates.

Chapter 1

Introduction

1.1 Self-forming layers in nature and their practical implication

Layering and zonation are ubiquitous in nature occurring as iron oxide bands in sandy gravelly sediments, in soils as iron pans (Crampton 1963; Conry *et al.*, 1996), or in cores of oceanic bottom sediments (van Cappellen and Gaillard 1996), or in limestones as shown in Figure 1.1. Among these the thin, wavy or convoluted, black to reddish zones forming iron pans are the most common naturally self-forming layer systems (Crampton, 1963), occurring as thin hard layers with low permeability. Chemically they contain primarily iron with some manganese and aluminum. Their mode of genesis is well understood starting with migration of reduced iron from the parent material followed by oxidation and precipitation in a thin layer, which can adsorb a large variety of cations and anions as well as organic matter (Conry *et al.*, 1996).

Besides occurring naturally such self-forming layers can also be the product of human activity. In the early 90's, Hockley and van der Sloot (1991a) reported an example of natural seal formation in stabilized coal fly ash disposed in the ocean. In 1992 Schuiling discovered a layer consisting of ferric oxyhydroxide and gypsum between an acidic fluid and underlying carbonate-bearing clay in a waste sulfuric acid lake of a TiO_2-plant at Armyansk, Crimea (Schuiling and van Gaans, 1997). The principal conceptual advance furthered in both studies has been that a self-forming layer can be initiated by precipitation reaction at the interface of two parents materials whenever physical but primarily chemical gradients are present. Such interfacial phenomena are symbiotic in nature: two substances coexisting together in a mutually beneficial relationship, the reward here being self induced isolation. This symbiosis may be induced by acid-base, redox or permeability variation. Such interfacial phenomena have been receiving increasing attention due to their impact on the mobility of chemical constituents and their potential to create a barrier for waste isolation (Côté and van der Sloot 1989, 1994; Schuiling 1989, 1990, 1996).

The above observations of layer formation at the interface between two adjacent materials inspired a search into the possibility if such layer could be created on purpose to isolate industrial waste from its surroundings and to immobilize the contaminants from their leachates. Such waste self-sealing isolation might be relatively cheap, and because of its self healing capacity might also be a very reliable technique with many possible applications in industrial waste management. For example research results at a waste-soil interface (Hockley 1992; Hockley and van der Sloot 1991a, 1991b, 1993; van der Sloot *et al.*, 1993, 1995a, 1997a) clearly indicated that

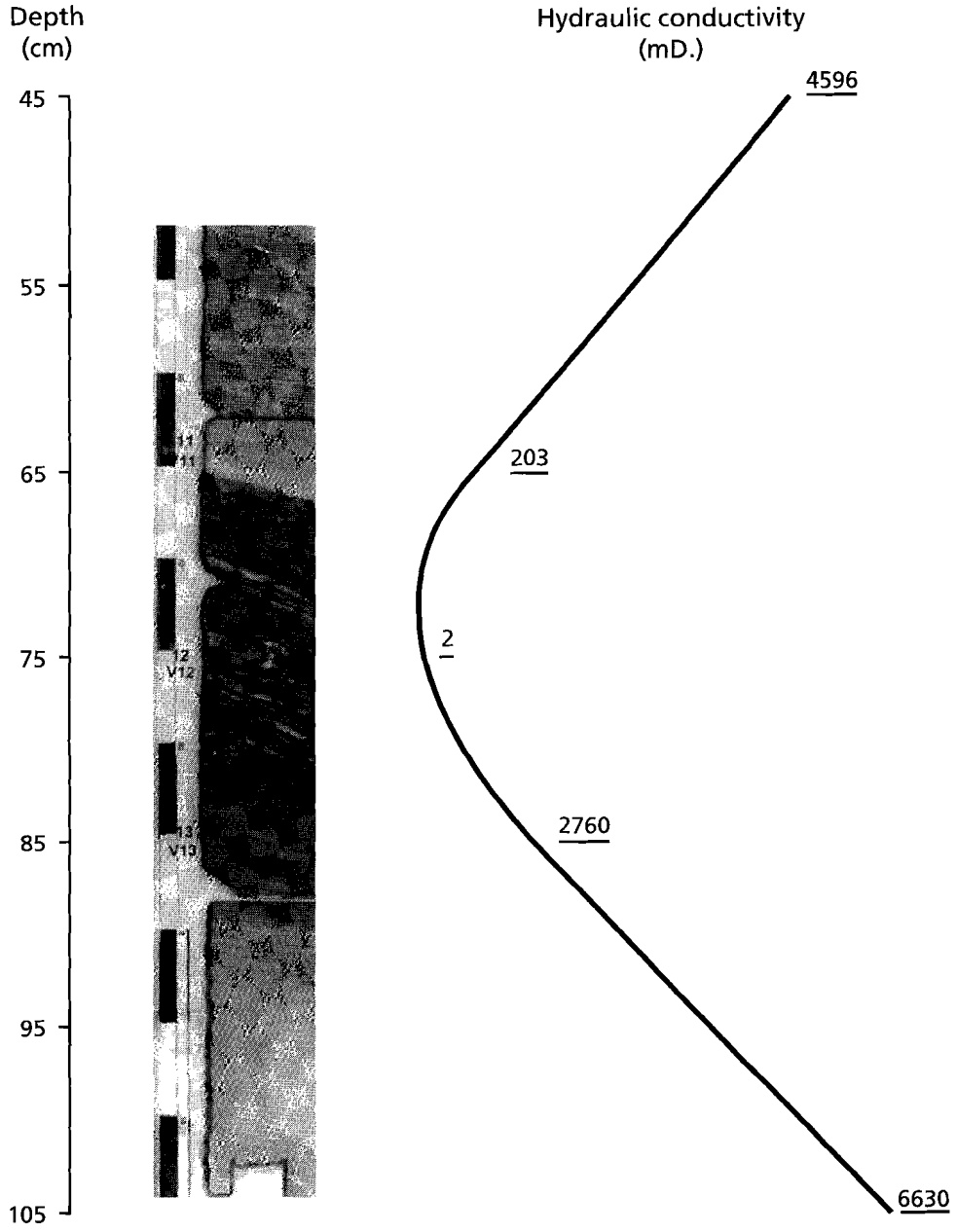

Fig 1.1 Drill core from Maastrichtien chalk, Quarry Nekami, Bemelen The Netherlands. The dark zone consists primarily of red brown ferric oxyhydroxide and has the lowest hydraulic conductivity (courtesy Dr. H. Zijlstra).

bulk release of contaminants from a waste depends not only on the properties of the waste itself but also on the type of interaction between the waste and its surroundings, and furthermore indicated that self-sealing/healing as an new environmental technique is worthy of further study. It therefore became necessary to probe in detail the mechanism of developing such self-sealing barrier and its impact on the transport and mobility of its chemical constituents.

1.2 Sealing layer in layered acidic jarosite/alkaline fly ash system

It is crucial to select the proper starting materials to fulfil the conditions necessary for self-sealing formation (van der Sloot *et al.*, 1993). These conditions are on the one hand that the concentration of reacting solutes in both materials ought to be high enough to initiate a precipitation reaction, on the other that the sources of reacting solutes should be sufficient to fill all the pores at the interface. For our purpose we selected acidic jarosite $[M]Fe_3(SO_4)_2(OH)_6$ ($M=Na^+$, K^+, NH_4^+, and Pb^{2+}), a waste product from the zinc industry, and alkaline coal fly ash as a model system, because their disposal is of environmental concern and their character has the potential to demonstrate acid-base induced symbiosis. By putting acidic jarosite and alkaline fly ash as two chemically contrasting wastes next to one another, we anticipated precipitation to occur at the interface. The reaction we envisioned can be expressed as follows:

$$[M]Fe_3(SO_4)_2(OH)_6 + 2CaO + 3H_2O \leftrightarrow M^+ + 3FeOOH \downarrow + 2CaSO_4.2H_2O \downarrow + OH^-$$

where M represents NH_4^+, Na^+, K^+, and Pb^{2+}. A consequence of this reaction would be that a self-forming layer with lower permeability will form due to pore filling of precipitates at the interface, causing in this process a reduction of the mobility of chemical constituents including contaminants from both wastes.

Therefore, characterizing both materials and assessment of their acid-base and leaching properties forms the first issue in need of research. The second problem needed to be faced is how to investigate experimentally the self-sealing layer in jarosite/alkaline coal fly ash. This task can be partitioned into three sub-tasks. The first one involves characterization of the interface precipitation, the next one measurement of the effective resistance of such self-forming layer to transport, and as final one determination of the chemical retention of constituents from both jarosite and fly ash.

1.3 Transport characteristics in layered materials: case of the jarosite/fly ash system

Reactive transport in porous medium has been receiving increased attention in recent years (Mangold and Tsang 1991; Lichtner *et al.*, 1996; Schnoor, 1996). Despite this increase there exist virtually no theories or models which describe transport in layered materials (Hassanizadeh and Gray, 1989a, 1989b; Hockley *et al.*, 1992). This is the more surprising once it is realized that physical but much more importantly chemical gradients at the interface of two materials can overwhelmingly affect the over all transport characteristics of the system (van der Sloot *et al.*, 1993, 1995a, 1997a). From a theoretical perspective such transport requires additional specification of boundary conditions in the mathematical description (Crank 1975; Hockely *et al.*, 1992), because phenomenology dictates that the transport characteristics of chemical constituents in the combined system can differ significantly from those of the single materials (Ding 1996a; Ding *et al.*, 1997, 1998).

Especially, when reactions occur at the interface between two chemically contrasting materials, a reaction zone may form which differs significantly in transport and thermodynamic properties from its parent medium. For example, during the process of sealing layer formation between jarosite and fly ash, local transport properties such as diffusivity and porosity will change in the reaction zone. Such change in local physical properties caused by precipitation will subsequently affect transport of chemical constituents. Thus diffusion and precipitation are highly dynamic and coupled with one another (Steefel and Lasaga, 1990, 1994; Carnahan 1990).

Having noticed the importance of reactive transport in layered materials in particular the absence of a viable model to describe the self-forming process in such a system, it is necessary to establish mathematical models to quantitatively describe the effect of physical and chemical discontinuities in porous media on a transport process in general. Especially, it is important to develop a computer program which can be used to simulate and predict the transport characteristics in layered materials where self-sealing layers may form due to interface precipitation. In practice, one also faces the question whether the amount of precipitates will suffice to form a sealing layer and the rate at which such layer can be formed in order to isolate the waste efficiently. Finally to calibrate and verify such model we need a proper experimental method specifically designed to test our model differing from the standard batch or flow through column experiments.

1.4 The chemical nature of the sealing layer in jarosite/fly ash

The chemical reactivity of the sealing layer in jarosite/fly ash is caused by amorphous ferric oxyhydroxide FeOOH, one of the newly formed minerals at the interface of the layered jarosite/fly ash system. FeOOH has been the subject of a large number of studies (Dzombak and Morel, 1990; Cornell and Schwertmann, 1996) due to its adsorption capacity for a large number of cations and anions. We anticipated that the layer consisting of FeOOH reacts strongly with toxic components leached from the wastes, adding an additional safety factor for the purpose of waste management.

Despite much theoretical and experimental work on cation and anion adsorption on ferric oxyhydroxide focussing primarily on solution chemistry (pH, ionic strength, concentration of solutes, and so on) (Benjamin and Leckie, 1981; Benjamin, 1983; de Jong, 1982; Dzombak and Morel, 1990; Juergens, 1995; Zachara *et al.*, 1987; Lützenkirchen and Behra, 1996; Pierce and Moore, 1982), much remains to be done in terms of detailed chemical reaction mechanisms involving chemical bonding between solid and solutes. Recent developments in analytical technique have provided more direct and quantitative information of the sorbed complex (Manceau, 1995; Scaini *et al.*, 1997; Becker *et al.*, 1997), as summarized by Brown (1990). Among these techniques, EXAFS has been widely adopted to probe the surface structure (Waychunas *et al.*, 1993, 1995, 1996; Fuller *et al.*, 1993) providing information about geometries of adsorption complexes such as inner-sphere, outer-sphere, mono-dentate, bi-dentate, and so on. From a quantum mechanical perspective the state of describing the interaction between solutes and substrate (Hoffmann 1993) involves first of all how and if electrons transfer from substrate to adducts and secondly determination of the relative position of ground and excited energy states of substrate and adduct to asses their mutual affinity. X-ray photoelectron spectroscopy (XPS), as a surface analytical technique sampling at most the top 5 nm of as solid , provides the proper level of information to answer these questions.

The purpose of this study is to combine the phenomenological results from adsorption experiments with XPS results to characterize the nature of the chemical interaction between aquatic solutes, such as arsenate, phosphate, chromate Pb^{2+} and Zn^{2+} ions, and the FeOOH substrate. An additional aim is to explore the nature of the electronic bonding between solid and solutes in terms of the theoretical framework laid down in the frontier molecular orbital concept.

1.5 Overview of this thesis

The following flow scheme shows the organization of this thesis:

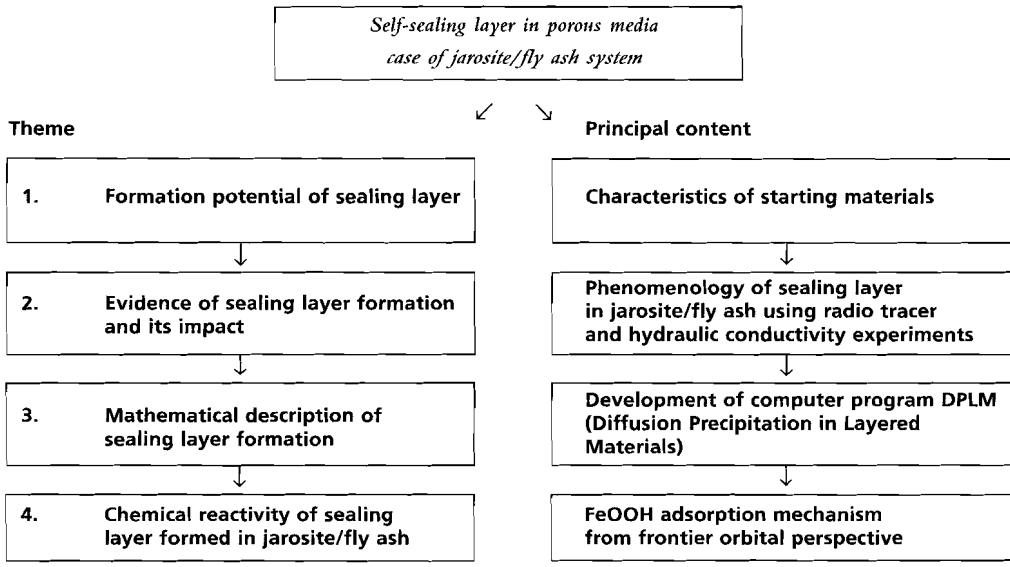

Chapter 2

Characteristics of Materials: acidic jarosite and alkaline coal fly ash

2.1 Introduction

Environmental problems caused by disposal of waste jarosite have received increasingly more attention in recent years (Dutrizac and Harris 1996). As a waste product of the zinc industry, it is intrinsically acidic and contains high concentration of heavy metals such as lead and zinc as well as toxic ones among which arsenic predominates. When exposed to the environment, these heavy metals and toxic elements will easily be released. Therefore the search is on for alternative options concerning the disposal of jarosite and propose a possible solution for this serious environmental problem.

Mimicing geochemical processes to solve environmental problems has been initiated by Schuiling (Schuiling 1989). One of the major subjects in this new discipline, environmental geochemical engineering, is self-sealing isolation and immobilization (Schuiling 1990, 1996; Davis *et al.*, 1996; Voronkevich 1994; Jurjovec *et al.*, 1995). As a means of an environmental technique dealing with waste disposal, it has been developed and studied since the late eighties (Côté and van der Sloot 1989, 1994; Hockley and van der Sloot 1991a). The technique is based on the formation of a layer with a low permeability to ground water and leachate by placing two chemically contrasting substances against one another, which simultaneously reduces the mobility of chemical constituents including pollutants.

The discovery of a layer consisting of iron oxyhydroxide and gypsum between an acidic fluid and underlying carbonate-bearing clay in an waste sulfuric acid lake of a TiO_2-plant at Armyansk, Crimea (Schuiling and Van Gaans 1994) provides a clue to solve the environmental problems caused by disposal of waste jarosite. One can anticipate that when waste jarosite is placed against alkaline coal fly ash, a waste product from power plants which presumably has a function similar to that of carbonate-bearing clay, precipitation will occur of newly formed minerals iron oxyhydroxide and gypsum, leading to pore filling at the interface between these two materials. Eventually a new zone with lower permeability will be created. As a consequence, one expects that waste isolation and immobilization will be realized by such self-sealing layer formation. The important problem addressed here is if precipitation will occur at the interface between these two materials; and, if so, if the amount of precipitate meets the requirement for a proper seal. Another issue concerns the optimal way of dealing with waste jarosite, either neu-

tralizing it by simple mixing with alkaline fly ash; or isolating and immobilizing it by co-disposal with alkaline coal fly ash in single or multilayers, resulting in single or multilayered seals.

Answering the above questions forms the purpose of this study. It starts by investigating the critical release behavior of waste jarosite and fly ash. Next the leaching behavior of the principal chemical components will be illustrated as a function of pH. These results will allow us to envision the state of those components at the interface between jarosite/fly ash, where a sharp pH discontinuity occurs. As third item we shall discuss whether the mass of principal reacting solutes in pore fluid of the parent materials is sufficient to result in a sealing layer. Furthermore we shall address the acidity, i.e. the capacity of water to donate protons, and the alkalinity, i.e. the capacity of water to accept protons, of jarosite and fly ash. With these results we can assess for both materials their neutralization capacity, which is used to predict the optimal proportion in which the two materials must be used. Finally, as a practical issue, alternative options dealing with disposal of waste jarosite are discussed.

It is important to point out that the acidity and alkalinity for suspensions include contributions from minerals and other solids present in addition to those from aqueous species. Commonly, minerals and other solids contribute to the long term acidity and alkalinity of natural waters via such reactions as ion exchange of protons, weathering, and hydrolysis. It is therefore necessary to separate instantaneous acidity and alkalinity from their equilibrium values.

To carry out these objectives, a series of standard leaching tests used extensively in the Netherlands Energy Research Foundation (ECN) (de Groot and Hoede 1994; van der Sloot 1995b, 1997b; van der Sloot *et al.*, 1991, 1994), such as availability test NEN 7341(NEN 7341 1993), the cascade test NEN 7349 (NEN 7349 1993), the column test NEN 7343 (NEN 7343 1994), and pH static (van der Sloot *et al.*, 1994) are performed on jarosite and fly ash separately. By combining the first three tests, the cumulative releases as a function of L/S ratio are obtained. From the pH static test, the leaching behavior as a function of pH is investigated.

To quantify the acid-base character of our solid wastes, we have carried out three series of experiments. Firstly we determined the immediate acidity and alkalinity of jarosite and coal fly ash by titrating their suspensions with a strong acid HNO_3 or a strong basic NaOH solution to an endpoint pH. Secondly we determined the long term acidity and alkalinity of jarosite and fly ash separately by adding to their suspension various amount of either HNO_3 or NaOH, reacting them till equilibrium, followed by measuring their solution pH. Finally we determined the neutralization capacity of fly ash relative to jarosite, by titrating suspensions made up of mixtures of coal fly ash and jarosite, and bringing these mixtures up to a specified pH.

2.2 Materials and methods

2.2.1 Materials

Jarosite

Jarosite is one of the most important members of a large group of isostructural minerals. The general formula of this group is $RA_3(BO_4)(OH)_6$ (Wang *et al.*, 1965; Menchetti and Sabelli 1976; Fleischer 1983), where R is a monovalent or divalent cation such as Na^+, K^+, NH_4^+, and Pb^{2+}, A stands for trivalent iron or aluminium, and B for sulphur, phosphorous, or arsenic. In jarosite the B position is occupied by sulphur and A mainly by Fe^{3+}. In nature, jarosite forms most commonly in acidic, sulphate-rich environments which can develop as a result of pyrite oxidation during weathering (Stoffregen 1993). In addition, jarosite precipitation is an important method for removing impurities from acidic waste (Norton *et al.*, 1991). Jarosite used in this studied comes from a zinc factory in the Netherlands (Elgersma 1992; Hage and Schuiling 1996). It is produced as a chemical waste during electrolytic production of zinc by removing iron from acidic, sulphate-rich solutions at elevated temperature. The general process can be expressed as:

$$3Fe^{3+} + 2SO_4^{2-} + 6H_2O + M^+ \leftrightarrow MFe_3(SO_4)_2(OH)_6\downarrow + 6H^+$$

where M represents NH_4^+, Na^+, K^+ and Pb^{2+}. As a waste product, jarosite concentrates a number of toxic and heavy metals. Table 2.1. lists the chemical composition of jarosite used in this study.

Table 2.1. Chemical composition of jarosite waste.

Major elements (>10000 mg/kg)	wt %	Minor elements (1000 to 10000 mg/kg)	wt %	Trace elements (< 1000 mg/kg)	mg/kg
SO_3	32.53	Al_2O_3	1.78	Mn	929
Fe_2O_3	22.41	K_2O	0.60	Ba	590
SiO_2	20.27	MgO	0.58	Ti	540
PbO	7.37	As_2O_5	0.51	Sb	450
NH_3	1.85	CuO	0.19	P	330
ZnO	3.64	Na_2O	0.15	Ag	20
CaO	2.79			Mo	6
Total	**90.86**	**Total**	**3.81**		

The mineralogical composition of the waste jarosite was examined by powder XRD analysis (Ding *et al.*, 1997). The dominant phases identified are ammoniumjarosite ($NH_4Fe_3(SO_4)_2(OH)_6$), and quartz (SiO_2) with a small amount of gypsum ($CaSO_4 2H_2O$). Figure 2.1 presents the particle size distribution of jarosite. The bulk and dry density of jarosite are 2.20 kg/m^3 and 2.86 kg/m^3, respectively.

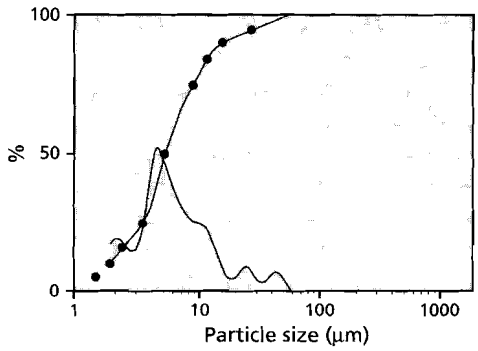

Fig. 2.1 Particle size distribution of jarosite

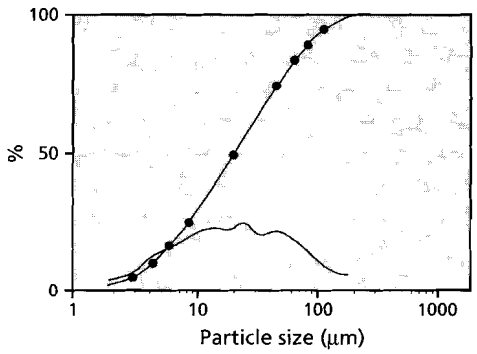

Fig. 2.2 Particle size distribution of fly ash

Alkaline coal fly ash

Fly ash is the residue from coal combustion that enters the flue gas stream (Carlson and Adriano, 1993), and can be divided into two categories: acidic and alkaline fly ash depending on the solution pH of its suspension. The waste used in this study is alkaline coal fly ash, the residue from a power plant. Table 2.2. lists its chemical composition.

Table 2.2. Chemical composition of coal fly ash.

Major elements (>10000 mg/kg)	wt %	Minor elements (1000 to 10000 mg/kg)	wt %	Trace elements (< 1000 mg/kg)	mg/kg
SiO_2	46.86	Na_2O	1.23	Zn	217
Al_2O_3	24.69	SO_3	1.03	Cu	214
Fe_2O_3	8.81	TiO_2	0.98	Ce	196
CaO	6.86	P_2O_5	0.66	Li	165
MgO	3.80	BaO	0.25	Zr	155
K_2O	2.10	SrO	0.17	Cr	154
		MnO	0.13	Ni	138
Total	**93.12**	**Total**	**4.45**		

XRD analysis (Ding *et al.*, 1997) shows that the fly ash used in this study consists mainly of amorphous phases, with a small amount of quartz (SiO_2), mullite ($Al_6Si_2O_{13}$), and hematite (Fe_2O_3). Figure 2.2 presents the particle size distribution of fly ash. The bulk and dry density of fly ash are 1.2 kg/m^3 and 2.0 kg/m^3, respectively.

2.2.2 Methods

Analytical techniques

The chemicals used in all our experiments were reagent grade. Except the elements As, Se and Ag which were analyzed with Zeeman-AAS(Atomic Absorption Spectrometer) on a PERKIN-ELMER Zeeman-410ZL, all other elements were analyzed with ICP-AES (Inductively Coupled Plasma-Atomic Emission Spectrometer) using a PERKIN-ELMER ICP-optima 3000. The X-ray Powder Diffractometer used for mineral phases identification is a PHILIPS PW 1730 using CuK_α radiation (1.5418Å). The particle size distribution of the materials was determined with a Malvern Particle Sizer 2600.

Leaching test methods

The leaching tests used, were developed in the Netherlands to assess the release from waste materials under a variety of conditions.

Availability test (NEN 7341) (NEN 7341 1993)
The purpose of the availability test is to determine the fraction of a component potentially available for release from the material under extreme environmental conditions. In this experiment, 8 grams of crushed and sieved sample (< 125μm) is added to 800 ml demineralized water with a liquid to solid ratio, L/S, of 100. The solution pH is kept at a constant pH of 4 by adjustment with 0.1 M NaOH or 0.1M HNO_3. The suspension is stirred for 3 hours. The ensuing solution provides the first extract. Next the suspension is filtrated, and to the residue on the filter, 800 ml acidified demineralized water is added with a constant pH of 7 maintained by adding 0.1M HNO_3 or 0.1 M NaOH, and stirred for another 3 hours. This last extract is combined with the earlier one for chemical analysis.

Batch test (NEN 7349) (NEN 7349 1993)
The purpose of the cascade test is to determine the long term leachability of a component at L/S ratios varying between 20 and 100. The test consists of successive batch extractions of a sample with acidified demineralized water of pH=4.

Column test (NEN 7343) (NEN 7343 1994)
The column test is aimed at simulating the short (<5 years) and intermediate (5-50 year) leaching behavior of a waste with a L/S varying between 0.1 and 10. Acidified dem-

ineralized water at a pH=4 is continuously percolated in this test through a column packed with waste. The leachate is sampled over various intervals and analyzed.

pH static test (van der Sloot *et al.*, 1994)
The leaching behavior of components from a waste as a function of pH is assessed by extracting waste, commonly at L/S=10 or L/S=100 under controlled pH by adding 1 M NaOH or 1 M HNO_3. After reaching equilibrium, the suspension is filtrated and the solution analyzed.

Titration

The total acid C_a (eq/L) or base C_b (eq/L) equivalents of a suspension (at liquid to solid ratio L/S = 100) is measured by titrating it with a standard solution of base (1.0 N NaOH) or acid (1.0 N HNO_3), respectively in a closed system. During titration, the volumes of the standard solution of base or acid, added to the suspension, are recorded along with the pH of the mixed solution. The titration is continued to an endpoint pH. C_a and C_b in the unknown solution are calculated from the relationship based on mass balance.

$$\text{Concentration (eq/L)} * \text{Volume (L)} = \text{Concentration (eq/L)} * \text{Volume (L)}$$
$$\text{titrated acid} \qquad \text{or} \qquad \text{base solution unknown}$$

It is necessary to point out that in the calculations of the titration results, the activity coefficients are ignored to avoid needlessly complicating the calculation.

In general, titration curves are presented in two ways (Langmuir 1997). One is the volume of a titrant acid or base V_a (L) or V_b (L) *versus* the pH of a solution. Another is the concentration of acid or base added C_a (eq/L) or C_b (eq/L) *versus* the solution pH. I have chosen the latter because of its advantage in indicating directly the buffer capacity of a solution.

2.3 Results and Discussions

2.3.1 Release from jarosite

Jarosite leaching behavior as a function of pH

The results of jarosite leaching as a function of pH, as depicted in Figure 2.3a - 2.3c, suggest that there are three mechanisms controlling the principal components release from jarosite. Release of Fe, Al, Zn, Cu, As and Pb are pH dependent. With increasing pH, the releases of these elements decrease rapidly reaching a minimum, then, at high pH their release starts to increase again. These phenomena are consistent with the

known solubility of their hydroxides as function of pH (Baes and Mesmer 1976), indicating that the release of these elements is solely controlled by the nature of their solubility. In contrast, the release of S is virtually pH independent. The release of Ca can be divided into two stages: at a solution pH below 7, the release of Ca is pH independent; at a solution pH above 7, the release of Ca slowly decreases with increasing pH, implying that a precipitation reaction occurs in which Ca, Si and/or Al participate

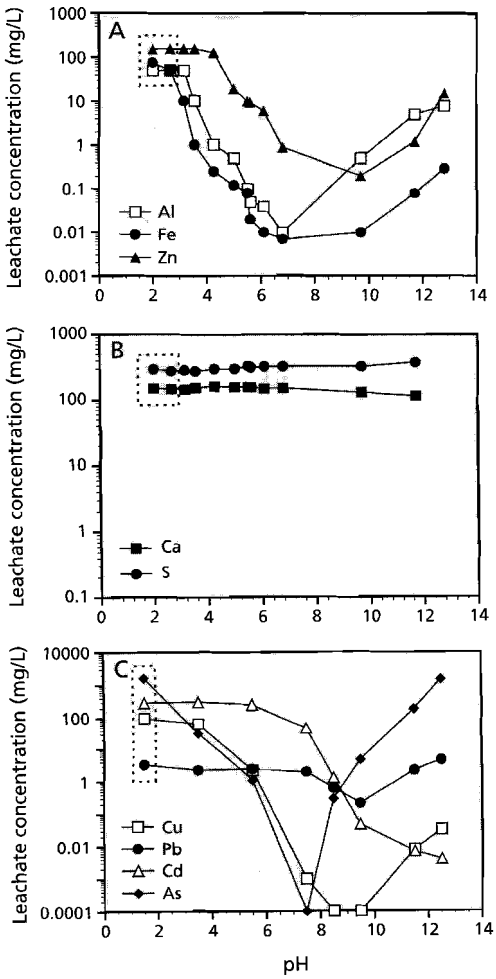

Fig. 2.3 Jarosite leaching as a function of pH
(a) L/S=100; (b) L/S=100; (c) L/S=10

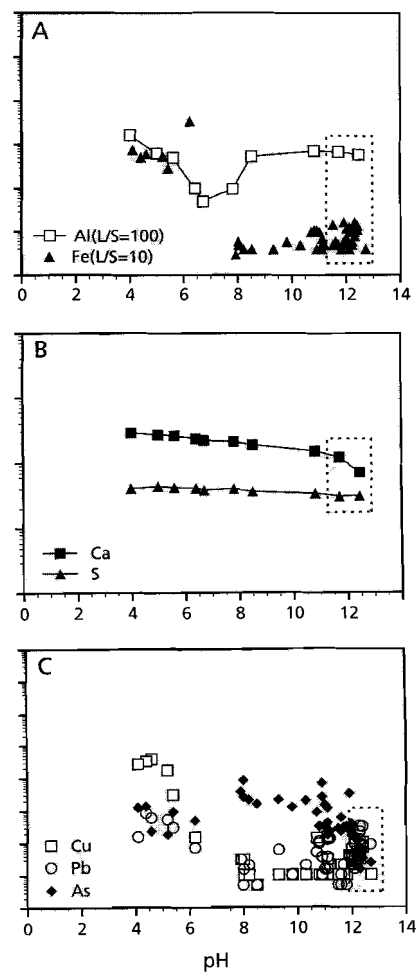

Fig. 2.5 Fly ash leaching as a function of pH
(a) L/S=100 (Al), L/S=10 (Fe)
(b) L/S=100, (c) L/S=10

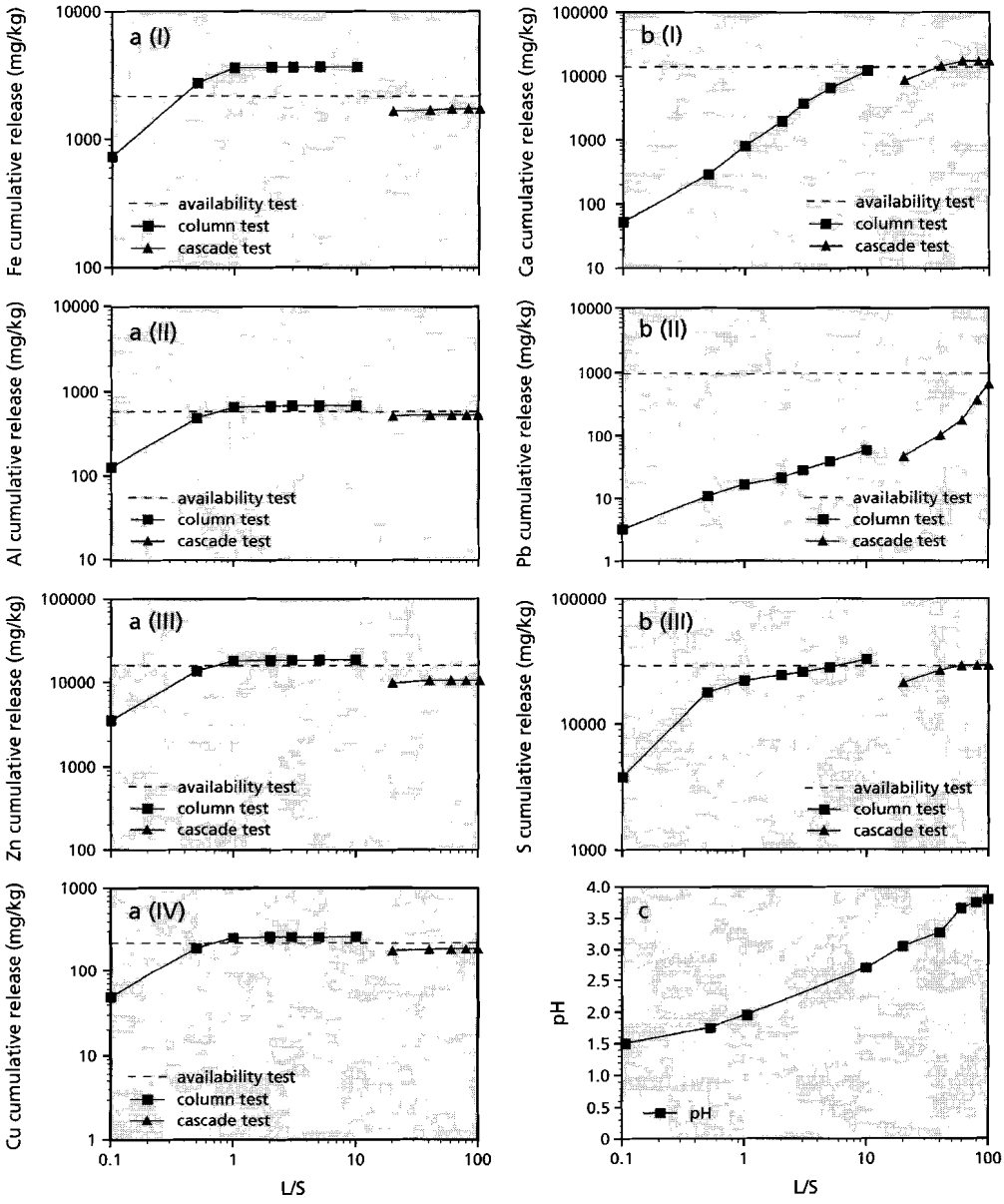

Fig. 2.4 Jarosite leaching as a function of L/S ratio

Jarosite leaching behavior as a function of L/S ratio

Besides solution pH, another important factor which affects the release property from solid is the Liquid to Solid ratio, L/S. Theoretically the time dependent release from a waste material in nature can be estimated in the laboratory from the cumulative release at different L/S ratio, according to the following relation (Kosson *et al.*, 1996):

$$L/S = \frac{(\inf)(t_{yr})}{\rho * H_{fill}} \qquad (2.1) \qquad\qquad M_{\Sigma} = (L/S)*(S_x) \qquad (2.2)$$

Where, inf is the annual infiltration at a given location (m^3/m^2yr), t_{yr} is the exposure time in the field(yr), H_{fill} is height or depth of residue fill material (m), and ρ is the bulk density of the material concerned (kg/m^3). M_{Σ} is the estimated cumulative release (mg/kg), and S_x is determined by solubility or availability(mg/L).

Figure 2.4a - 2.4c show cumulative release of the principal components from jarosite as a function of L/S ratio. As illustrated in Figure 2.4a, the release of Al, Fe, Zn, and Cu each reaches within L/S < 1 their maximum release capacity value, i.e. availability. Figure 2.4a also shows that the column test results of these element are slightly higher than their avalability value, probably due to the highly pH dependent release of these elements, as inferred from Figure 2.3a. The solution pH at low L/S ratio in column tests, as indicated in Figure 2.4c, is lower than that availability tests which remains constant at a pH of 4. The results of cumulative release of these elements on the other hand also provide evidence for their pH dependence. The release of Ca, S and Pb increases with increasing L/S ratio and eventually reaches their availability value. These results show a very good fit between column and cascade tests, as displayed in Figure 2.6b. Figure 2.4c presents the solution pH as a function of L/S ratio. Figure 2.4 clearly indicates the seriousness of environmental problems which can be caused by jarosite leaching. Thus even short time exposure to prevailing climatological conditions will result in a substantial release of a variety of chemicals including toxics due to the very high acidity of the leachate.

2.3.2 Release from fly ash

For pH static tests at L/S=100, the number of detectable elements in the leachate using ICP are limited for reasons of dilution. Figure 2.5a – 2.5c shows the results of releasing Fe, Al, Ca, S, Pb, Cu, and As as a function of pH. As expected, the release of Fe, Al is solubility controlled, similar to what we observed in the leaching tests of jarosite. Similarly, the release mechanism of Ca and S resembles that of jarosite. However it should be noted that in contrast to jarosite, the total elemental release of fly ash is small.

2.3.3 Acidity of jarosite

Contributing to the short term acidity of jarosite are strong and weak acids, salts of strong acids and weak bases, and hydrolysis of transition metals among which Fe^{3+} predominates. Contributions to the long term acidity include ion exchange of protons and weathering. Figure 2.6 presents the titration curves for a jarosite suspension (L/S=100 ml/g) with a strong base (1.0 N NaOH), to show the difference between short and long term (under equilibrium condition after 10 days exposure) acidity. The results from both short and long term acidity suggest that two proton sources affect the acidity of jarosite. Between a pH of about 2 and 5, the acidity is dominated by protons in a solution which has itself a low pH buffer capacity. Resultant reactions include:

$$H^+ + OH^- \leftrightarrow H_2O$$
$$H_2SO_4 + OH^- \leftrightarrow HSO_4^- + H_2O$$
$$HSO_4^- + OH^- \leftrightarrow SO_4^{2-} + H_2O$$

As indicated in Figure 2.6 between a pH 5 and 7, the slope of the curve is much smaller relative to the previous one, suggesting that in this pH range, the acidity of jarosite is caused mainly by hydrolysis of M^{n+} This reaction can be written:

$$M^{n+} + nOH^- \leftrightarrow M(OH)_n\downarrow$$

where M represents Fe^{3+}, Al^{3+}, Pb^{2+}, and Zn^{2+}. Figure 2.6 also shows that the long term acidity of jarosite is larger than the short term one. At pH 6, the long term C_b is almost three times the short term one.

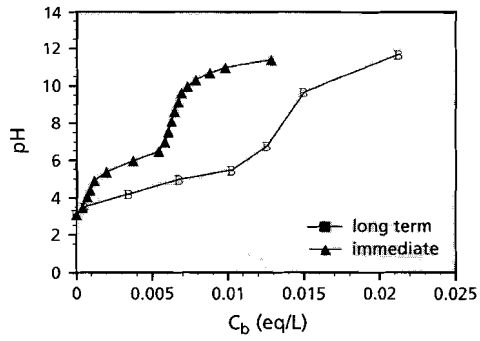

Fig. 2.6 Titration of jarosite suspension (L/S=100) with a strong base (1.0 M NaOH) in a closed system

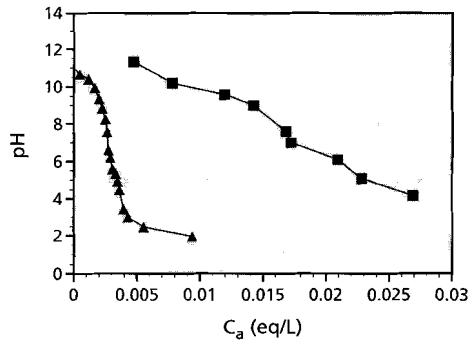

Fig. 2.7 Titration of fly ash suspension (L/S=100) with a strong acid (1.0 M HNO_3) in a closed system

2.3.4 Alkalinity of coal fly ash

The titration results for alkaline coal fly ash suspension (liquid/solid=100 ml/g) by a strong acid (1.0 N HNO_3) are shown in Figure 2.7. As illustrated in this Figure, there is a large and clearly observable difference between short and long term (under equilibrium condition after 20 days exposure) alkalinity of fly ash. Our results suggest that the contribution to the short term alkalinity of fly ash differs from that of the long term one. The short term alkalinity of fly ash involves only strong bases and may be expressed as:

$$M_xO_y + H_2O \leftrightarrow xM^{2y/x+} + (y+1)HO^- \qquad (M=Ca, Mg, K, etc.)$$

The rapid pH decrease with acid addition indicates a poor short term pH buffer capacity of fly ash from pH about 11 to pH about 2.

However, the long term alkalinity of fly ash suggests a potential pH buffer capacity larger than anticipated. At pH 6, the long term C_a is about 6 times the short term one. The difference between the long term *vis a vis* short term alkalinity presumably involves cation exchange of protons and geochemical weathering.

2.3.5 Titration of the jarosite and fly ash mixture

One of the potential uses of fly ash involves neutralization of waste acid, for example acidic jarosite. Figure 2.8 shows the neutralization capacity of alkaline fly ash with respect to jarosite. During the experiments, the amount of jarosite in the mixture was fixed. All titrations were carried out under L/S of 100. As indicated in Figure 2.8, with increasing amount of fly ash in the mixture less base is needed to bring the suspension pH of the mixture up to a specific value. Figure 2.10 also shows that there is a big difference between pH=5 curve and pH 7 curve, which is mainly due to hydrolysis of Fe^{3+} , Al^{3+}, Zn^{2+} and Pb^{2+} in jarosite and in turn indicates its buffer capacity.

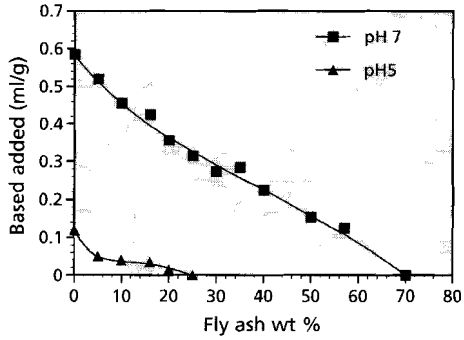

Fig. 2.8 Titration of suspension (L/S=100) of the jarosite and fly ash mixture with a strong base (1.0 M NaOH) in a closed system. The amount of jarosite in the mixture is constant and equals 2.0 g. The pH=5 line is the plot of the volume of base added to bring the suspension of the mixtures (the weight percentage of fly ash in the mixture is variable) up to pH of 5. The pH=7 line is the plot of the volume of base added to bring the suspension of the mixtures (the weight percentage of fly ash in the mixture is variable) up to pH of 7. The graphs reflect the neutralization capacity of fly ash in relation to jarosite, e.g. when the fly ash in the mixture is about 25 wt%, the suspension (L/S=100) pH of the mixture will be 5, whereas the suspension (L/S=100) pH of jarosite alone is about 2.3.

2.3.6 Potential initiating precipitation at the interface of jarosite/fly ash

As stated by van der Sloot (van der Sloot *et al.*, 1995a) the necessary condition for self-sealing is that the concentration of the reacting solutes in both parent materials ought to be high enough to initiate a precipitation reaction. In this particular case, we could estimate the feasibility for precipitation reaction to occur based on previous leaching results. Table 2.3 summarizes the calculational results (assuming that L/S=1, pH = 7 at the interface, and ignoring activity)

Table 2.3 Estimate of the feasibility for precipitations at the interface of jarosit/fly ash

Elements	Conc. in jarosite (g/L)*	Conc. in fly ash (g/L)**	Precipitation	Solubil. produc.	Feasibility
Al	5	$7*10^{-2}$	$Al(OH)_3$	10^{-25}	yes
Fe	10	$5*10^{-5}$	$Fe(OH)_3$	10^{-39}	yes
Zn	10	n.d.	$Zn(OH)_2$	10^{-16}	yes
Ca	15	1	$Pb(OH)_2$	10^{-20}	yes
S	20	$2*10^{-1}$	$CaSO_4 \cdot 2H_2O$	10^{-5}	yes

* these values come from Figure 2.4

** these values come from Figure 2.5

2.3.7 Sealing layer formation in relation to the mass of precipitates

Theoretically, a sealing layer will be formed when all the pores are filled with precipitates. Before precipitates start pore filling:

$$V_{pore} = A \cdot b \cdot \theta \tag{2.3}$$

where, V_{pore} is the volume of pores (m^3), A is a hypothetical sealing layer area (m^2), b is the hypothetical thickness of the layer (m) and θ is the porosity of the initial matrices. By definition, we have:

$$V_{pore} = A \cdot b \cdot \theta = \sum_{i=1}^{n} \frac{M_i}{\rho_i} \tag{2.4}$$

Here, assuming that the number of precipitates in the system is n, M_i and $_i$ are the mass and density of precipitate i in the system taken separately. The density of precipitate i is a constant parameter, whereas the mass of precipitate M_i can be obtained from the concentration change of chemical components which are contained in the precipitate and in the pore fluid. For example, $M_{Fe(OH)_3} = (C^{Fe}_{initial} - C^{Fe}_{equilibrium}) \cdot A \cdot L$, in which C represents concentration, and L the length of the system.

Based on Eq. 2.3 and 2.4, we can make a preliminary prediction concerning the self-sealing layer formation in jarosite/fly ash system under various conditions. Table 2.4 lists our predictions. In this particular case, the interface precipitation reaction can be expressed as:

$$MFe_3(SO_4)_2(OH)_6 + 2CaO + 3H_2O \leftrightarrow 3FeOOH\downarrow + M^+ + OH^- + 2CaSO_4 \cdot 2H_2O\downarrow$$

Clearly, filling of the original pore space at the interface is caused by some fraction of the two newly formed minerals; one of which being iron oxyhydroxide the other gypsum. Therefore, $V_{pore} = V_{FeOOH} + V_{gypsum}$. According to stoichiometry, production of three moles of FeOOH will result in two moles of $CaSO_4 \cdot 2H_2O$. The mole volumes of FeOOH and $CaSO_4 \cdot 2H_2O$ can be derived from their constant densities. Thus,

$$\frac{V_{FeOOH}}{V_{gypsum}} = \frac{3 * (1/\rho_{FeOOH})}{2 * (1/\rho_{gypsum})} \tag{2.5}$$

When ρ_{FeOOH} = 4.0 Kg/m^3, ρ_{gypsum} = 2.4 Kg/m^3, we can express,

$$V_{pore} = V_{FeOOH} + V_{gypsum} = V_{FeOOH} + 2.14 * V_{FeOOH} = 3.14 * V_{FeOOH} \tag{2.6}$$

Hence,

$$A \cdot b \cdot \theta = V_{pore} = 3.14 * V_{FeOOH} = 3.14 * \frac{(C^{Fe}_{initial} - C^{Fe}_{equilibrium})}{\rho_{FeOOH}} \cdot A \cdot L \quad (2.7)$$

and finally we have,

$$b \cdot \theta = 3.14 * \frac{(C^{Fe}_{initial} - C^{Fe}_{equilibrium})}{\rho_{FeOOH}} \cdot L \quad (2.8)$$

Table 2.4 Necessary Conditions Concerning Sealing Layer Formation in Jarosite/Fly Ash System

(Assuming that $\theta = 0.45$, and $C^{Fe}_{equilibrium} = 10^{-15}$ M at pH = 6)

b = 1 cm	L = 5.7 cm	C = 0.1 mg/ml
b = 1 cm	L = 57.3 cm	C = 0.01 mg/ml
b = 1 cm	L = 573 cm	C = 0.001 mg/ml
L = 5 cm	b = 0.87 cm	C = 0.1 mg/ml
L = 5 cm	b = 0.87 mm	C = 0.01 mg/ ml
L = 5 cm	b = 0.087 mm	C = 0.001 mg/ml
C = 0.01 mg/ml	L = 2.5 cm	b = 0.44 mm
C = 0.01 mg/ml	L = 100 cm	b = 1.74 cm
C = 0.01 mg/ml	L = 50 cm	b = 8.7 mm
C = 0.1 mg/ml	L = 2.5 cm	b = 0.44 cm

The results listed in Table 2.4 are based on Eq. 2.8.

2.3.8 Alternative options for waste jarosite management

The principal information from our investigation of acid-base and leaching properties of jarosite are its strong acidity and the release of a variety of chemicals, which has aroused environmental concern. In addition we noted that the release of jarosite is reduced significantly with increasing pH. Thus, one could select, based on these characteristics, alternative options to eliminate or reduce the environmental problems of waste jarosite.

Neutralization:

As indicated from the titration of jarosite and fly ash mixture Fig. 2.8, only 25 wt% fly

ash presence in the mixture will result in the solution pH of the suspension at L/S=100 rising up to about 5, which falls within an environmentally safe range. At the same time immobilization of various cations and anions such as Pb^{2+}, Zn^{2+}, and AsO_4^{3-} will take place due to precipitation. However, the drawback of this option is that the waste cannot be recycled. Looking for another option which on the one hand eleminates the environmental problems associated with jarosite on the other hand can keep it as a resource for recycling, is the challenge for the future.

Isolation

As one of the most common environmental option, isolation (Artiola 1996; Schuiling 1989) has been widely applied in Modern Sanitary Landfills (Artiola 1996) and suggested as a long term option (Schuiling 1989), especially in situations where a proper way to treat the waste is lacking. The previous discussion showed that self-sealing layers form when putting waste jarosite layer against alkaline coal fly ash layer by interface precipitation, which leads to pore filling. Additional support for isolation as an effective option comes from recent study on the development of a reliable, integrated and efficient treatment process for jarosite waste (Hage and Schuiling 1996). One can envision that in the near future, integrated using of waste jarosite will become possible. Thus, it is recommended to choose isolation as the option of choice requiring additional study.

2.4 Conclusions

The principal elements released from jarosite are Fe, Al, Zn, Pb, S, Ca, As and those of from fly ash are Al, Ca and S, the release of jarosite being much larger than that of fly ash, as indicated from the dotted outlines in Figure 2.3 and Figure 2.5. In general, the release of Fe, Al, Zn, Pb and As is controlled by the solubility of their hydroxides depending highly on pH. With increasing pH, the release of these elements decreases rapidly reaching a minimum value at pH range between 5 to 7. With continuously increasing pH, their release will rise again. The release of S is pH independent. Release of Ca at a pH below 7 is pH independent. Whereas at pH above 7, release of Ca from both jarosite and fly ash increases with increasing pH.

The results of our acid-base properties study suggests that it is crucial to take into account the long term acidity and alkalinity in studies involving minerals and groundwater. The long term acidity of jarosite is larger then the short term one. Contribuants to the short term acidity of jarosite are acids in solution and Fe^{3+} Al^{3+}, Zn^{2+}, and Pb^{2+} hydrolysis, the later causing the buffer capacity of jarosite. Similarily, the long term alkalinity of fly ash is also much larger than its short term one. In addition, the long and short term alkalinity of fly ash are about two times that of the long term and short term acidity of jarosite. The neutralization capacity of fly ash with respect to jarosite is pH specific. The amount of base needed to bring a 25-75 weight percent jarosite fly ash

mixture to a pH of 5 is about 1/8 of the amount needed to bring such mixture to a pH of 7. This difference is caused by hydrolysis of Fe^{3+}, Al^{3+}, Zn^{2+}, and Pb^{2+} in jarosite, which consumes a large amount of base.
It is because of their leaching and acid-base properties, we can expect that placing jarosite and fly ash adjacent to one another will result at the interface, in precipitation reactions among the principal releasing solutes.

The amount of precipitate determines the potential to form a sealing layer at the interface of jarosite/fly ash depending on practical initial and boundary conditions. Therefore, it is feasible and significant to select jarosite waste and alkaline coal fly ash as two objects in our study of self-sealing isolation and immobilization caused by chemical discontinuities in porous media.

The results of leaching and acid-base tests performed on jarosite and fly ash provide on the one hand the information of self-sealing layer formation potential in jarosite/fly ash system, on the other hand the initial and boundary conditions for model practical usage, which will be discussed in Chapter 4 of this thesis. Finally, the recommended environmental option to waste jarosite is self-sealing isolation and immobilization by placing it as a layer on top of a fly ash layer.

Acknowledgements

I would like to acknowledge Dr. H. A. van der Sloot for providing comparable data measured by ECN and for discussing the leaching tests in detail. All the analytical data were measured by Analytical Laboratory, Faculty for Earth Sciences, Utrecht University. Professor Dr. B. H.W.S de Jong read the manuscript and improved its language.

Chapter 3

Self-sealing isolation and immobilization in layered jarosite/fly ash

Chapter 3.1

Interaction of Fe^{3+}, Ca^{2+}, and SO_4^{2-} at the jarosite/alkaline coal fly ash interface

Abstract: Radio tracer diffusion experiments have been carried out to study self-sealing/healing isolation and immobilization of two chemically contrasting wastes: acidic jarosite and alkaline coal fly ash. Precipitation of iron oxyhydroxide FeO(OH) and gypsum $CaSO_4 \cdot 2H_2O$ occurs at the interface between jarosite and fly ash due to diffusion and interaction among the principal reacting solutes Fe^{3+}, SO_4^{2-}, Ca^{2+}, and OH^-. A layer with low permeability is formed at this interface because of pore filling by such precipitates causing a change in the transport properties of the bulk system. Precipitation at the interface between jarosite and fly ash affects also the mobility of chemical constituents including contaminants from the wastes. Co-disposal of chemically contrasting wastes may therefore lead to a self-forming barrier layer between them, which, next to isolating the wastes, also immobilizes contaminants from their leachates. Such systems will have a wide application in waste management.

Key words: *interface precipitation, self-sealing/healing isolation, jarosite, alkaline fly ash, effective diffusion coefficient, permeability, hydraulic conductivity.*

3.1.1 Introduction

Studies dealing with multicomponent-multiphase reactive transport in porous media have been receiving increasingly more attention due to their inherently closer similarity to realistic systems (Lichtner *et al.*, 1996). Some research emphasis has been placed on the study of interfaces between media in which large physical or chemical gradients occur (Hassanizadeh and Gray 1989a, 1988b). It can be anticipated that chemical reactions at such interfaces must influence the transport properties of a system and the mobility of its constituents, especially in the presence of solutions.

A new concept was introduced by Côté and van der Sloot (Côté and van der Sloot 1989, 1994) who developed "self-forming and self-repairing seals", as a waste isolation technique utilizing interface induced chemical reactions. The principle of this technique involves forming a layer with low permeability to groundwater and leachate at the interface of waste-soil or waste-waste based on diffusion and precipitation of react-

ing solutes. Damage to such seal will self-repair by continued diffusion and precipitation. Additional studies employing mathematical formulations for different types of chemical reactions, which dominate waste-soil interfaces have been carried out by Hockley *et al.*, (1992). Their results indicated that migration of contaminants from both waste and soil not only depends on the property of the waste but is also strongly influenced by the type of interface reaction between the waste and its surroundings.

The results of these pioneering researches provided the impetus to address the solution of a serious environmental problem: the disposal of acidic jarosite and alkaline coal fly ash. We surmised that there could be a potential benefit by co-disposal of these two chemically contrasting wastes. The process we envisioned was that by putting them adjacent to one another, precipitation would happen at the interface. As result a decrease in the permeability of the bulk system occurs together with a decrease in mobility of its constituents including contaminants from both wastes. Support for our working hypothesis came from the discovery of hematite and gypsum between a layer of acidic waste and limestone in a waste sulfuric acid lake of a TiO_2-plant at Armyansk, Crimea, Ukraine (Schuiling and van Gaans 1997). Combining this observation with our preliminary batch and flow through experimental results (Ding 1994) on these two wastes reinforced the idea that the interaction of Fe^{3+}, SO_4^{2-}, Ca^{2+}, and OH^- at the jarosite/fly ash interface would lead to precipitation. These newly formed minerals might eventually completely fill the pores, leading to the formation of a seal and hence to waste isolation.

In light of the above, this study has three goals. The first one is to determine the nature of the precipitates at the interface between acidic jarosite and alkaline fly ash. The second one is to investigate the effects of precipitation reactions at this interface on the transport properties of the bulk system and on the mobility of its constituents. The third one is to explore the quantitative relation between the change in transport properties of the bulk system and the microstructural change caused by pore filling precipitates at this interface.

Our principal result is that reactions involving Fe^{3+}, Ca^{2+}, SO_4^{2-}, and OH^-, tend to form a layer with low permeability to groundwater and leachate at the interface between acidic jarosite and alkaline coal fly ash. Constituents including contaminants from both wastes are thus immobilized at the interface. Such combined systems may provide a superior solution to the disposal of acidic jarosite and alkaline fly ash.

3.1.2 The principle of self-sealing/healing isolation

Isolation is the most common environmental option to dispose hazardous waste (Schuiling 1996). The key issue addressed in this technique is how to create a barrier between waste and its surroundings. This barrier can consist of compacted soil with low

permeability to form a so-called liner, as commonly used in Modern Sanitary Landfills (Artiola 1996). However such liner can also be developed by decreasing the permeability at the interface between waste and soil or waste and waste by chemical reactions such as precipitation, which results in filling the pores at the interface causing so-called self-sealing/healing (Côté and van der Sloot 1989, 1994). This precipitation occurs due to chemical interaction either between existing reacting solutes at the waste-waste or waste-soil interface (Schuiling and van Gaans 1997) or by introducing chemical discontinuities in the pore fluid of one of the materials (Côté and van der Sloot 1989, 1994). It is obvious, as stated by van der Sloot (van der Sloot *et al.*, 1995a) that the necessary condition for self-sealing is that the concentration of the reacting solutes in both materials ought to be high enough to initiate a precipitation reaction.

Figure 3.1.1 shows the principle of self-sealing/healing isolation. Suppose there are two materials adjacent to one another. Reacting solute A occurs in one material and solute B in the other. Due to the concentration gradient of solutes A and B between these two materials, diffusion of A and B will occur in opposite direction. Once the concentrations of A and B are sufficiently high, a precipitation reaction involving A and B will start. This precipitation will cause a local lowering of the concentration of A and B in the pore fluid, thus maintaining a concentration gradient, which will lead to further diffusion of A and B towards the interface, resulting in more precipitation. These coupled processes of diffusion and precipitation will continue until the pores are completely filled with precipitate, resulting in self-sealing layer formation at the interface. As long as sufficiently large amounts of solutes A and B are present at opposite sites of the interface, this coupling process will be maintained and any mechanical damage to the interface, i.e. the liner, will cause further diffusion and precipitation thus healing the liner. In this manner the interface seals as well as heals hence the term self sealing/healing layer. This built in security of healing upon damage can without doubt be considered as the principal advantage of the self-sealing/healing isolation technique.

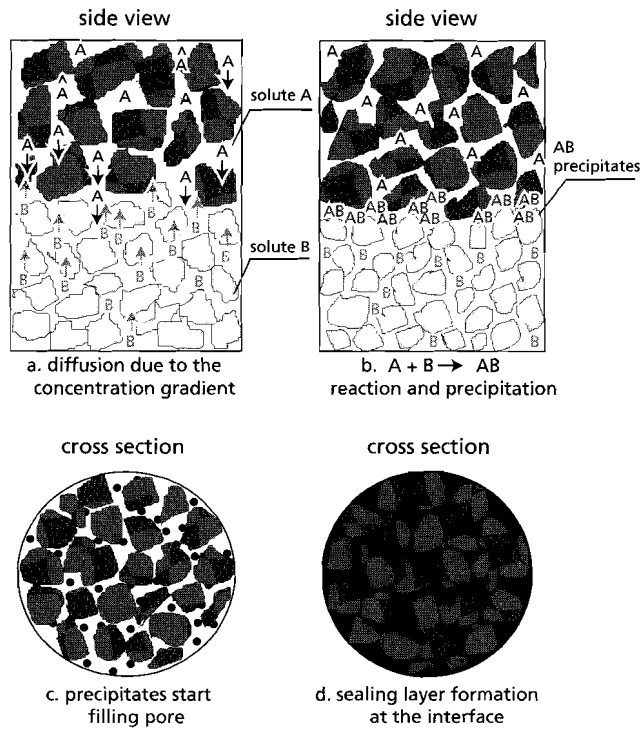

Fig. 3.1.1 The principle of self-sealing/healing isolation.

3.1.3 Experimental methods and materials

Materials

Jarosite and alkaline fly ash

Jarosite is one of the most important members of a large group of isostructural minerals. The general formula of this group (Stoffregen 1993) is $MA_3(BO_4)_2(OH)_6$, where M is a monovalent or divalent cation such as Na^+, K^+, NH_4^+, or Pb^{2+}, A stands for iron or aluminium, and B for sulphur, phosphorous, or arsenic. The jarosite used in this study comes from a zinc manufacturing plant and is the result of removing Fe from acidic, sulphate-rich solutions (Elgersma 1992). The alkaline fly ash used in this study is the residue from a power plant. It consists mainly of an amorphous phase, with small amounts of quartz (SiO_2), mullite ($Al_6Si_2O_{13}$), and hematite (Fe_2O_3). The physical and chemical characteristics of jarosite and alkaline fly ash are summarized in Table 3.1.1.

Table 3.1.1 Physical and chemical characteristics of jarosite and alkaline fly ash

	Jarosite	Alkaline Coal Fly Ash
Composition	$[M]Fe_3(SO_4)_2(OH)_6$ [M=Na^+, K^+, NH_4^-, and Pb^{2+}]	Amorphous Phase Quartz(SiO_2) Mullite($Al_6Si_2O_{13}$) Hematite(Fe_2O_3)
Particle Size (mm)	5.2	20.1
Dry Density (kg/m³)	2.9	2.0
Bulk Density (kg/m³)	2.2	1.2
Natural pH*	1.7	12.0
Principal Leachates	S, Fe, Pb, Zn, Ca, As, Mg	Ca, K, Na, S

** Determined at a Liquid/Solid ratio of 10*

^{59}Fe tracer

In Table 3.1.2 the characteristics of the $^{59}Fe^{3+}$ radiotracer used in this study are presented.

Table 3.1.2 $^{59}Fe^{3+}$ tracer characteristics

Nuclide	Chemical Form	Concentration (mg/ml)	Initial Activity (counts/min•ml)	Half-life ($T_{1/2}$)
^{59}Fe	Fe^{3+}	9.21	$2.33*10^7$	45.1 days

Experimental methods

Diffusion tube measurement

A schematic of a diffusion tube measurement is depicted in Figure 3.1.2 (van der Sloot *et al.*, 1991). In these small diffusion tubes (Ø8 mm, L50 mm), either one material (jarosite or fly ash) or a combination of two materials (jarosite with fly ash) were compacted. One half-space contained the material to be labelled with a radiotracer, the other half-space contained the tracer-free material. Both ends of the tube were closed by pistons. These diffusion tubes remained stored in a constant moisture atmosphere at room temperature and zero fluid flow condition. The exposure times were one day, one week, two weeks, one month and two months. After exposure, both the labelled and unlabelled segments were sliced and counted with L 1282 Compugamma Universal Gamma Counter.

Preparation and slicing of diffusion tube contents

Figure 3.1.3 shows the preparation and slicing of the diffusion tube contents (van der Sloot *et al.*, 1991). Thirty grams of jarosite and fly ash were mixed with 12 ml and 9 ml distilled water respectively, to form a non-labelled paste. Meanwhile, another 30 grams of jarosite and fly ash were mixed with 12 ml and 9 ml diluted tracer solution respectively, to form the labelled paste. Half of the tube was filled with the non-labelled paste, the remaining half with the labelled one. The amount of solution used to mix with solid proved experimentally to be the best scheme to avoid any liquid spilling from the tubes. The degree of dilution was chosen such that 10^{-2} % of the originally added activity level (counts/min.g) could be detected in each sliced sample. The 50 mm long tube was sliced into about 40 slices.

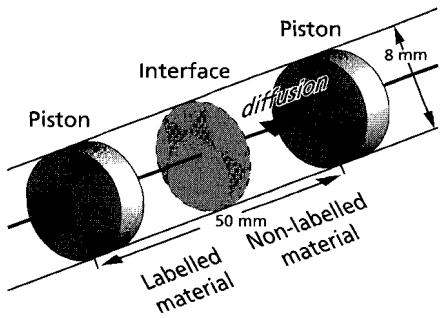

Fig. 3.1.2 Schematic view of a diffusion preparation and slicing measurement.

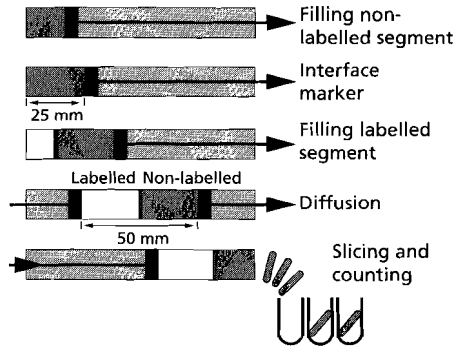

Fig. 3.1.3 Tube of diffusion tube contents.

pH gradient measurement

pH tube measurements were designed to track the variation in the pH gradient during transport and chemical reaction in the layered jarosite/fly ash system. The preparation and slicing of the pH tube content is exactly the same as that for the diffusion tube experiment except that no tracer was added in either of the segments. The procedure consists in adding a specific amount of distilled water to each sliced segment for a liquid to solid ratio of 10. The measured pH refers to the pH of such solution.

Hydraulic conductivity measurement

Hydraulic conductivity measurements were carried out in a triaxial cell (Ø50 mm, L140 mm) under controlled three-dimensional stress conditions (flexible wall) to prevent

leakage as well as flow along the wall. One half part of the cell was filled with 70 mm jarosite with a dry weight of 293 g, the other part with 70 mm alkaline fly ash with a dry weight of 234 g. The fly ash was placed on top of the jarosite, the fluid flow direction was from the bottom upwards. The samples were compacted mechanically and saturated with pure water.

X-ray power diffraction

X-ray power diffraction of jarosite, fly ash, and interface samples were determined with a Philips Power Diffractometer PW 1050/PW 1730 and ADM Software Packet.

3.1.4 Results

pH development in the layered jarosite and alkaline fly ash system

The variation in pH as a function of time and distance across the interface in the layered jarosite/alkaline fly ash system is shown in Figure 3.1.4. It is essential to pay particularly attention to the pH variation in the 2 mm zone at the both sides of the interface because of its central importance in self-sealing formation. Inspection of Figure 3.1.4 shows that the initial pH gradient in this 4 mm thick zone (2 mm at both sides) is about 10 pH units. After one day this gradient is reduced to 7 units, and continues to decrease with time. This interfacial pH gradient is reduced to 4 units in about one month and the pH reached a value of about 6 across the zone after about two months. Note that three relatively steady pH states can be clearly distinguished in this layered system after two months: the first one in the alkaline fly ash segment with a pH of about 10, the second in the interface zone with a pH of about 6, and the third one in the jarosite segment with a pH around 4. These three pH states imply that in a closed system, in which the size of the tubes is limited, the pH gradient over the interface will continuously decline as long as the interface has not been sealed completely. Moreover

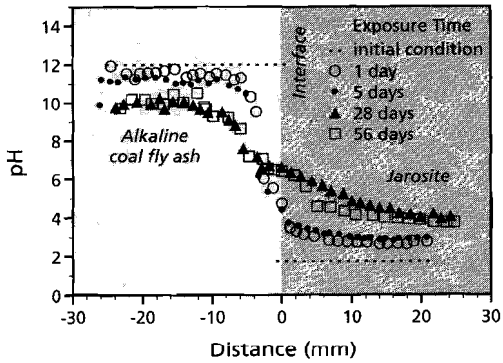

Fig. 3.1.4 pH development in the layered jarosite/fly ash system.

the existence of a zone of precipitation causes the jump in gradient to appear non-linear, as illustrated in Figure 4 where the second pH region extends about 2 mm into the alkaline fly ash zone. If, on the other hand, the pores are fully filled, a discontinuous steady state across the interface will develop. We also anticipate that with the use of longer tubes or in an open system, pH gradients will be maintained longer.

Radio tracer experiment

The radiotracers we have been using include all the principal reacting solute components such as $^{59}Fe^{3+}$, $^{45}Ca^{2+}$, and $^{35}SO_4^{2-}$ as well as $^{22}Na^{+}$ and $^{3}H^{+}$. The choice of the last two was predicated by their supposedly inert nature. In this paper we shall focus only on the behavior of $^{59}Fe^{3+}$, as representative of the behavior of one of the principal reacting solutes, Fe^{3+}, in the jarosite/fly ash system.

$^{59}Fe^{3+}$ diffusion in jarosite

Figure 3.1.5 presents the $^{59}Fe^{3+}$ diffusion profiles in jarosite. Two principal results can be inferred from inspection of Figure 3.1.5. Firstly, the diffusion of $^{59}Fe^{3+}$ in jarosite slows down with increasing exposure time. As indicated from our radiotracer data for $^{59}Fe^{3+}$, the measured effective diffusion coefficients of $^{59}Fe^{3+}$ in jarosite decreases in about two months from $10^{-10.1}$ m²/s to $10^{-11.5}$ m²/s (Ding 1996). Secondly, the characteristic diffusion pattern of $^{59}Fe^{3+}$ in jarosite does not coincide with the anticipated standard diffusion pattern which should result in a horizontal line through the point at C/C_0 equal to 0.5 under the same controlled boundary condition. The difference between the measured $^{59}Fe^{3+}$ diffusion profile and the ideal diffusion profile is due to the time dependent isotopic exchange reaction which can occur between $^{59}Fe^{3+}$ introduced into the pore water and stable Fe^{3+} in the jarosite matrix.

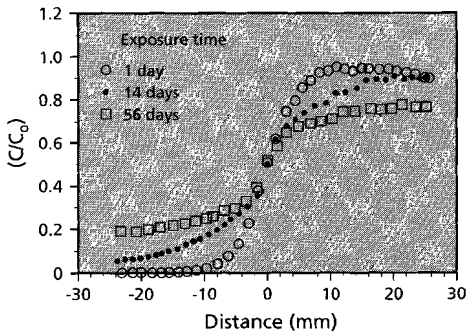

Fig. 3.1.5 $^{59}Fe^{3+}$ diffusion profiles in jarosite.

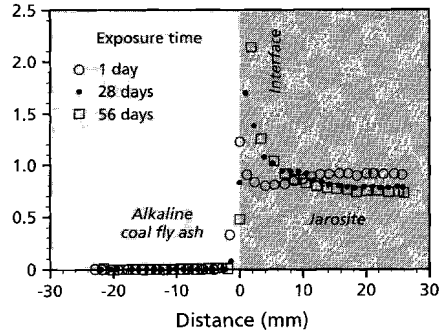

Fig. 3.1.6 Profiles of $^{59}Fe^{3+}$ diffusion from jarosite to alkaline fly ash.

$^{59}Fe^{3+}$ diffusion from jarosite to alkaline fly ash

Figure 3.1.6 shows $^{59}Fe^{3+}$ diffusion profiles in a combined jarosite and alkaline fly ash layered system. Our principal results, as can be seen in Figure 3.1.6, are: firstly, $^{59}Fe^{3+}$ tracer accumulation at the interface of jarosite/fly ash where a sharp peak can be observed, which indicates that iron oxyhydroxide precipitation occured; secondly, a curious first day profile showing just before and after the midpoint of the total length of labelled jarosite, a gradual decline in Fe-59 tracer concentration followed by a rapid rise near the jarosite/fly ash interface, and a sharp drop in the alkaline fly ash. Integrating the results of $^{59}Fe^{3+}$ diffusion and pH profile in the layered jarosite/fly ash system suggests that two processes are characteristic for the behavior of Fe^{3+} at the interface. The diffusion of Fe^{3+} is caused by its concentration gradient between jarosite and fly ash. The sharp peaks appearing at the interface are caused by the exceedingly low solubility of Fe^{3+} due to the marked pH jump at the interface. The thermodynamics of ferric hydrolysis (Baes and Mesmer 1981) indicates that due to its extremely low solubility at room temperature between pH 5 and 9 , Fe^{3+} in pore water will be completely transferred to the insoluble state in the form of FeO(OH).

Gypsum formation at the interface of the layered jarosite/fly ash system

Figure 3.1.7 shows X-ray power diffraction results of jarosite, of the interface, and of fly ash. Inspection of this Figure reveals that the major component in fly ash is glass, together with small amounts of quartz, mullite and hematite. The jarosite used in the study, was mineralogically pure except for a small amount of quartz. In the interface gypsum as major phase could be identified next to a minor amount of bassanite. The interface sample also contains some jarosite and quartz which are contaminants from the starting materials due to the experimental difficulty in selecting a pristine interface sample.

Hydraulic conductivity development in the layered jarosite/fly ash bulk system

The variation in hydraulic conductivity as a function of time and hydraulic head needed to maintain a flow through the system is depicted in Figure 3.1.8. As can be seen, the hydraulic conductivity of the first system(Test 1) decreases slowly in the first 15 days, followed by a faster decrease in the next five days, from an initial value of 10^{-7} m/s to $5\star10^{-9}$ m/s. The hydraulic head increases concomitant with this decrease in hydraulic conductivity. The increase in hydraulic head causes some damage to the self-forming layer, with as consequence that the hydraulic conductivity after 20 days starts to increase up to roughly 10^{-8} m/s. This situation is maintained for about one more month, indicating that no additional diffusion and precipitation occurred. We interpret this phenomenon as being due to shortage of the Fe^{3+} source. Note that the starting pH in the first system was 6.6 rather than 2.0 as mentioned previously for jarosite. Thus the amount of Fe^{3+} needed for precipitation is much less than that needed in the seond

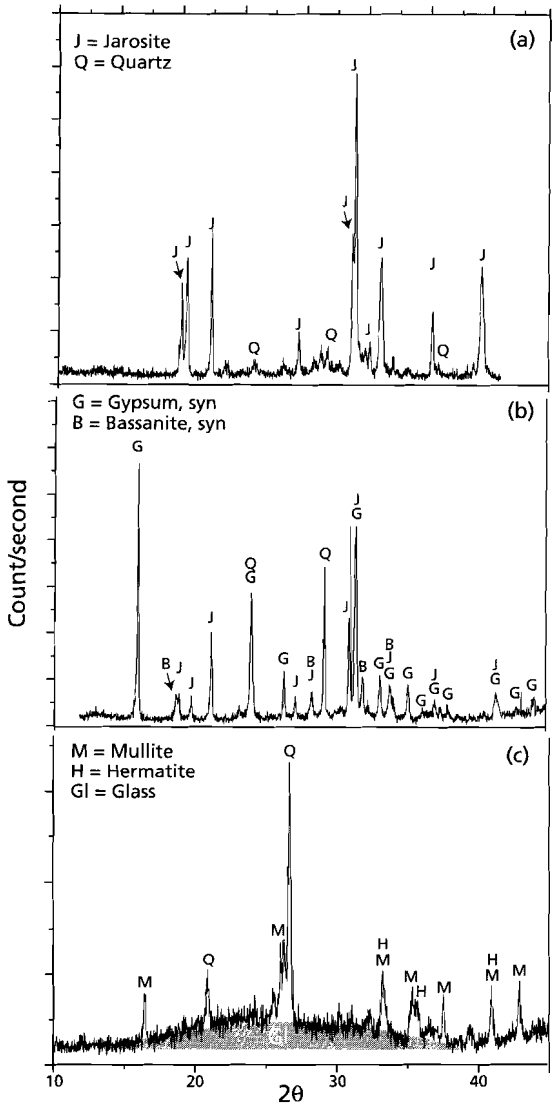

Fig. 3.1.7 X-ray power diffraction of (a): jarosite; (b): interface; (c): fly ash.

system(Test 2) in which the starting conditions were similar to those of the diffusion tube measurement. As we mentioned already, the solubility of Fe^{3+} at a pH above 4 is very low in comparison to that at pH 2. Therefore, the hydraulic conductivity in the second system continuous to decrease after 75 days.

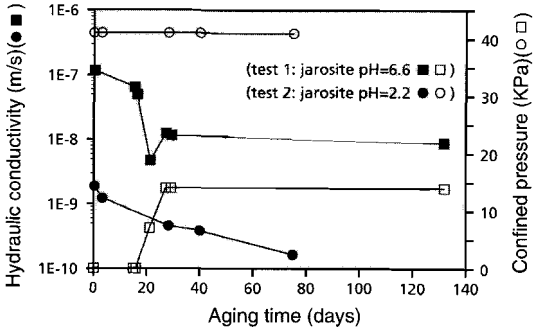

Fig. 3.1.8 Development of hydraulic conductivities jarosite/fly ash system.

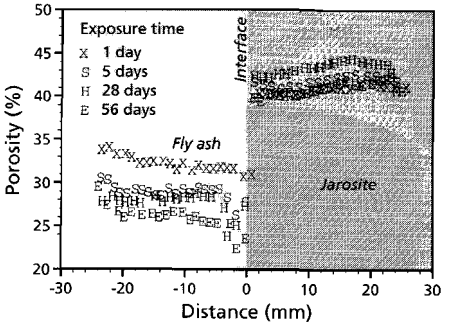

Fig. 3.1.9 Porosity variation in the in the jarosite/fly ash bulk system.

Porosity variation in the jarosite/fly ash system

One of our most interesting results, the porosity variation in the jarosite/fly ash system, is illustrated in Figure 3.1.9. This Figure shows that the decrease in porosity occurs at the interface slightly penetrating the fly ash side. This decrease in porosity (hence the microstructural change) at the interface depends on reaction time and is due to precipitation, which results in filling pores. Figure 3.1.9 also shows that the disadvantages of diffusion tubes measurements are a lack of unique initial porosity among different tubes and limited resolution imposed by slicing of the tubes.

3.1.5 Discussion

The effect of precipitation on the mobility of constituents in the jarosite/fly ash system

Theoretical considerations

One of the major effects of chemical reactions in porous media is to change the mobility of reactive solutes, as can be inferred from our particular results for the jarosite/fly ash system. According to our pH measurement results, a pH gradient exists in the bulk system, and in particular a pH switch occurs at the interface. This phenomenon requires special attention because of its potential effect on immobilizing constituents including contaminants from the wastes. Recalling some thermodynamics of cation hydrolysis in aqueous solution, the general equilibrium equation for oxyhydroxide or hydroxide compound formation can be expressed as:

$$M(OH)_n \leftrightarrow M^{n+} + nOH^-, \quad K_s=[M^{n+}]\cdot[OH^-]^n \qquad \text{(Eq. 1)}$$

Where K_s is the solubility product and n is the formal charge of the cation (M). Thus, the solubility of a cation is given by:

$$[M^{n+}]=K_s/[OH^-] \qquad \text{(Eq. 2)}$$

This formula implies that for basic and amphoteric oxides, the higher the pH of the aqueous solution, the lower the solubility of cations. Table 3.1.3 lists the hydroxide solubility product of ferric iron (Fe^{3+}), aluminum (Al^{3+}), zinc (Zn^{2+}), and lead (Pb^{2+}), which are encountered as principal components in the leachates from both jarosite and alkaline fly ash. It can be inferred from Eq. 1 together with the data from Table 3.1.3 that Fe^{3+} will become immobile ($[M] < 10^{-6}$ mol/L) at a pH above 4.5 , followed by Pb^{2+} at a pH above 5, Al^{3+} above 7.5, and Zn^{2+} above 8. Referring to our pH determinations in the layered jarosite/fly ash system, we expect that immobilization of these four constituents would occur in different zones from just before or at the interface, to the interface slanted towards the fly ash side, and finally into the fly ash segment.

Table 3.1.3 Solubility product of ferric iron, aluminium, zinc, and lead hydroxide (Handbook of chemistry and physics 1980-1981).

	$Fe(OH)_3$	$Al(OH)_3$	$Zn(OH)_2$	$Pb(OH)_2$
log K_s	-38.58	-24.57	-16.16	-19.85

Effect of interface precipitation on the Fe^{3+} mobility in the jarosite/alkaline fly ash

Considering $^{59}Fe^{3+}$ as an example, the observed $^{59}Fe^{3+}$ profile (Figure 3.1.6) reflects, as mentioned previously, the coupled processes of diffusion and precipitation. In other words, the observed $^{59}Fe^{3+}$ diffusion profile can be divided into a mobile and immobile ferric cation profile, as shown in Figure 3.1.10. The mobile $^{59}Fe^{3+}$ profile is based on knowledge about the diffusion as well as thermodynamics of ferric hydrolysis which states that at a pH of about 4.5, $^{59}Fe^{3+}$ will be transferred completely to the insoluble state. The pH is about 5 at the interface of jarosite/fly ash, indicating that the concentration of mobile $^{59}Fe^{3+}$ at this point ought to be zero. Additionally, diffusion occurs only when a concentration gradient exists in the fluid state, implying that the lowest point of the observed $^{59}Fe^{3+}$ profile is still caused by mobile $^{59}Fe^{3+}$. Once the concentration starts to increase, precipitation of ferric oxyhydroxide occurs. Linking these two points, results in the mobile $^{59}Fe^{3+}$ profile. The profile of immobile $^{59}Fe^{3+}$ can be calculated by subtracting the mobile $^{59}Fe^{3+}$ profile from the measured one.

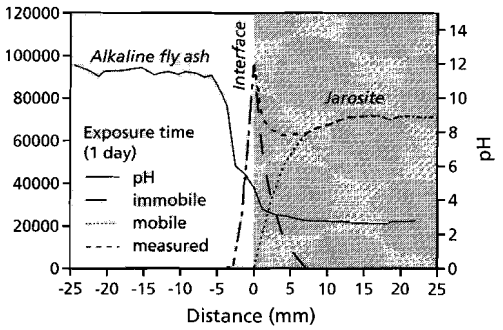

Fig. 3.1.10 $^{59}Fe^{3+}$ accumulation at the interface due to coupling between diffusion and precipitation.

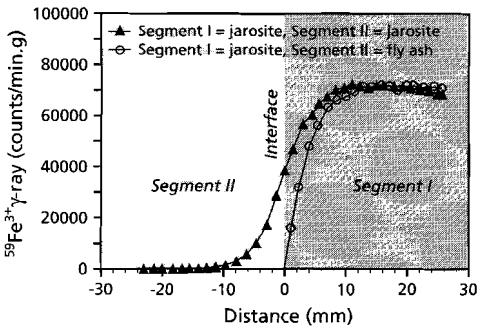

Fig. 3.1.11 Effect of interface precipitation on Fe^{3+} mobility.

Combining the mobile $^{59}Fe^{3+}$ profile in layered jarosite/fly ash system with the $^{59}Fe^{3+}$ profile in jarosite only, gives our most important result, as illustrated in Figure 3.1.11. This Figure shows that the mobility of Fe^{3+} in the jarosite/fly ash system decreases with respect to that observed for Fe^{3+} in jarosite. This decrease is due to ferric oxyhydroxide precipitation at the jarosite/fly ash interface leading to a substantial concentration of immobile Fe^{3+} even after only one day.

The effect of precipitation on the transport properties of the jarosite/fly ash system

Of crucial concern in this study is to assess the relation between microstructural changes caused by precipitation leading to pore filling in porous media and transport properties, such as hydraulic conductivity, and effective diffusion coefficient of inert components in the bulk system. We shall use as porosity parameter the symbol θ which is characteristic of the microstructure in a porous medium. Note that the transport properties of ions in porous media are determined not only by porosity but include many other factors, such as tortuosity, particle size, method of compaction, the manner of pore filling, *inter alia*. Consequently an explicit mathematical formulation taking these parameters into account becomes next to intractable. Therefore, most studies use empirical or semi-empirical formulas to rationalize their experimental results.

Hydraulic conductivities and effective diffusion coefficients

van der Sloot *et al.*, (1995) conducted a study on the relation between hydraulic conductivity and effective diffusion coefficients for inert components. They tested a wide range of materials with different porosities. Their results suggest that within a specified range the relation between K, the hydraulic conductivity (m/s), and D_e, the effective diffusion coefficient (m^2/s), can be summarized as follows:

$$\log K = a \log De + b \qquad \text{Where, } a \approx 1.06, b \approx 2.10, \qquad \text{(Eq. 3)}$$

$$10^{-12} < K(m/s) < 10^{-8.4} \qquad 10^{-13} < De(m^2/s) < 10^{-9.73}.$$

Our predictions concerning the variation of the effective diffusion coefficients for inert components in the jarosite/fly ash system based on this equation are collected in Table 3.1.4.

Table 3.1.4 Hydraulic conductivity K (m/s) and effective diffusion coefficient D_e (m^2/s) in the jarosite/alkaline fly ash.

Aging Time (days)	K_1(m/s, Test 1)	D_{e1}(m^2/s)	K_2(m/s, Test 2)	D_{e2} (m^2/s)
0 initial condition	1.2E-07	3.0E-09*	1.9E-09	6.2E-11
3			1.2E-09	4.1E-11
15	6.5E-08	1.7E-09*		
16	5.0E-08	1.3E-09*		
21	4.8E-09	1.5E-10		
26			4.6E-10	1.6E-11
40			3.9E-10	1.4E-11
132	8.9E-09	2.7E-10		

*** outside the range for which Eq. 3 is applicable.**

Inspection of this table shows that the effective diffusion coefficient of an inert component will decrease in about one month from $6.2 \star 10^{-11}$ m^2/s to $1.4 \star 10^{-11}$ m^2/s in the jarosite/fly ash system, and will continue to decrease with decreasing bulk hydraulic conductivity.

Permeability, hydraulic conductivity, and porosity

Two models which relate permeability and porosity show good agreement with the permeability derived from our experimental hydraulic conductivity measurement results. The relation between permeability k (m^2) and hydraulic conductivity K (m/s) is given by (Freeze and Cherry 1976):

$$k = K \cdot \mu / \rho \cdot g \qquad \text{(Eq. 4)}$$

Where k is the permeability (m^2); K the hydraulic conductivity (m/s); μ the viscosity of the fluid (g/cm.s); ρ the density of the fluid (g/ml); and g the gravitational acceler-

ation (9.8 m/s²). In our calculation, we have considered water as the fluid.
The relation between porosity and permability is according to Model 1 (Freeze and Cherry, 1976) :

$$k = \frac{\theta^3}{(1-\theta)^2} \cdot \frac{d_m^2}{180} \qquad \text{(Eq. 5)}$$

In which, k is the permeability (m²), θ the porosity (dimensionless), and d_m is the representative particle diameter.

According to Model 2 (Sahimi 1995) this relation is :

$$\frac{k_s}{k} = \frac{10\theta}{(1-q)^3} \qquad \text{(Eq. 6)}$$

Where $10^{-12} < K(m/s)$ called the Stokes permeability, and r is the mean sphere radius in meters.

Note that both models contain a parameter which describes the particle geometry of the particle, which cannot be determined in the jarosite/fly ash system. One way to avoid this difficulty is to consider the relative value of k. If we assume that changes in the value of d_m as well as r are negligible during the experiment, we obtain the following functions:

$$\frac{k_0}{k_i} = \frac{\theta_0^3}{\theta_i^3} \cdot \frac{(1-\theta_i)^2}{(1-\theta_0)^2} \qquad \text{(Eq. 7)} \qquad \frac{k_0}{k_i} = \frac{\theta_0^2}{\theta_i^2} \cdot \frac{(1-\theta_i)^3}{(1-\theta_0)^3} \qquad \text{(Eq. 8)}$$

Eq. 7 is derived from model 1, whereas Eq. 8 is derived from model 2. From both equations we are able to calculate K_i as a function of θ_i. Note that K_o and θ_o represent the initial values of the system. Porosities used in this calculation are obtained from our previous porosity measurement results. Figure 3.1.12 shows the permeability change as a function of time in the jarosite/fly ash system. Our result indicates that in the begining stage of aging time, the measured permeability declines with time and agrees well with the models. However, after aging for 8 days, the measured permeability decreases faster with time than is indicated by the models. The reasons for this discrepancy are , as mentioned before, firstly, limited resolution imposed by slicing of the tubes, which implies that the actural porosity should be lower than our measured result; secondly, in real life the permeability of the system does not depend solely on porosity.

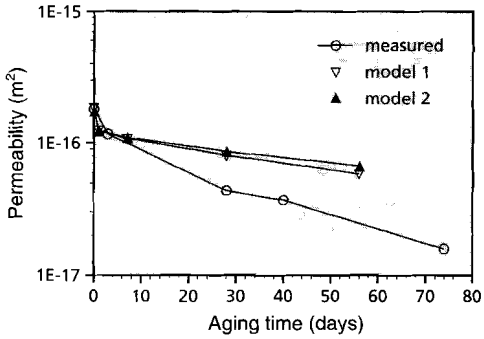

Fig. 3.1.12 Permeability as a function of time.

3.1.6 Conclusion and significance

A layer with low permeability was formed at the interface of acidic jarosite and alkaline fly ash. This layer formation is due to a coupling between diffusion and precipitation of principal reacting chemical components in leachates from the two wastes. The diffusion of Fe^{3+}, Ca^{2+}, SO_4^{2-}, and OH^- is caused by their concentration gradient between jarosite and fly ash. Precipitation occurred between these species at the interface, leading to pore filling (hence the porosity decrease), resulting in a hydraulic conductivity decrease of the bulk system. Immobilization of principal reacting solutes such as Fe^{3+} in the wastes occurred due to newly formed minerals at this interface, and that of contaminants from the wastes presumably because of coprecipitation or surface adsorption. The results of our study indicate that interfacial chemical reactions in porous media exert a crucial effect on the transport properties of the bulk system as well as on the mobility of environmentally harmful constituents. Particularly, one can make use of the interfacial phenomena in the acidic jarosite/alkaline fly ash system as a means of relatively safe and effective environmental technique to neutralize, immobilize and isolate them.

Acknowledgements

Work was carried out at the Soil and Waste Research Laboratory, Netherlands Energy Research Foundation (ECN), Petten. Professor Dr. R.D. Schuiling is gratefully acknowledged for financial and scientific support. Special thanks go to Professor Dr. B. H.W.S. de Jong for critical reading of the manuscripts and smoothing the language.
P. van Oudenallen of the Audiovisual Service at the Institute of Earth Sciences at Utrecht is thanked for making beautiful poster and slides.

Chapter 3.2

Interface precipitation affects the resistance to transport in layered jarosite/fly ash

Abstract

We have studied the effect of interface precipitation on the transport properties under fluid flow condition in a layered jarosite/fly ash system as part of an ongoing case study in geochemical engineering dealing with isolation and immobilization of chemically contrasting wastes. The experiment was carried out to determine the development of hydraulic conductivity in such system. However rather than hydraulic conductivity, we used resistance as the characteristic parameter. Our experimental results show that the overall resistance to transport increases by about two orders of magnitude due to the formation of a self-forming layer at the interface between jarosite and fly ash. Our modelling results suggest that this increase in resistance causes a more than sixty times delay in breakthrough of an inert constituent. We explore also the advantage of using the theory of electrical conductivity to describe fluid transport in a layered porous medium. Additionally, our results enable a proper assessment of the efficiency of self-sealing/healing isolation.

3.2.1. Introduction

A major topic in environmental geochemical engineering dealing with waste disposal is self-sealing/healing isolation (Schuiling, 1996; van der Sloot *et al.*, 1993b; van der Sloot *et al.*, 1995). It is based on the formation of a layer with a low permeability to ground water and leachate by placing two chemically reactive substances together. We have shown in previous work (Ding 1996; Ding *et al.*, 1996; Ding *et al.*, 1997) that such option is operational in chemically contrasting wastes: acidic jarosite and alkaline fly ash. In this particular case, precipitation of iron oxyhydroxide FeO(OH) and gypsum $CaSO4 \cdot 2H2O$ occurs at the interface in the layered jarosite/fly ash due to diffusion and interaction among the principal reacting solutes Fe^{3+}, SO_4^{2-}, Ca^{2+}, and OH^-, creating a barrier because of pore filling. As indicated by our radio tracer diffusion experiments (Ding *et al.*, 1996), the bulk diffusivity in the jarosite/fly ash system decreases in comparison to that of either jarosite or fly ash separately. Doubtless the change in the

resistance to transport is due to the reactions happening at the interface. In order to asses the proficiency of self-sealing/healing isolation in jarosite/fly ash, it is essential to quantify this change.

Here we shall address in detail the problem of how and to what extent interface precipitation affects the resistance to transport in this system. In contrast to using hydraulic conductivity or permeability as a parameter to describe the transport characteristics, we shall use resistance. Discussing it in this manner brings out on the one hand the similarity in mathematical formalism between fluid flow in porous media and the more familiar flow of electrical charge in a conductor, semiconductor, or insulator. On the other hand it has as advantage that the resistance defined in this paper is an independent intensive variable as opposed to hydraulic conductivity and thickness of layers both of which are extensive.

We have discovered that the overall resistance to transport in the bulk system increases by about two orders of magnitude after only 3 days. Furthermore, this increase in overall resistance is primarily due to the increase in resistance of the interface layer. Finally, by simulating breakthrough curves of an inert constituent as a function of resistance, a quantitative assessment is made on how the change in resistance in a porous medium affects the transport process.

3.2.2 Theoretical consideration

As a start a brief overview is given of concepts dealing with flow perpendicular to a layered porous medium.

Fluid flow perpendicular to layered porous media (Bear, 1972)

In this particular case the discharge, Q (m^3/s) remains constant, whereas the total hydraulic head ΔH and the total length L are the sum of the individual ΔH_i and L_i, respectively. According to Darcy's law:

$$Q = K \cdot A \cdot \frac{\Delta H}{L} \quad \Rightarrow \quad \Delta H = \frac{Q}{A} \cdot \frac{L}{K} \tag{1}$$

Here, K is the bulk hydraulic conductivity (m/s) and A is the cross sectional area (m^2). For an assemblage of layers;

$$Q = K_i \cdot A \cdot \frac{\Delta H_i}{L_i} \quad \Rightarrow \quad \Delta H_i = \frac{Q}{A} \cdot \frac{L_i}{K_i} \qquad i=1, 2, 3 \ldots\ldots N \tag{2}$$

Substituting Eq. 1 and Eq. 2 in $\Delta H = \sum_{i=1}^{N} \Delta H_i$ gives;

$$\frac{L}{K} = \sum_{i=1}^{N} \frac{L_i}{K_i} \tag{3}$$

Our hydraulic conductivity measurements are based on Equation 1 and represent the bulk hydraulic conductivity. We know that this bulk system consists of a layer of jarosite, a layer of fly ash, and the variable interface layer. Equation 3 clearly indicates that if we want to know how much the hydraulic conductivity of the interface precipitation layer contributes to the bulk hydraulic conductivity, it is required to have the corresponding data dealing with the variable thickness of such layer, which are experimentally difficult to obtain. Plus, K_i and L_i are both extensive variables , i.e., the values of these two parameters depend on the amount of matter being used, adding another difficulty to describing fluid flow by using hydraulic conductivity or permeability. These difficulties can be circumvented by considering the analogy between fluid flow in a porous medium and flow of electrical current. Their similarity is that the transport of a given physical quantity (mass, electrons), occurs as a response to spatial differences in the concentration of that quantity.

The resistance to transfer of matter in layered porous media

We know for any transport process (e.g. Poirier, 1991):

$$rate\ of\ \ transport\ \ process(v) = \frac{driving\ \ force}{resistance}$$

Returning to Darcy's law, $Q = K \cdot A \cdot \frac{\Delta H}{L}$,

we have , $v = \frac{Q}{A} = K \cdot \frac{\Delta H}{L} = \frac{\Delta H(driving\ \ force)}{(L/K)(resistance)}$

substituting in Equation 3, the resistance R (s) to flow perpendicular to layered porous media can be written as:

$$R = \frac{L}{K} = \sum_{i=1}^{N} \frac{L_i}{K_i} = \sum_{i=1}^{N} R_i \qquad \text{where, } R_i = L_i/K_i \tag{4}$$

Equation 4 is identical to the law of electrical resistance in series. In this way, we are able to determine the flow by using the resistances of the layers. If we keep the driving force, ΔH, constant in a flow system, a decrease in velocity will occur with increasing resistance according to the relation $v_0R_0=\Delta H=vR$, where the o subscript indicates the initial condition.

3.2.3 Method and materials

Method

Hydraulic conductivity measurements were carried out in a triaxial cell (∅ 50 mm, L 140 mm) under controlled three-dimensional stress conditions (flexible wall) to prevent leakage as well as flow along the wall. One half part of the cell was compacted with 70 mm jarosite with a dry weight of 293 g, the other part with 70 mm fly ash with a dry weight of 234 g. The fly ash was placed on top of the jarosite, the fluid flow direction was from the bottom upwards. Before starting measurements, the cell was saturated with distilled water. During the measurement, the fluid flowing through the cell was also distilled water.

Materials

Jarosite used in this study is a waste product from a zinc manufacturing plant and is produced during the removal of ferric ions from acidic, sulphate-rich solution. The alkaline fly ash used in this study is the residue from a coal burning power plant. Table 3.2.1 lists the major physical and chemical characteristics of jarosite and fly ash.

Table 3.2.1 Physical and chemical characteristics of jarosite and alkaline fly ash

	Jarosite	Alkaline Coal Fly Ash
Composition	$[M]Fe_3(SO_4)_2(OH)_6$ $[M=Na^+, K^+, NH_4^-$, and $Pb^{2+}]$	Amorphous Phase Quartz(SiO_2) Mullite($Al_6Si_2O_{13}$) Hematite(Fe_2O_3)
Particle Size (mm)	5.2	20.1
Dry Density (kg/m^3)	2.9	2.0
Bulk Density (kg/m^3)	2.2	1.2
Natural pH*	1.7	12.0
Principal Leachates	S, Fe, Pb, Zn, Ca, As, Mg	Ca, K, Na, S

**** Determined at a Liquid/Solid ratio of 10***

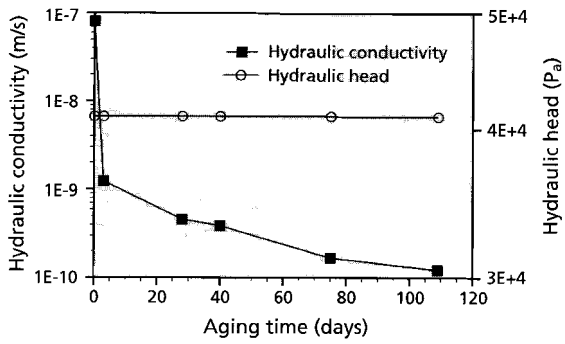

Figure 1. Hydraulic conductivity development in layered jarosite/fly ash

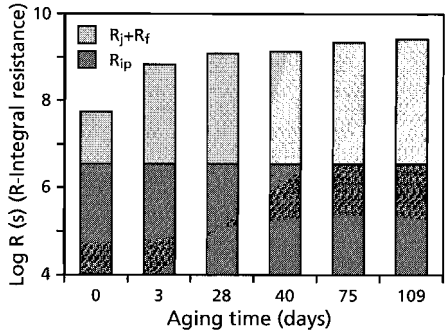

Figure 2. Resistances and their evolution in layered jarosite/fly ash.

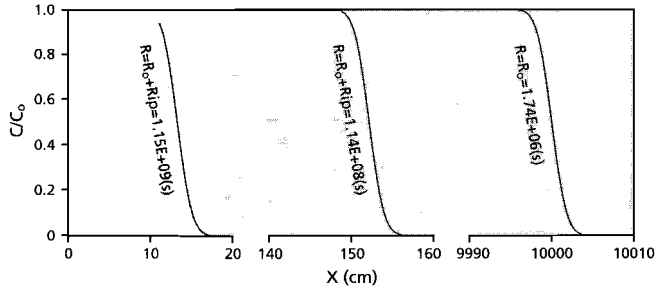

Figure 3. Concentration profile in a hypothetical column of layered jarosite/fly ash at various resistances. The formula used to construct this figure is $C/C_o = (1/2) \cdot \{1+\text{erf}[(x-v \cdot t)/2 \cdot (D \cdot t)1/2]\} + (1/2)\text{erfc}[(x-v \cdot t)/2 \cdot (D \cdot t)1/2]$, with the conditions $V_0 = 10^{-4}$ m/s, $t = 10^6$ s, $D = 10^{-10}$ m^2/s, and the relation $V = V_0 \cdot (R_0/R)$

3.2.4 Results

Figure 3.2.1 presents the variation in hydraulic conductivity as a function of time and hydraulic head needed to maintain a flow through the system. As can be seen, the hydraulic conductivity decreases rapidly in the first three days from about 10^{-7} m/s to 10^{-9} m/s, i.e. almost two orders of magnitude, followed by a slower decrease in the next three months, suggesting a rapid rate of chemical reaction between acidic jarosite and alkaline fly ash soon after placing jarosite and fly ash adjacent to one another. The applied hydraulic head was kept constant for each measurement as indicated in Figure 3.2.1.

3.2.5 Discussion

Relation between the overall resistance and resistances of the individual layers in jarosite/fly ash

To apply Equation 4 to our particular case, it has to be realized that there are initially two layers in the system. One is jarosite with an initial porosity of about 0.28, another
fly ash with an initial porosity of about 0.15. The formation of the interface layer will occur as soon as these two materials are placed in contact with one another. In terms of the law of electrical resistance in series, this additivity can be described as:

$$R=R_j + R_{ip} + R_f \qquad (5)$$

the subscripts j, ip, and f indicate jarosite, interface layer, and fly ash, respectively. Clearly the initial R_{ip} equals zero. Thus,

$$R_0 = R_j + R_f \qquad (6)$$

Our radio tracer diffusion experiments (Ding, 1996) show that the porosity change in either jarosite or fly ash is negligible. The precipitation zone resides solely at the interface between jarosite and fly ash, causing there a time dependent porosity decrease, as confirmed by our microscopic investigation of epoxy impregnated transverse thin sections across the interface. Consequently, the change in measured bulk hydraulic conductivity with time is due to the development of an interface layer. In other words, R_j and R_f remain almost constant during measurement, whereas $\Delta R = R_{ip}(t)$, the change in R can be attributed primarily to the resistance developed over the interface layer. We are therefore able to determine precisely how interface precipitation affects the resistance to transport in jarosite/fly ash.

Interface precipitation affects the resistance to transport in layered jarosite/fly ash

The time evolution of resistance to transport in layered jarosite/fly ash is shown in Figure 3.2.2. Inspection of Figure 3.2.2 clearly indicates that the overall resistance increases with time and is due to the increase in resistance of the interface layer. Initially (time = 0), the resistance due to the interface layer is zero followed by a rapid increase in resistance within the first few days, slowing down in the subsequent period. Figure 2 also shows that in comparison with the combined constant resistance of jarosite and fly ash, the resistance of the interface layer is much larger by about two to three orders of magnitude. This result points to the essential role played by the resistance of the interface layer in characterizing fluid flow in the overall system.

In order to reveal the consequence of a change in resistance to material transport in general, we have simulated the flow of an inert component through a hypothetical column (Freeze and Cherry, 1979) of layered jarosite/fly ash while varying its resistance. We assumed a flow with constant hydraulic head, a continuous supply of an inert component with a concentration C_o, and a constant effective diffusion coefficient. Note that the effective diffusion coefficient in reality decreases with time, which should result in a flatting of the concentration profiles. The results of our simulation are shown in Figure 3.2.3 as the spatial evolution of the concentration profiles of an inert component as a function of resistance. Our results suggest that in the absence of a chemical reaction between jarosite and fly ash, i.e. when the resistance of the system will be R_o, the front of the inert component will move roughly 100 meters for a specific time. However interface precipitation increases the total resistance of the system. As a consequence, the front of the inert component moves roughly 1.5 meters in the same time, a factor about sixty times less. It should be noted that these results are indistinguishable from those of transport of absorbable constituents in porous media, where commonly a retardation factor is used to describe the effect of interaction between a chemical constituent and the medium on material transport.

3.2.6 Conclusion

Interface precipitation in layered jarosite/fly ash not only decreases the bulk diffusivity of the system but also creates a resistance to flow. This increase in bulk resistance is mainly due to an increase in resistance of the interface layer in such system. Rather than using hydraulic conductivity or permeability to determine these chemical effects on transport of flow, the concept of resistance is used in the layered jarosite/fly ash system to emphasize the analogy with the more familiar laws of electrodynamics. Using resistance makes it possible to describe flow of matter through a layered porous medium in terms of flow of electrons.

Acknowledgement

I would like to thank the Faculty of Earth Sciences at Utrecht University for providing an 'AIO' fellowship making it possible to carry out my Ph.D. research. I am grateful to Professor Dr. R.D. Schuiling for pointing out the jarosite/fly ash environmental problem and for supporting this research. Dr. H.J.S. Dorren showed me how to think about flow through porous media in terms of the laws of electrodynamics. Professor Dr. B.H.W.S.de Jong read the manuscript critically and improved its language.

Interface reaction affects Fe^{3+} mobility in jarosite and alkaline coal fly ash

Abstract

To investigate the effects of interface precipitation on the mobility of constituents in layered acidic jarosite and alkaline fly ash systems, small diffusion tube (Ø 8 mm, L50mm) experiments have been carried out using $^{59}Fe^{3+}$ as a radiotracer. Our principal result indicates that $^{59}Fe^{3+}$ accumulates at the interface of jarosite and fly ash due to the coupling of diffusion and precipitation. Diffusion of $^{59}Fe^{3+}$ is caused by the concentration gradient between jarosite and alkaline fly ash, whereas precipitation of ferric hydroxide is due to the exceedingly low solubility of Fe^{3+} at the interface where the pH changes markedly. Based on our $^{59}Fe^{3+}$ results the behavior of aluminium, zinc, and lead in jarosite and alkaline fly ash can be predicted.

3.3.1 Introduction

It is well known that chemical reactions such as oxidation-reduction, ion-exchange, adsorption, dissolution, and precipitation may take place in porous media, particularly at the interface of those media where large variations in chemical characteristics occur. In recent years, such reactions at the waste-soil interface have received attention due to their effects on the mobility of environmentally harmful constituents. A novel concept was introduced by van der Sloot *et al.*, (1993a) who developed " self-forming and self-repairing seals " as a means of waste isolation. Processing such self-forming and self-repairing seals requires first of all knowledge about the diffusion of chemical components. Moreover an assessment of possible precipitation reactions among these reacting components is needed together with the extent to which precipitates fill soil pores at the waste-soil interface. Damage to such seals will self-repair by additional diffusion and precipitation.

Additional research on systematic modelling and experimental study of waste-soil was carried out by Hockley *et al.*, (1992) These authors started with classifying categories of waste-soil interfaces. Together with each of their categories, a mathematical model was constructed concomitant with experimental verification. Their results clearly indicated that the migration of components from both waste and soil was strongly influenced by the type of interface reaction between the waste and its surroundings.
The results of this pioneering research inspired us to start an inquiry into the problem

of co-disposal of two chemically different wastes. In particular, we surmised that there could be a potential benefit for the environmental problems of acidic jarosite and alkaline coal fly ash. The anticipated result was that the precipitation reaction at the interface of jarosite and alkaline fly ash would change the transport properties of the bulk system and the mobility of its constituents. Chemical analyses of the effluent in preliminary flow through column experiments (Ding 1994) did indeed show a decrease in their mobility presumably due to a coupling between transport and chemical reaction. In order to describe this coupling in detail, a radiotracer ,$^{59}Fe^{3+}$ as representative of the behavior of one of the principal constituents, Fe^{3+}, in the jarosite-flyash system was selected.

The purpose of the study is twofold: the first one is to investigate the effect of interface precipitation on the Fe^{3+} mobility in the layered jarosite/alkaline fly ash system under the condition of zero fluid flow; the second one to make use of the Fe^{3+} results to extrapolate its behavior to other constituents in jarosite and alkaline fly ash.

In this paper, we present a study on Fe^{3+} mobility in jarosite only and in the layered jarosite/alkaline fly ash systems using results of $^{59}Fe^{3+}$ tracer experiments carried out in small (Ø 8mm, L 50 mm) diffusion tubes. Subsequently, these data are interpreted phenomenologically in combination with the thermodynamics of ferric hydrolysis. Finally, extension of these results to aluminium, zinc, and lead mobility in the jarosite/fly ash system will be discussed.

The principal result is that two processes characterize Fe^{3+} mobility in jarosite/alkaline fly ash. The first process is diffusion caused by the Fe^{3+} concentration gradient between jarosite and alkaline fly ash; the second is the precipitation of ferric hydroxide caused by the exceedingly low solubility of Fe^{3+} at the interface where a marked change in pH occurs. This pH change results in a reduced mobility of Fe^{3+} in jarosite/alkaline fly ash interface. Interface precipitation in the jarosite/fly ash system causes not only a reduction in Fe^{3+} mobility but also of other constituents, such as Al^{3+}, Zn^{2+}, and Pb^{2+}. Extension of our calculational results to Fe-free systems predicts that immobilization of aluminium and zinc at the jarosite/fly ash interface will occur at a pH range between 7.5 and 8.0, penetrate into the fly ash segment, whereas that of lead will occur at a pH of about 5 at the interface slanted towards the fly ash side. With this argument we can predict whether immobilization of constituents including contaminants from wastes occurs due to chemical reactions at the interface.

3.3.2 Materials and methods

Materials

Jarosite and Alkaline Fly Ash:

Jarosite is one of the most important members of a large group of isostructural minerals. The general formula of this group (Stoffregen 1993) is $MA_3(BO_4)_2(OH)_6$, where M is a monovalent or divalent cation such as Na^+, K^+, NH_4^-, or Pb^{2+}, A stands for iron or aluminium, and B for sulphur, phosphorous, or arsenic. The jarosite used in this study comes from a zinc manufacturing plant and is the result of removing Fe from acidic, sulphate-rich solutions (Elgersma 1992). The alkaline fly ash used in this study is the residue from a power plant. It consists mainly of an amorphous phase, with small amounts of quartz (SiO_2), mullite ($Al_6Si_2O_{13}$), and magnetite (Fe_3O_4). The physical and chemical characteristics of jarosite and alkaline fly ash are summarized in Table 3.3.1.

Table 3.3.1 Physical and chemical characteristics of jarosite and alkaline fly ash

	Jarosite	Alkaline Coal Fly Ash
Composition	$[M]Fe_3(SO_4)_2(OH)_6$ [M=Na^+, K^+, NH_4^-, and Pb^{2+}]	Amorphous Phase, Quartz(SiO_2), Mullite($Al_6Si_2O_{13}$), Magnetite(Fe_3O_4)
Particle Size (μm)	5.2	20.1
Dry Density (kg/m³)	2.9	2.0
Bulk Density (kg/m³)	2.2	1.2
Natural pH*	1.7	12.0
Major Leachate	S, Fe, Pb, Zn, Ca, As, Mg	Ca, K, Na, S

* *Liquid/Solid*: 10

^{59}Fe Tracer:

In Table 3.3.2 the characteristics of the $^{59}Fe^{3+}$ radiotracer used in this study are.presented.

Table 3.3.2 ^{59}Fe tracer

Nuclide	Chemical Form	Concentration (μg/ml)	Initial Activity (counts/min•ml)	Half-life-life ($T_{1/2}$)
^{59}Fe	Fe^{3+}	9.21	$2.33*10^7$	45.1 days

Methods

Diffusion tube measurement:

Figure 3.3.1 (van der Sloot *et al.*, 1991) shows a schematic of the diffusion tube measurements. In these small diffusion tubes (Ø 8 mm, L 50 mm), either one material (jarosite or fly ash) or a combination of two materials (jarosite with fly ash) were compacted. One half-space contained the material to be labelled with radiotracer, the other half-space contained the tracer-free material. Both ends of the tube were closed by pistons. These diffusion tubes remained stored in a constant moisture atmosphere at room temperature. After one day exposure, both the labelled and unlabelled segments were sliced and counted with L 1282 Compugamma Universal Gamma Counter.

Preparation and slicing of diffusion tube contents:

Thirty grams of jarosite and fly ash were mixed with 12 ml and 9 ml distilled water respectively, to form a non-labelled paste. Meanwhile, another 30 grams of jarosite and fly ash were mixed with 12 ml and 9 ml diluted tracer solution respectively, to form the labelled paste. Half of the tube is filled with the non-labelled paste, the remaining half with the labelled paste as shown in Figure 3.3.2 (van der Sloot *et al.*, 1991). The amount of solution used to mix with solid proved experimentally to be the best scheme to avoid any liquid spilling from the tubes. The degree of dilution was chosen such that 10^{-2} % of the originally added activity level (counts/min.g) could be detected in each sliced sample. The tube was sliced into about 40 slices over a total length of 50 mm.

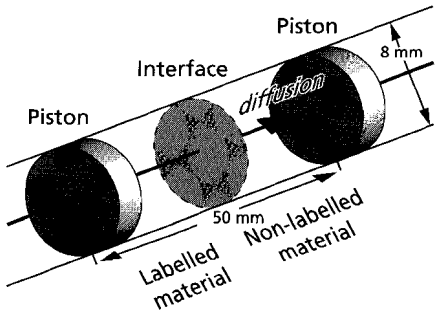

Fig. 3.3.1 Schematic view of diffusion tube measurements.

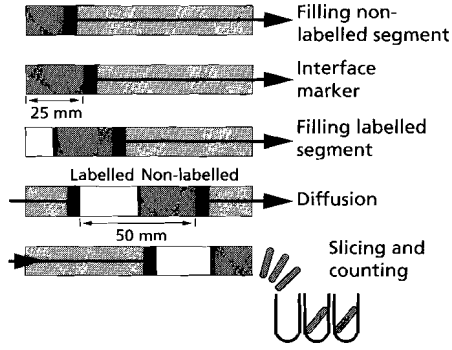

Fig. 3.3.2 Preparation and slicing of diffusion tube contents

pH Gradient Measurement:

pH tube measurements were designed to track the pH gradient change during transport and chemical reaction in the layered jarosite/fly ash system. The preparation and slicing of the pH tube content is exactly the same as that for the diffusion tube experiment except that no tracer was added in either of the segments.

3.3.3 Results

$^{59}Fe^{3+}$ Diffusion in Jarosite

Figure 3.3.3 shows the $^{59}Fe^{3+}$ diffusion profile in jarosite after 1 day. Inspection of Figure 3 indicates that $^{59}Fe^{3+}$ diffusion in jarosite coincides with the standard diffusion pattern expected of two half-spaces with uniform initial concentration. Its measured diffusion coefficient is $10^{-10.56}$ m^2/s (Ding 1996). Consequently, we can infer that given time and in the absence of a chemical reaction between $^{59}Fe^{3+}$ and jarosite, a horizontal diffusion profile will result passing through the point at half the initial specific activity due to the complete mobility of $^{59}Fe^{3+}$ in acidic jarosite which has a constant pH of 1.7.

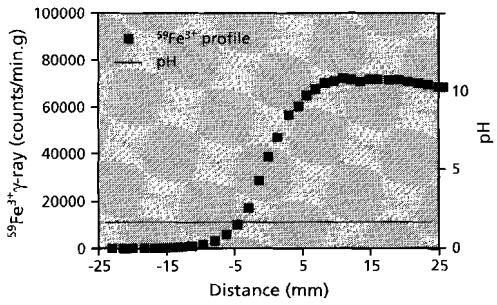

Fig. 3.3.3 $^{59}Fe^{3+}$ profile in jarosite.

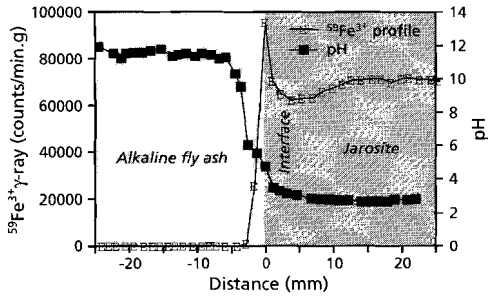

Fig. 3.3.4 $^{59}Fe^{3+}$ profile in jarosite/alkalinefly ash.

$^{59}Fe^{3+}$ Diffusion in layered jarosite/alkaline fly ash

The principal result after 1 day, illustrated in Figure 3.3.4, shows that the $^{59}Fe^{3+}$ tracer accumulates at the interface of jarosite/alkaline fly ash as indicated by the sharp peak. An additional point of interest is that the measured $^{59}Fe^{3+}$ radiotracer profile starts to decline about halfway along the total length of labelled jarosite followed by a rapid rise, as mentioned before, resulting in the sharp peak. Note that Figure 3.3.4 also shows the marked pH switch at the interface. These results suggest that two processes characterise Fe^{3+} behavior in the layered jarosite/fly ash system. One is the diffusion of $^{59}Fe^{3+}$

caused by its concentration gradient between jarosite and fly ash, the other is the brown coloured precipitation of amorphrous ferric hydroxide caused by the exceedingly low solubility of Fe^{3+} at the interface.

3.3.4 Discussion

The relation between solubility, mobility, and immobility

The general equilibrium equation of cation (M) hydrolysis and hydroxide compound formation in water can be expressed as:

$$M(OH)n \leftrightarrow M^{n+} + nOH^- \qquad K = [M^{n+}]\cdot[OH^-]^n$$

where K is the solubility product and n the formal charge on the cation (M). Thus, the solubility of a cation is given by:

$$[M^{n+}] = \frac{K}{[OH^-]^n}$$

The mobility of cations as defined in this study is a parameter which is normalised with respect to a Fe^{3+} reference solubility of 10^{-6} mol/L. The relation between mobility and immobility is defined as:

$$\text{mobility}_{(M)} + \text{immobility}_{(M)} = 1$$

In this way, the solubility , mobility and immobility of a cation (M) as a function of pH can be calculated. In our particular case, the focus was on iron (Fe^{3+}), aluminium (Al^{3+}), zinc (Zn^{2+}), and lead (Pb^{2+}) because they constitute the principal components in leachates from both jarosite and alkaline fly ash. Especially, Fe^{3+}, a major constituent according to our $^{59}Fe^{3+}$ tracer diffusion test, is one of the principal reacting components participating in the precipitation reaction at the jarosite/alkaline fly ash interface. The solubility products used in the calculation are listed in Table 3.3.3.

Table 3.3.3 Solubility product of iron, aluminium, zinc, and lead hydroxide (Handbook of chemistry and physics 1980-1981)

	$Fe(OH)_3$	$Al(OH)_3$	$Zn(OH)_2$	$Pb(OH)_2$
logK	-38.58	-24.57	-16.16	-19.85

Figure 3.3.5 presents the relation of Fe^{3+} solubility and immobility as a function of pH and Figure 3.3.6 reveals the immobility of Al^{3+}, Zn^{2+}, and Pb^{2+} as a function of pH. Inspection of Figure 3.3.5 indicates that at about a pH of 4 all Fe^{3+} becomes immobile.

This is caused by the rapid logarithmic decrease in solubility of Fe^{3+} at pH values above 4 (Baes and Mesmer 1976). Inspection of Figure 3.3.6 shows that Al^{3+}, Zn^{2+} and Pb^{2+} cations become immobile at approximate pH values of 8, 7, and 5, respectively.

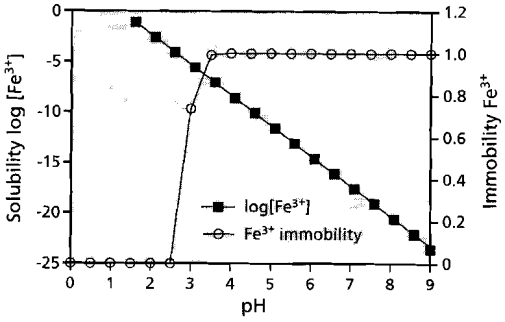

Fig. 3.3.5 Fe^{3+} solubility and immobility as a function of pH.

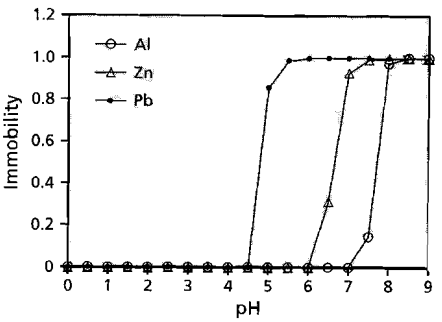

Fig. 3.3.6 Al^{3+}, Zn^{2+}, and Pb^{2+} immobility as a function of pH.

Effect of Interface Precipitation on Fe^{3+} Mobility in Jarosite/Alkaline Fly Ash

The observed $^{59}Fe^{3+}$ profile (Figure 3.3.4) reflects the coupled effects of diffusion and precipitation, as mentioned previously. In other words, the observed $^{59}Fe^{3+}$ diffusion is the sum of mobile and immobile ferric cations. The mobile $^{59}Fe^{3+}$ profile is based on knowledge about diffusion as well as the thermodynamics of ferric hydrolysis. As indicated in Figure 3.3.5, at the interface (pH about 5) $^{59}Fe^{3+}$ will completely be transferred to the insoluble state. In other words, the mobile $^{59}Fe^{3+}$ concentration at this point will be zero. Additionally, diffusion occurs only when a concentration gradient exists, which implies that the lowest point of the observed $^{59}Fe^{3+}$ profile is still due to mobile $^{59}Fe^{3+}$. Once the concentration starts increasing, precipitation of ferric hydroxide occurs. Linking these two points, the one at the interface with the other at the lowest point of measured $^{59}Fe^{3+}$ concentration, results in the mobile $^{59}Fe^{3+}$ profile. Next, the profile of immobile $^{59}Fe^{3+}$ can be calculated by subtracting the mobile $^{59}Fe^{3+}$ from the measured profile at each pH which itself has been parametrized with distance. Figure 3.3.7 shows the distribution of $^{59}Fe^{3+}$ in jarosite/fly ash system between fluid and solid. Note that the observed profile is the sum of the $^{59}Fe^{3+}$ concentration in solid together with fluid.

The most important result, illustrated in Figure 3.3.8, indicates that the mobility of Fe^{3+} in the jarosite/fly ash system decreases relative to that observed for Fe^{3+} in jarosite. This is due to ferric hydroxide precipitation at the jarosite/fly ash interface leading to a substantial amount of immobile Fe^{3+} after only 1 day.

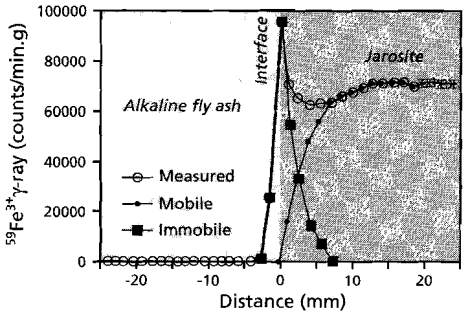

Fig. 3.3.7 $^{59}Fe^{3+}$ accumulation at the interface due to coupling of diffusion and precipitation.

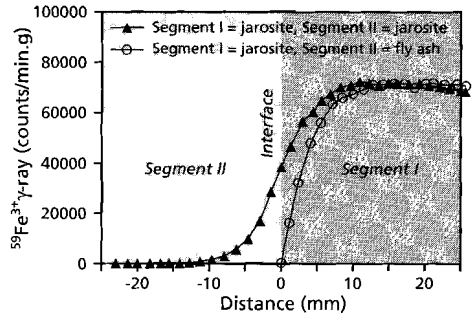

Fig. 3.3.8 The effect of interface reaction on Fe^{3+} mobility.

Aluminium and lead containing system

Generalization of these Fe^{3+} results leads to predictions concerning the immobilization of Al^{3+} and Pb^{2+} in jarosite/alkaline fly ash. It is our claim that just as for Fe^{3+}, the change in mobility of Al^{3+} and Pb^{2+} due to interface precipitation reactions can be estimated. Figure 3.3.9 presents the calculated results for Al^{3+} and Pb^{2+} immobility in jarosite/alkaline fly ash. This figure predicts that aluminium accumulates at a pH of about 8 and that the accumulation zone penetrates into the fly ash part; that lead accumulates at a pH of 5 close to the interface still at the fly ash side; whereas Fe^{3+} accumulates at a pH of around 4 right at the interface as is confirmed by our experimental results. These results demonstrate that with the aid of cation mobility and immobility as defined in this paper, the distribution of constituents can be predicted in layered systems varying in acid-base as well as redox characteristics. Note that the predicted behavior of Al^{3+} and Pb^{2+} depends purely on their thermodynamic properties assuming that there is no effect of diffusion. Therefore, the calculated results of Al^{3+} and Pb^{2+} immobility can only qualitatively describe the spatial effect of immobilization but not the actual profiles.

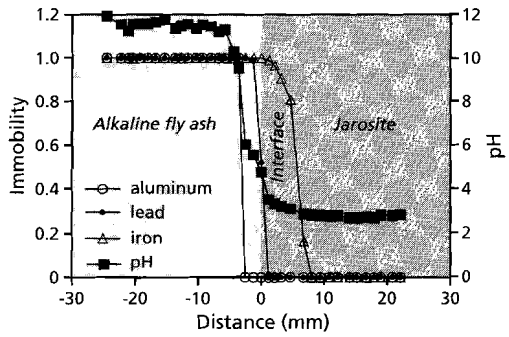

Fig. 3.3.9 Prediction Al^{3+} and Pb^{2+} immobility in jarosite/alkaline fly ash

3.3.5 Conclusion

Consideration of interface chemical reactions in porous media is crucial in describing transport properties of their chemical constituents. The reduction of Fe^{3+} mobility in jarosite/alkaline fly ash relative to that of Fe^{3+} in jarosite is due to ferric hydroxide precipitation. This precipitation is caused by the exceedingly low solubility of Fe^{3+} at the interface of jarosite/fly ash in the presence of a marked pH change. Interface precipitation in the jarosite/fly ash system not only reduces Fe^{3+} mobility but also that of other constituents, such as Al^{3+}, Zn^{2+}, and Pb^{2+}. The calculational results for Fe-free systems predict that immobilization of aluminium will occur at the jarosite/fly ash interface at a pH of about 8 and that the maximum aluminium concentration zone will penetrate into the fly ash segment, whereas that of lead will occur at a pH of 5 approximately at the interface slanted towards the fly ash side. Following this argument, we can predict whether immobilization of constituents including contaminants from wastes occurs due to chemical reactions at the interface.

Acknowledgements

Work was carried out at the Soil and Waste Research Laboratory, Netherlands Energy Research Foundation (ECN), Petten. Financial, and scientific, support of Professor Dr R.D.Schuiling, and a travel grant from the Dutch Organization for Scientific Research(NWO) are gratefully acknowledged.

Chapter 4

Discontinuities in porous media affect the transport and mobility of chemical constituents

4.1 Introduction

The systematic study of the relation between mathematical formulation and the chemical nature of reactions as applied to the transport of reacting solutes in porous media has been initiated by Rubin in the early eighties (Rubin, 1983). The ongoing concern about the fate of pollutants in the environment has added to the pertinence of this subject as attested to by the increasing number of publications especially directed towards modeling of reactive transport in porous media (Mangold and Tsang, 1991; Lichtner *et al.*, 1996; Schnoor, 1996). The common strategy to tackle such problems involves taking existing theories and models which are used in analyzing transport of reacting solutes in a single matrix and account for the influence of chemical reactions by adding or appropriately modifying the transport equation for non-reacting solutes.

However, most of these models do not suffice when transport in more than one matrix is considered. Here physical and chemical discontinuities across the interface between the matrixes often occur. Such "jump conditions" (Hassanizadeh and Gray, 1989a, 1989b) will impact profoundly the overall transport and speciation of chemical components. From a theoretical point of view the existence of such jumps requires a more detailed specification of boundary conditions in the mathematical description of a transport problem. It is known from experiments (Ding 1996; Ding *et al.*, 1996) that concentration profiles of chemical components in such system will differ from those in either of the matrices taken separately. Especially, when reactions occur at the interface between chemically contrasting media, a reaction zone may form differing significantly in transport and thermodynamic properties from both parent media (Ding *et al.*, 1997, 1998).

Several phenomena observed in natural processes clearly show the consequence of reactive transport in layered materials when physical or chemical gradients occur at an interface. As examples might be mentioned the formation of a reaction zone in aquatic sediments (van Cappellen and Gaillard, 1996), iron pans in soil (Crampton, 1963; Conry *et al.*, 1996), natural seal formation caused by anthropogenic activities such as stabilized coal fly ash in the ocean (Hockley and van der Sloot, 1991) or self-sealing layers formed

in waste sulfuric acid lake of a TiO_2-plant at Armyansk, Crimea (Schuiling and van Gaans, 1997; van Gaans and Schuiling, 1997), as well as research combining modelling with laboratory studies of waste/soil and waste/waste interface (van der Sloot and Côté, 1989; van der Sloot, 1993; Hockley and van der Sloot, 1991b, 1993; Hockley *et al.*, 1992). The results of these last pioneering studies showed that the release of contaminants from a waste depends not only on the properties of the waste itself but also on the characteristics of the interface between the waste and its surrounding. The above examples clearly indicate that discontinuities in porous media are common in natural or man made environments and that they may have a significant effect on the transport and mobility of chemical constituents.

It is for this reason crucial to consider why such discontinuities occur in porous media and the extent to which elemental mobility is affected. To reveal its nature hinges largely on subtle spatial and temporal concentration distributions of chemical components especially in the interface region. To grasp the underlying physics and chemistry requires mathematical formulation and model simulation. In addition, it requires a proper experimental technique different from batch or flow through column experiments to track reacting solutes in the processes and to determine experimentally the relevant parameters needed for model verification.

The principal aim of this paper is then to demonstrate mathematically and experimentally how the transport and mobility of chemical constituents is affected by chemical and physical discontinuities in porous media. We shall emphasize in particular systems where a self-forming zone is generated due to precipitation at the interface of layered materials. Secondly we shall state the laboratory method required to accomplish the above mentioned aims. Finally, as an application of our model, we shall predict a case of practical interest in waste management: sealing layer formation in the acidic jarosite/alkaline coal fly ash system. Such sealing layer is caused by chemical discontinuities between jarosite and fly ash.

To accomplish these goals, we shall start by stating the general mathematical formulation of reactive transport in porous media and establish analytical and numerical solutions taking into account discontinuities across the boundary between the media. The numerical method we have adopted is the classical implicit fourth-order Runge-Kutta method (Albarède, 1995; Press *et al.*, 1987). I have developed two programs. One is designated DNLM*, which stands for **D**iffusion **N**eutralization in **L**ayered **M**aterials. The second one is designated DPLM*, which stands for **D**iffusion **P**recipitation in **L**ayered **M**aterials. Next, we shall simulate several cases, where chemical reactions such as acid-base, adsorption and precipitation occur at the interface between the media. We have selected acidic jarosite $NH_4Fe_3(SO_4)_2(OH)_6$ and alkaline fly ash as our two canonical materials and conducted radio tracers $^3H^+$, $^{22}Na^+$, $^{59}Fe^{3+}$, $^{45}Ca^{2+}$, and $^{35}SO_4^{2-}$ diffusion tube experiments (Das *et al.*, 1989; Das, 1992; 1994; van der Sloot *et al.*, 1991) on each separately as well as combined. The diffusion experiments with inert tracers

* *Information about the programs is available from M. Ding, E-mail: ding@geo.uu.nl.*

$^{3}H^{+}$ and $^{22}Na^{+}$ for each matrix are needed to obtain their tortuosities required as input physical parameters for our model. Based on those parameters, diffusivities of principal reacting components in jarosite (Fe^{3+}, $SO4^{2-}$) and coal fly ash (Ca^{2+}) can be derived (Paterson, 1995; Schaefer *et al.*, 1995). Model verification is done by comparing our modelled results of $^{59}Fe^{3+}$ in the layered jarosite/fly ash system with the measured ones. Finally, we shall predict the transport and reaction characteristics for an hypothetical jarosite/fly ash disposal site.

4.2 Mathematical model

4.2.1. Reactive transport in a single porous medium

The general continuity equation, in one-dimensional form, based on the principle of mass conservation, to describe the reactive transport of constituent i in a porous medium is :

$$\frac{\partial (\theta C^i)}{\partial t} = -q\frac{\partial C^i}{\partial x} + D_e^i \frac{\partial^2 C^i}{\partial x^2} - \sum R^i \qquad (4.1)$$

Where $\partial C^i / \partial t$ is the concentration change of constituent i per unit of time, C^i is the concentration of constituent i in the medium, θ is the porosity of the medium, and q is the velocity of pore fluid. In this paper, we shall use the term D_e as effective diffusion coefficient rather than molecular diffusion coefficient D_o as defined in Fick's first law (Crank 1975), because D_e involves interactions (Cussler 1984; van Cappellen and Gaillard 1996; Nakashima 1995; Schaefer *et al.*, 1995) between ions and mimicks the actual situation better. The relation between these two parameters is given by (Paterson 1995; Schaefer *et al.*, 1995):

$$D_e = (q/T)*D_o \qquad (4.2)$$

where T is the tortuosity of the medium (dimensionless with $T > 1$).

In Eq. 4.1, R^i is the sum of chemical or biological reaction rates involving constituent i. Eq. 4.1 describes the spatial and temporal evolution of constituent i in pore fluid due to advectional and diffusional transport as well as removal due to chemical reaction.

To simplify let us consider a system with zero flow, i.e. q=0 where diffusional transport dominates. In this case Eq. 4.1 reduces to

$$\frac{\partial (\theta C^i)}{\partial t} = D_e^i \frac{\partial^2 C^i}{\partial x^2} - \sum R^i \qquad (4.3)$$

In principle, Eq.4.3 describes the coupled processes of diffusion and reaction of a constituent in a porous medium. Here, R^i is the reaction rate of component i and equals $\rho_{mediium} \frac{\partial SS^i}{\partial t}$, which reflects the removal of component i from pore fluid into solid per unit time or the dissolution of this component from solid into pore fluid per unit time. SS^i is the concentration of component i in the medium, and ρ_{medium} is the bulk medium density.

In the case of no reaction, Eq. 4.3 can be reduced further to:

$$\frac{\partial (\theta C^i)}{\partial t} = D_e^i \frac{\partial^2 C^i}{\partial x^2} \qquad (4.4)$$

Thus, Eq. 4.4 reflects diffusion of an inert species in a porous medium, with as analytical solution under proper initial and boundary conditions (Albarède 1995a; Appelo and Postma 1993; Freeze and Cherry 1979):

$$C^i = \frac{C_0^i}{2} \cdot (1 + erf \frac{|x|}{2\sqrt{D_e^i \cdot t / \theta}}) \qquad 0 \le x \le \frac{1}{2}L, t > 0 \qquad (4.5)$$

$$C^i = \frac{C_0^i}{2} erfc \frac{x}{2\sqrt{D_e^i \cdot t / \theta}} \qquad \frac{1}{2} \le x \le L, t > 0 \qquad (4.6)$$

with as initial conditions:

$$C^i_{(x,t=0)} = 0 \qquad 0 \le x \le \frac{1}{2}L$$

$$C^i_{(x,t=0)} = C_0^i \qquad \frac{1}{2} \le x \le L$$

and as boundary conditions:

$$\frac{\partial C^i}{\partial x}\Big|_{x=0} = 0 \qquad \frac{\partial C^i}{\partial x}\Big|_{x=L} = 0$$

Where L is the transport distance.

4.2.2 Reactive transport in layered materials

Assume two materials in contact with each other at x = o. One half space -L< x < o has the initial concentration $C_{(x,\ t=o)} = C_o$ ($C_o > o$); the other half-space L > x > o, $C_{(x,t=o)} = o$. Each of the two half spaces has a constant and specific porosity and diffusivity. Assuming that in each half-space the diffusion reaction equation is valid, we have a set of formulas consisting of two diffusion equations:

$$\theta_1 \frac{\partial C_1^i}{\partial t} = D_{e1}^i \cdot \frac{\partial^2 C_1^i}{\partial x^2} - \sum R_1^i \qquad (4.7)$$

$$\theta_2 \frac{\partial C_2^i}{\partial t} = D_{e2}^i \cdot \frac{\partial^2 C_2^i}{\partial x^2} - \sum R_2^i \qquad (4.8)$$

Subscript 1 denotes the region x < o. Obviously, the model used to describe the characteristic transport of a reacting solute in a system of layered materials requires additional boundary conditions at the interface. Physically the following boundary conditions are necessary (Crank 1975) :

$$C_1^i\big|_{x=0} = C_2^i\big|_{x=0} \qquad \frac{D_{e1}^i}{\theta_1} \cdot \frac{\partial C_1^i}{\partial x}\Big|_{x=0} = \frac{D_{e2}^i}{\theta_2} \cdot \frac{\partial C_2^i}{\partial x}\Big|_{x=0} \qquad (4.9)$$

Chemically the situation is variable depending on the chemical nature of the interface. These interfacial characteristics are crucial in the study of discontinuities in porous media and need to be adressed in detail.

4.2.3 Discontinuities in porous media caused by physical gradient

The physical properties of a medium include its porosity, tortuosity, diffusivity, and water content. The discontinuities in porous media caused by physical contrast display an abrupt change in these parameters between the two media. The mathematical description of the transport problem in this case will be:

$$\theta_1 \frac{\partial C_1^i}{\partial t} = D_{e1}^i \cdot \frac{\partial^2 C_1^i}{\partial x^2} \qquad (4.10)$$

$$\theta_2 \frac{\partial C_2^i}{\partial t} = D_{e2}^i \cdot \frac{\partial^2 C_2^i}{\partial x^2} \qquad (4.11)$$

Analytical solutions of Eq. 4.10 and Eq. 4.11 are available and given by (Crank 1975):

$$C_1^i = \frac{C_0^i}{1+\sqrt{D_{e2}^i \cdot \theta_1 / D_{e1}^i \cdot \theta_2}} \cdot (1+\sqrt{D_{e2}^i \cdot \theta_1 / D_{e1}^i \cdot \theta_2} \cdot erf \frac{|x|}{2\sqrt{D_{e1}^i \cdot t / \theta_1}}) \quad x<0 \tag{4.12}$$

$$C_2^i = \frac{C_0^i}{1+\sqrt{D_{e2}^i \cdot \theta_1 / D_{e1}^i \cdot \theta_2}} erfc \frac{x}{2\sqrt{D_{2e}^i \cdot t / \theta_2}} \quad x>0 \tag{4.13}$$

Substituting Eq. 4.2 in Eq. 4.12 and 4.13, gives the following solutions in terms of tortuosity :

$$C_1^i = \frac{C_0^i}{1+\sqrt{T_1 / T_2}} (1+\sqrt{T_1 / T_2} erf (\frac{|x|}{2\sqrt{D_o^i \cdot t / T_1}})) \tag{4.14}$$

$$C_2^i = \frac{C_0^i}{1+\sqrt{T_1 / T_2}} erfc(\frac{x}{2\sqrt{D_o^i \cdot t / T_2}}) \tag{4.15}$$

Clearly, Eq. 4.10 and 4.11 and their solutions can be used to simulate the effect of discontinuities caused by contrasting physical properties such as porosity, tortuosity and diffusivity in porous media.

4.2.4 Discontinuities in porous media caused by chemical gradient

As stated before the nature of chemical reaction of reacting solutes at the interface is essential in describing reactive transport in layered materials. We shall address three typical categories: pH interface, linear reaction interface, and precipitation interface.

pH-interface

Here we give a brief overview of the case involving a pH gradient (Hockley *et al.*, 1992) across the interface between two media. We assume that the effective diffusion coefficients of H^+ and OH^- are constant and equal to one another, and that diffusion occurs in double layered homogeneous porous media. In addition, neither H^+ nor OH^- will participate in any other reaction besides with each other.

Hence, $R = \dfrac{\partial [H_2O]}{\partial t}$

Substituting in Eq. 4.3 results in:

$$\theta_1 \frac{\partial [H^+]}{\partial t} = D_{e1}^H \frac{\partial^2 [H^+]}{\partial x^2} - \frac{\partial [H_2O]}{\partial t} \tag{4.16}$$

$$\theta_1 \frac{\partial [OH^-]}{\partial t} = D_{e1}^{OH} \frac{\partial^2 [OH^-]}{\partial x^2} - \frac{\partial [H_2O]}{\partial t} \tag{4.17}$$

Assuming $D_{e1}^H = D_{e1}^{OH}$ and after operating Eq. 4.16 and 4.17, we have:

$$\frac{\partial \beta_1}{\partial t} = D_1 \frac{\partial^2 \beta_1}{\partial x^2} \tag{4.18}$$

Similarily,

$$\frac{\partial \beta_2}{\partial t} = D_2 \frac{\partial^2 \beta_2}{\partial x^2} \tag{4.19}$$

Where, $D_1 = (D_{e1}^H / \theta_1) = (D_1^{OH} / \theta_1)$ *and* $D_2 = (D_{e2}^H / \theta_2) = (D_{e2}^{OH} / \theta_2)$,

$$\beta_1 = [H^+] - [OH^-] = [H^+] - \frac{K_w}{[H^+]}, \text{ and } \beta_2 = [OH^-] - [H^+] = [OH^-] - \frac{K_w}{[H^+]}$$

K_w is the ionization constant for water, which at 25°C equals 10^{-14}.

Eq. 4.18 and 4.19 resemble in appearance Eq. 4.10 and 4.11, but due to neutralization at the interface, require additional boundary conditions reflecting the chemical nature of the interface. It is for this reason that Eq. 4.18 and 4.19 cannot be solved analytically and that one has to resort to a numerical solution. We developed a FORTRAN (Koffman and Friedman 1997) program DNLM (Diffusion Neutralization in Layered Materials) using the implicit classical fourth-order Runge-Kutta method (Press *et al.*, 1987; Albarède 1995b). The development of β as a function of time and space can be obtained by a numerical solution of the above model. We can simulate the pH profiles in such layered system by solving the relation between β and H^+.

Linear reaction interface

In this case the reaction between solute and medium can be described by the following relation:

$$SS^i = K_d \cdot C^i \tag{4.20}$$

where K_d is a temperature dependent parameter, reflecting the distribution of component i between the solid and aqueous phase.

Thus, $R = \rho_{mediium} \frac{\partial SS^i}{\partial t} = \rho_{medium} \cdot K_d \frac{\partial C^i}{\partial t}$. Substitution in Eq. 4.7 and 4.8 results in the following diffusion equations of component i in two adjacent media: (if θ remains constant)

$$\frac{\partial C_1^i}{\partial t} = \frac{D_{o1}^i}{R_T \cdot T_1} \cdot \frac{\partial^2 C_1^i}{\partial x^2} \tag{4.21A}$$

$$\frac{\partial C_2^i}{\partial t} = \frac{D_{o2}^i}{R_T \cdot T_2} \cdot \frac{\partial^2 C_2^i}{\partial x^2} \tag{4.21B}$$

in which, $R_T = (1 + \frac{\rho_{medium}}{\theta} \cdot K_d)$, commonly defined as the retardation factor, is considered a constant parameter. R_T is the ratio of the total concentration of component i to that in the aqueous phase ($R_T = C_T / C$). As is well-known, the Langmuir adsorption isotherm (Stumm 1992; Langmuir 1997) falls within this category of linear reactions.

Equation 4.21A and 4.21B are identical to the classical diffusion equations Eq. 4.10 and 4.11, except for the constant D_e which is replaced by the constant $D_o/R_T \cdot T$. An analytical solution of two half-spaces with uniform initial concentration is therefore available. It is important to point out that the simulation describes the concentration in the aqueous phase. The total concentration profile can be obtained by converting C into C_T via their relation to R_T.

Precipitation interface

In previous cases, we have assumed that physical properties such as porosity, tortuosity and diffusivity of the media do not change during chemical reaction. However as several studies (Steefel and Lasaga, 1990, 1994; Carnahan 1990) have shown, chemical reac-

tions such as precipitation or/and dissolution influence the local porosity by filling of pores with precipitates. The effect of coupling chemical reactions and fluid flow on 'space-time evolution' is geologically important. Self-forming layer formation in two adjacent materials is observed in nature and laboratory study (Schuiling and van Gaans 1997, Ding *et al.*, 1997, 1998a; Hockley and van der Sloot 1991b; Hockley *et al.*, 1992; Côté and van der Sloot 1989; van der Sloot *et al.*, 1993b, 1997a). It is primarily due to interface precipitation, leading to reduction in permeability of the system, and an increase in resistance to transport with as extreme case the formation of a self-sealing layer. Yet, the current study on modeling of precipitation interface in layered system does not take into account the induced porosity change. For the purpose of waste isolation, one needs to simulate if self-sealing layers can effectively form and how thick such layers will be. It is therefore crucial to take this change in physical property into account.

Referring back to Eq. 4.3, the reaction term can be expressed as:

$$R^i = \rho_{medium} \frac{\partial SS^i}{\partial t} = \frac{M_{medium}}{V_{medium}} \frac{\partial M^i}{M_{medium} \partial t} = \frac{\partial C^i_{medium}}{\partial t} = \frac{\partial M^i}{V_{mediun} \cdot \partial t} \quad (4.22)$$

M^i = (molecular weight of component i) $\star$ (mole number of i)

When a new mineral involving component i is formed, the following equation is valid.

$$mole\ number\ of\ i = \frac{number\ of\ mole\ i}{1\ mole\ of\ mineral} * mole\ number\ of\ mineral \quad (4.23)$$

By definition:

$$M^i = W^i_m * \frac{number\ of\ mole\ i}{1\ mole\ of\ mineral} * \frac{mass\ of\ mineral}{W^{\min}_m} \quad (4.24)$$

Consider an actual sample of a *Representive Elemental Volume* $V_{Medium} = \Delta x \cdot A$, where A is the area of the sample:

$$M^i = \nu^i_{\min} \cdot \omega^i_{\min} \cdot \rho_{\min} \cdot V_{\min} \quad (4.25)$$

where $\nu^i_{\min}$ indicates the number of moles i in one mole of mineral, $\rho_{\min}$ is the density of the mineral, $\omega^i_{\min}$ is the ratio of the molecular weight of i to that of the mineral. $\nu^i_{\min}$, $\rho_{\min}$, and $\omega^i_{\min}$ are considered constant parameters.

In a *Representative Elemental Volume*, a newly formed mineral involves removal of component i and affects the porosity due to pore filling. Thus, the difference between the volume of the solid before and after chemical reaction is the volume of the newly formed mineral, which can be expressed as:

$$V_{\min} = [(1-\theta)\cdot\Delta x\cdot A]-[(1-\theta_{initial})\cdot\Delta x\cdot A] = \Delta x\cdot A\cdot(\theta_{initial}-\theta) = V_{medium}(\theta_{initial}-\theta) \tag{4.26}$$

Substituting Eq. 4.25 and 4.26 in Eq. 4.24, gives

$$C^i_{medium} = \nu^i_{\min}\cdot\omega^i_{\min}\cdot\rho_{\min}(\theta_{initial}-\theta) \tag{4.27}$$

in which, $\theta_{initial}$ is a known constant parameter. Substituting Eq. 4.27 in Eq. 4.22, gives

$$\frac{\partial\theta}{\partial t} = -(\nu^{i\ -1}_{\min}\cdot\omega^{i\ -1}_{\min}\cdot\rho^{-1}_{\min})\cdot R^i \tag{4.28}$$

By combining Eq 4.28 and 4.3, we obtain a diffusion equation including a change in porosity due to chemical reactions such as precipitation:

$$\frac{\partial(\theta C^i)}{\partial t} = \frac{\partial}{\partial x}(D^i_e\frac{\partial C^i}{\partial x}) - \nu^i_{\min}\cdot\omega^i_{\min}\cdot\rho_{\min}\frac{\partial\theta}{\partial t} \tag{4.29}$$

Clearly, Eq. 4.29 indicates the specific case in which chemical precipitation reactions affect the porosity and diffusivity of the system as well as the mobility of chemical components. This equation has no analytical solution and must be solved numerically.

4.2.5 Numerical Method

The numerical method adopted in this study is the implicit Runge-Kutta method. The general form of the classical fourth-order Runge-Kutta formula is the following (Albarède 1995b; Press *et al.*, 1987):

$$k_1 = h\,f(x_n, y_n)$$

$$k_2 = h\,f(x_n+\frac{h}{2}, y_n+\frac{k_1}{2})$$

$$k_3 = h\,f(x_n+\frac{h}{2}, y_n+\frac{k_2}{2})$$

$$k_4 = h f(x_n + h, y_n + k_3)$$

$$y_{n+1} = y_n + \frac{k_1}{6} + \frac{k_2}{3} + \frac{k_3}{3} + \frac{k_4}{6} + O(h^5)$$

Referring to Eq. 4.29, rewriting it in a finite difference scheme, and rearranging result in:

$$C_m^{n+1} = C_m^n + \Delta t \cdot [(\frac{D_m^n}{\theta_m^n})(\frac{C_{m-1}^n - 2 \cdot C_m^n + C_m^n}{\Delta x^2}) + \frac{(C_{m+1}^n - C_m^n)(D_{m+1}^n - D_m^n)}{\theta_m^n \cdot \Delta x^2} + (N - C_m^n)(\frac{\theta_m^{n+1}}{\theta_m^n} - 1)] \quad (4.30)$$

Here, the subscript m denotes distance and the superscript n denotes time.
$N = \nu_{min}^i \cdot \rho_{min} \cdot \omega_{min}^i$ is a constant. Clearly, Eq. 4.30 can be regarded as being of the form

$$y_{n+1} = y_n + h f(x_n, y_n)$$

In which,

$$f(x_n, y_n) = [(\frac{D_m^n}{\theta_m^n})(\frac{C_{m-1}^n - 2C_m^n + C_{m+1}^n}{\Delta x^2}) + \frac{(C_{m+1}^n - C_m^n)(D_{m+1}^n - D_m^n)}{\theta_m^n \cdot \Delta x^2} + (N - C_m^n)(\frac{\theta_m^{n+1}}{\theta_m^n} - 1)] \quad (4.31)$$

Hence, we can employ the Runge-Kutta method to advance C_m^{n+1} from C_m^n, $h = \Delta t$, under the condition that the spatial and temporal variation of diffusivities and porosities are known. We have developed a FORTRAN program DPLM (Diffusion Precipitation in Layered Materials) to carry out such numerical calculation.

4.2.6 Model calibration and verification: laboratory study

The model simulations represented above suggest how to design purposeful experiments needed for its verification. These are:

a. as parameters of the model, the physical properties of material such as their porosity, tortuosity and diffusivity.
b. the variation in space and time of reactive or non-reactive solutes.

In order to do so experimentally requires first of all two materials in contact with one another, followed by properly designed radio tracer (Das *et al.*, 1989; Das 1992, 1994; van der Sloot *et al.*, 1991) diffusion experiments in two-half spaces with uniform initial concentration. Next a choice has to be made concerning the proper tracers to be used. For instance, an inert tracer is needed to determine the physical transport properties of

the medium to calibrate the corresponding model against experimental data. A reactive tracer needs to be selected on the other hand when investigating the coupled processes of transport and reaction in a reactive solute. Another crucial point is that the tracer component must be distributed homogeneously in one half-space, $C^i_{(x,t=o)} = C^i_o$ $x<o$ (labelled part), and no tracer component must be present in the other half-space, $C^i_{(x,t=o)} = o$ $x<o$ (unlabelled part) in order to get a uniform initial concentration. Finally, the spatial and temporal variation in concentration of the tracer has to be measured. The measured specific activity of a radiotracer can be converted into concentration, in which radioactive decay during the experiment must be taken into account.

4.3 Experiments

4.3.1 Materials

Jarosite and alkaline coal fly ash

The jarosite used in this study comes from a zinc manufacturing plant and is the result of removing Fe from acidic, sulphate-rich solutions (Elgersma 1992; Hage and Schuiling 1996). The alkaline fly ash used in this study is the residue from a power plant. The major physical and chemical characteristics of jarosite and alkaline coal fly ash used in this study are summarized in Table 4.1.

Table 4.1 Physical and chemical characteristics of jarosite and alkaline coal fly ash

		Jarosite	Alkaline coal fly ash
Composition	major:	ammoniumjarosite $NH_4Fe_3(SO_4)_2(OH)_6$	amorphous phase
	minor:	gypsum $CaSO_4 \cdot 2H_2O$	quartz SiO_2
		quartz SiO_2	mullite $Al_6Si_2O_{13}$
			hematite Fe_2O_3
representative partical size (μm)		5.2	20.1
dry density kg/m^3		2.9	2.0
bulk density kg/m^3		2.2	1.2
natural pH*		1.7	12.0
principal elements in leachate**		Al, Fe, Zn, Ca, S, Pb, As, Cu	Al, Ca, S

*** Determined at a liquid/solid radio of 10** **** results from chapter 2**

Radiotracers

The radiotracers and their characteristics are collected in Table 4.2.

Table 4.2 Characteristics of radiotracers

Element	Nuclide	Valence state	Concentration (μg/ml)	Initial activity (CPM*/ml) (1 june, 95')	Half-life ($T_{1/2}$)
H	tritium	H^+	n.d.	1.05*108	12 years
Na	Na-22	Na^+	0.0074	1.80*107	2.6 year
S	S-35	SO_4^{2-}	n.d.	9.6*105	87.5 day
Ca	Ca-45	Ca^{2+}	0.119	5.8*106	163 days
Fe	Fe-59	Fe^{3+}	9.21	2.33*107	45.1 day

*** CPM represents Counts Per Minute**

4.3.2 Methods

Figure 4.1 depicts the flow scheme of the radio tracer diffusion experimental procedure

I. Preparation and tracer addition
⇓
II. Diffusion
⇓
III. Analysis

Fig. 4.1 Flow scheme of radio tracer diffusion experimental procedures

Preparation and tracer addition

Experimentally the tracers were introduced into each material by first preparing a diluted tracer solution. We used this solution to form a labelled paste by mixing it with dry material to obtain a homogeneous initial concentration. The non-labelled paste we made by mixing distilled water with dry material. We experimentally determined the proper liquid to solid ratio to avoid any liquid spilling from the diffusion tube. The diffusion tubes were filled first with non-labelled paste followed by labelled paste to avoid contamination. More detailed information dealing with radio tracer diffusion experiments can be obtained from several references (van der Sloot *et al.*, 1991, 1993, 1995a; 1995, Hockley *et al.*, 1992; Das *et al.*, 1989; Das 1992, 1993, 1994; Ding 1996; Ding *et al.*, 1997, 1998).

Diffusion

The filled diffusion tube, with one half-space containing the labelled, the other unlabeled material, was stored at controlled relative humidity at room temperature and zero fluid flow condition. The exposure time were one day, one week, two weeks, one month, and two months.

Analysis

Each 50 mm long diffusion tube was sliced into about 40 slices, by pushing the material out of the non-labelled segment. Thus, cross contamination of slices is avoided. The slices are transferred to counting tubes. The weight of the individual slices is determined after drying.

For $^{59}Fe^{3+}$ and $^{22}Na^{+}$ determination, the samples were dried overnight in an oven at 850°C and counted with L 1282 Compugamma Universal Gramma Counter. However, to detect tritium, samples should not be dried by virtue of the volatility of tritium. Another essential point is that reliable β counts require separation of the solid and the pore fluid because of the very high susceptibility of β rays to adsorption by the solid matrix. To do so, we added 5 ml distilled water to each sample and mixed it intimately. After standing for 4 hours, 4 ml of a clean supernatant was extracted and mixed with 10 ml gel before β counting using Philips PW 4700 Liquid Scintillation Counter.

pH gradient measurement

We designed pH tube measurements to track the spatial and temporal development of pH in the layered jarosite/fly ash system. The preparation and slicing of the tubes for these experiments is identical to that of the diffusion tube experiments except that no tracer was added to either of the segments. 20 ml distilled water was added and mixed with each sample individually. The measured pH refers to the solution pH.

4.4 Results

4.4.1 Radiotracer experiments performed in a single material

The spatial and temporal developments of tritium, $^{59}Fe^{3+}$, and $^{22}Na^{+}$ in jarosite, and of $^{22}Na^{+}$ in coal fly ash are presented in Figure 4.2, 4.3, 4.4, and 4.5 respectively. The results shown in Figure 4.2 and 4.5 indicate that tritium and $^{22}Na^{+}$ transport of diffusion in jarosite and fly ash are fairly fast and eventually reach a steady state as inferred by their horizontal profile lines. These results are consistent with the notion of non-reactive diffusion profiles of two half-spaces with uniform initial concentration.

Therefore, tritium can be regarded as an inert component in jarosite whereas the same holds for $^{22}Na^{+}$ in coal fly ash.

Figure 4.3 shows that $^{22}Na^{+}$ diffusion in jarosite resembles initially that observed in coal fly ash, i.e. relatively fast diffusion close to an ideal diffusion pattern. However, the profiles measured after 28 and 56 days differ significantly from the previous two and from those observed in fly ash. Note that the 28 and 56 days patterns overlap with one another hence indicating that no concentration gradients existed in the pore water of the labelled nor of the unlabelled segments in this system. This absence of a concentration gradient can only be caused by a reaction of the sodium tracer with the matrix reaching a steady state after 28 days. It can be concluded that $^{22}Na^{+}$ cannot be considered inert in jarosite and that the rate of such reaction is time dependent and comparable to diffusional transport. The mass of Na in jarosite, with which the Na-22 tracer can be exchanged is larger compared to that in fly ash leading to the different tracer levels on both half cells after equilibrium has been established.

Analogous to $^{22}Na^{+}$, $^{59}Fe^{3+}$ diffusion in jarosite, as illustrated in Figure 4.4, slows down with increasing exposure time. The characteristic diffusion pattern of $^{59}Fe^{3+}$ in jarosite does not coincide with the anticipated standard diffusion pattern which should result in a horizontal profile line through the point at C/C_0 equal to 0.5. This result suggests that there is an exchange reaction between $^{59}Fe^{3+}$ in the pore fluid and Fe in jarosite. Again, the rate of exchange is time dependent and comparable with iron tracer transport of diffusion.

4.4.2 Radio tracer experiments in the layered jarosite/coal fly ash system

The intrinsic difference between jarosite and coal fly ash lies in their acid base contrast. Hence, the discontinuity in the layered jarosite/fly ash system is essentially caused by a pH gradient. The variation in pH as a function of time and distance across the interface in such system is shown in Figure 4.6. This Figure indicates that the interfacial pH gradient in this closed system, in which the size of the tubes is limited, decreases with increasing exposure time. The pH gradient over the interface will continuously decline as long as the interface has not been sealed completely. If, on the other hand, the pores are fully filled, a discontinuous steady state across the interface will develop. We also anticipate that with the use of longer tubes or in an open system, pH gradients will be maintained longer. Consequently, the chemical reactions taking place at the interface will procede more thoroughly.

Figure 4.7 shows our most interesting $^{59}Fe^{3+}$ diffusion profiles in the layered jarosite/coal fly ash system. The principal results, are: firstly, a $^{59}Fe^{3+}$ tracer accumulation at the interface of jarosite/fly ash where a sharp peak

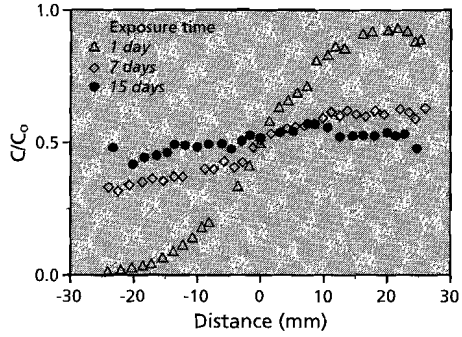

Fig. 4.2 Tritium diffusion profiles in jarosite

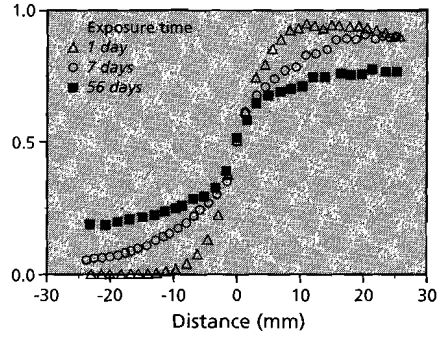

Fig. 4.3 $^{59}Fe^{3+}$ isotope diffusion profiles in jarosite

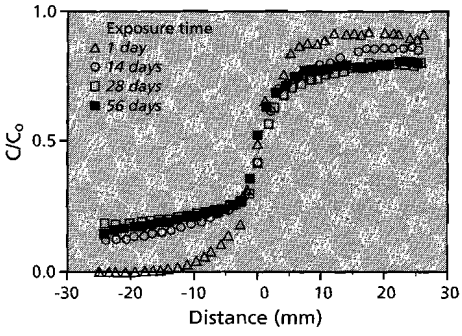

Fig. 4.4 $^{22}Na^{+}$ isotope diffusion profiles in jarosite

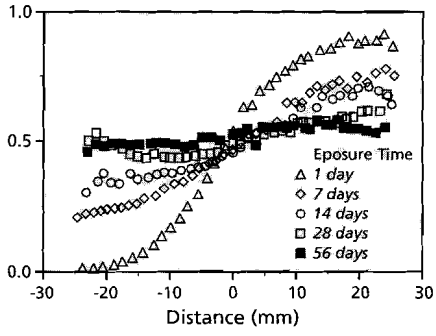

Fig. 4.5 $^{22}Na^{+}$ isotope diffusion profiles in fly ash

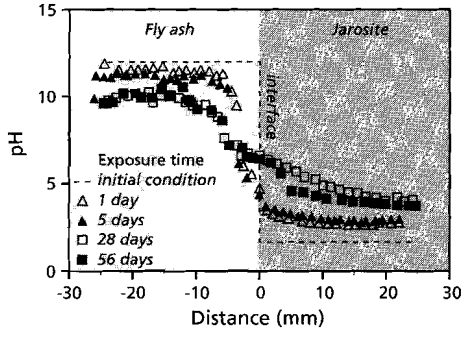

Fig. 4.6 pH development in jarosite/fly ash

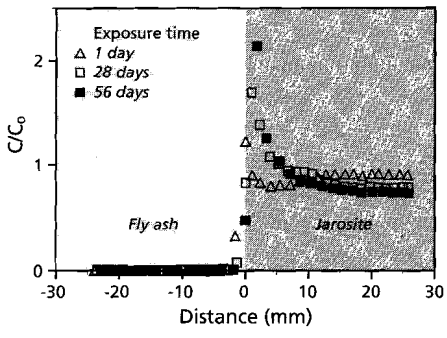

Fig. 4.7 $^{59}Fe^{3+}$ profiles in layered jarosite/fly ash

can be observed, indicating that $^{59}Fe^{3+}$ exchange from pore fluid to solid occured; secondly, a curious first day profile hinting that a coupled process of diffusion and precipitation characterises the behaviour of Fe^{3+} in such system; and thirdly, a shift in the position of these peaks towards the jarosite part. These phenomena point towards a process which involves hydroxide diffusion from alkaline fly ash and a reaction with Fe^{3+} in jarosite. Integrating the results of $^{59}Fe^{3+}$ diffusion and pH profiles in the combined jarosite and alkaline fly ash layered system suggests that two processes are characteristic for the behaviour of Fe^{3+} in the system. The diffusion of Fe^{3+} is caused by the concentration gradient between jarosite and fly ash. The sharp peak at the interface is caused by precipitation of FeOOH due to very low solubility of Fe^{3+} at pH about 7. In accordance with the thermodynamics of ferric hydrolysis (Baes and Mesmer 1976) Fe^{3+} in pore water will be completely transferred into the insoluble state in the form of amorphous FeO(OH).

4.5 Discussion

4.5.1 Effective diffusion coefficients

The effective diffusion coefficient of chemical constituents is the most crucial parameters required in the mathematical description of transport equations. To describe an actual process precisely and accurately with a model and verify it with experimental data, it is essential to determine the effective diffusion coefficients experimentally rather than to calculate them from empirical formulas or estimates. For an inert solute, its effective diffusion coefficient can be obtained directly by calibrating the diffusion model Eq. 4.10 and 4.11, which describes a non-reacting solute transport process, against measured profiles. Calibration is effectuated by adjusting the model parameter, i.e. the effective diffusion coefficient, to get a statistically best fit between model results and measurements. Based on the effective diffusion coefficients of the inert components: tritium and $^{22}Na^{+}$, we can calculate the tortuosity of the medium according to Eq. 4.2. Going a step further, we can derive effective diffusion coefficients of other components in the same medium, once more by using Eq. 4.2. Table 4.3 lists the diffusivities of principal constituents in jarosite and coal fly ash. The mathematical description of the above stated data processing can be summarized as follows:

Based on inert tracer diffusion tube experimental data

$$D^i_{jarosite} = \frac{\theta_{jarosite}}{T_{jarosite}} \cdot D^i_o \Rightarrow D^i_{jarosite} \qquad i = {}^{59}Fe^{3+},\ {}^{45}Ca^{2+},\ and\ {}^{35}SO_4^{2-}$$

$$D^i_{fly\ ash} = \frac{\theta_{fly\ ash}}{T_{fly\ ash}} \cdot D^i_o \Rightarrow D^i_{fly\ ash}$$

Based on principal constituents radiotracer diffusion tube experimental data

$$\theta_{jarosite}\frac{\partial C^{^3H^+}}{\partial t} = D^{^3H^+}_{jarosite}\cdot\frac{\partial^2 C^{^3H^+}}{\partial x^2} \Rightarrow \frac{\partial C^{^3H^+}}{\partial t} = \frac{D_o^{^3H^+}}{T_{jarosite}}\cdot\frac{\partial^2 C^{^3H^+}}{\partial x^2} \Rightarrow T_{jarosite}$$

$$\theta_{fly\ ash}\frac{\partial C^{^{22}Na^+}}{\partial t} = D^{^{22}Na^+}_{fly\ ash}\cdot\frac{\partial^2 C^{^{22}Na^+}}{\partial x^2} \Rightarrow \frac{\partial C^{^{22}Na^+}}{\partial t} = \frac{D_o^{^{22}Na^+}}{T_{fly\ ash}}\cdot\frac{\partial^2 C^{^{22}Na^+}}{\partial x^2} \Rightarrow T_{fly\ ash}$$

Table 4.3. The diffusivities of principal constituents in jarosite and alkaline coal fly ash

matrix	porosity	tortuosity	diffusivities									
			tritium		$^{22}Na^+$		Fe^{3+}		Ca^{2+}		SO_4^{2-}	
			pD_o	pD_e	pD_o	pD_e	pD_o	pD_e	pD_o	pD_e	PD_o	pD_e
jarosite	0.45	10.7	8.0	9.3	8.9	10.3	9.2	10.6	9.1	10.5	9.0	10.4
fly ash	0.30	1.5	8.0	8.7	8.9	9.6	9.2	9.9	9.1	9.8	9.0	9.7

*pD = - log D

4.5.2 Effect of discontinuities in porous media caused by physical gradient

Diffusivity, porosity, and tortuosity

The equations presented in Eq. 4.10, 4.11 and their solutions presented in Eq. 4.12-4.15 give a precise mathematical description of how a sudden fluctuation in diffusivity and porosity affects the transport process. The influence of tortuosity can be inferred from the other two parameters based on the relation presented in Eq. 4.2. Figure 4.8 demonstrates a non reacting solute diffusion profile with different ratios of $\frac{D_{e1}\cdot\theta_2}{D_{e2}\cdot\theta_1}$ or $\frac{T_2}{T_1}$.

In the specific situation that $T_1 = T_2$, the profile reflects diffusion of a component in a homogeneous medium. Its concentration at the interface is constant and equal to $C_0/2$. The distribution remains symmetrical at x = 0. That is what we are familiar with: an ideal diffusion pattern of two half spaces with uniform initial concentration. We can anticipate that applying such model to the layered jarosite/fly ash system, will not lead to a dramatic change in transport of components, due solely to physical gradient as reflected by their tortuosity ratio ($T_{jarosite}/T_{fly\ ash}$) of about 7.

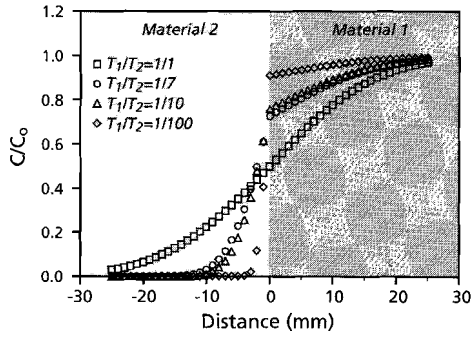

Fig. 4.8 Normalized concentration C/C_0 versus distance x for different ratios of T_1/T_2.

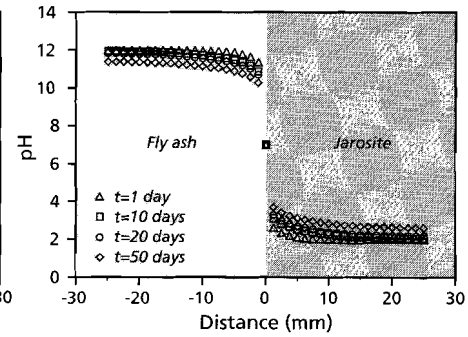

Fig. 4.9 pH profiles calculated using program DNLM

Water content

The amount of water in a system is of extreme importance for diffussional transport. As we know, diffusional driving forces depend on concentration gradients. In saturated porous media, the difference in water content of each half-space is indicative of their difference in porosity. However, in unsaturated porous media, an inhomogeneous distribution of water will influence the transport process and therefore needs to be considered. In this paper, for reasons of simplification, we have assumed all media to be saturated.

4.5.3 Effect of discontinuities in porous media caused by chemical gradients

Contrary to physical restrictions, chemical gradients between two adjacent materials may change significantly the transport process and constituent mobility. As mentioned in the introduction, natural phenomena, such as the formation of a reaction zone between oxidizing and reducing matrices or the formation of a sealing layer between acidic jarosite and carbonate-bearing clay, are generated primarily by chemical discontinuities in the system. In the last case, chemical reactions adversely influence the physical properties of the system due to pore filling precipitates. The diversity and complexity of chemical reactions add a lot of difficulties to the mathematical description of reactive transport in porous media. In general, chemical reactions are introduced into the transport equation either as chemical equilibria in the case of fast kinetics or as time dependent reactions when kinetics is slow. In this section, we consider three cases. The first one is acid-base neutralization, which is a sufficiently fast reaction with as consequence that the rate of transport of H^+ and OH^- will dominate the process. The implementation of this chemical reaction requires modification of the transport equation to include chemical equilibria. The second one is chemical adsorption following the Langmuir adsorption mechanism, in which the kinetics of the reaction involving com-

ponent i is proportional to first order in concentration and the reaction rate comparable to diffusion. The final one is precipitation with a sufficiently fast reaction rate. Similarly to acid-base reactions, precipitation reactions are introduced into the transport problem by including chemical equilibria into mass action.

pH dominant interface

Figure 4.9 presents the simulation results of pH development in layered jarosite/fly ash based on the model of Eq. 4.18 and 4.19. The model is calculated using the DNLM program. Our results show that the pH gradient at the interface decreases with increasing exposure time. Comparing the results of our pH model prediction with experiment, as shown in Figure 4.6, does not show a good agreement possibly for the following reasons. First, in the model we assumed that only H^+ reacts with OH^-, but in reality OH^- also reacts with Fe^{3+}. Second, in the model the intrinsic acidity and alkalinity of jarosite and fly ash are equivalent, which means that they have the same neutralization capacity. However, the results from Chapter 2 indicate that the neutralization capacity of fly ash is about three times higher in comparison to that of jarosite. Last, in the model, we assumed that the physical properties such as diffusivity, porosity and tortuosity of the system remain constant.

Adsorption dominant interface

When the interaction between a solute and the matrix obeys the Langmuir equation, we can simulate reaction and diffusion of the reacting solute with Eq 4.21A and 4.21B. Figure 4.10 demonstrates the profiles of reacting solute i in a system of layered materials as a function of time and distance. The retardation factor of material 2 is much larger than of material 1 ($R_{T_2} > R_{T_1}$). If it is assumed that reacting solute i originally was distributed homogeneously in the fluid of material 1 but not present in the fluid of material 2, diffusion of solute i from material 1 to material 2 will occur due to the presence of a concentration gradient. In addition, adsorption of component i on to the solid of material 2 will start when this component comes in contact with material 2, whith as result an accumulation of component i at the interface between the two materials. Thus this component will gradually penetrate into the main body of material 2, as illustrated in Fig. 10a, b, the diffusional transport depending on the ratio of the two retardation factors, R_{T_1}/R_{T_2}.

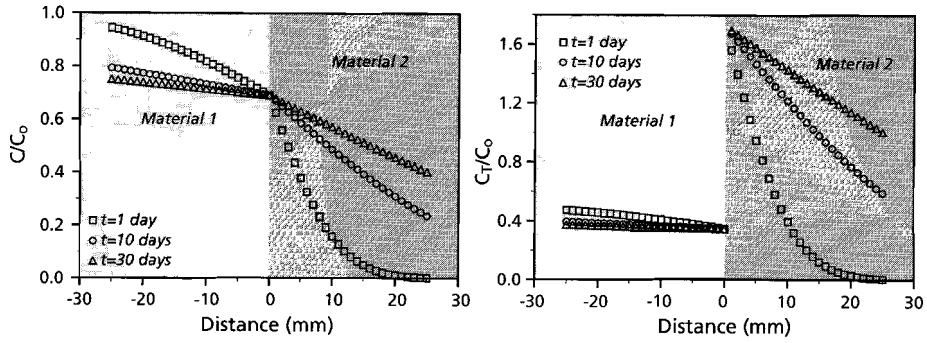

Fig. 4.10 Diffusion profiles of a component in a hypothetical layered material. The retardation factors of the two materials differ from each other, i.e. R_{T1} / R_{T2} = 1/5. (a) Diffusion profiles of the component in fluid flow, (b) Profiles of the component in the overall system (solution +solid).

Precipitation dominant interface

To demonstrate how large this effect on transport and mobility of chemical components can be, we illustrate in Figure 4.11 and 4.12 our $^{59}Fe^{3+}$ radio tracer diffusion experimental results on acidic jarosite solely (without the effect of discontinuities) and in the layered acidic jarosite/alkaline fly ash (with the effect of discontinuities). These Figures show the marked accumulation of $^{59}Fe^{3+}$ tracer at the jarosite/alkaline fly ash interface as indicated by the sharp peak caused by the pH switch from strongly acidic (jarosite) to strongly basic (fly ash). Note that the measured profiles of $^{59}Fe^{3+}$ in the layered jarosite/fly ash is the sum of mobile and immobile ferric cations.

Clearly, discontinuities in porous media caused by chemical contrast not only affect transport but also the mobility of chemical constituents. Conversely, change in physical properties in porous media are caused by chemical reaction, e.g. reduction in permeability and diffusivity due to precipitates filling pores (Carnaban 1990; Ding 1996; Ding et al., 1997, 1998; Steefel and Lasaga 1990, 1994; van der Sloot et al., 1993, 1997a). In order to describe these coupled chemical and physical processes mathematically and furthermore to predict the consequence in various, not experimentally accessible circumstances, it is not enough if one remains stuck in phenomenology. In the previous section, we established a model taking into account the spatial and temporal change in porosity and diffusivity. We also formulated a numerical solution to such model. Next, we must address the validity of this model.

4.5.4 Model verification in layered jarosite/fly ash

The model presented in Eq. 4.29 has been calibrated and verified using $^{59}Fe^{3+}$ radio tracer experiments in the layered jarosite/fly ash system. Figure 4.13 shows our modeled profiles of Fe^{3+} in the layered jarosite/fly ash system. Figure 4.14 presents the

porosity development in the interface region. Figure 4.15 indicates that the modeled result is the sum of Fe^{3+} present in fluid and in solid. Comparing Figure 4.7, i.e. measurements profiles of $^{59}Fe^{3+}$ and Figure 4.13 clearly shows that the model and our measurements agree well with some exceptions. The exceptions are probably due to the concentration contrast between tracer $^{59}Fe^{3+}$ and bulk Fe^{3+} in the pore fluid; as well as precipitation which not only involves FeOOH but also $CaSO_4 \cdot 2H_2O$, whereas in the model FeOOH is considered as the only precipitating phase. In addition, some discrepancy between practical operation and theoretical calculation can hardly be avoided. Despite this discrepancy, the model and measurements agree quite well, encouraging us to use the model to predict the fate and transport of Fe^{3+} and other principal constituents under various boundary and initial conditions. Among these were the development of physical properties of a system, the transport, and the mobility of its constituents in an industrial disposal site of layered jarosite/fly ash. Figure 4.14 also shows that the porosity change calculated from the model in the designed system is not able to induce a sealing layer after 56 days when steady state is almost reached.

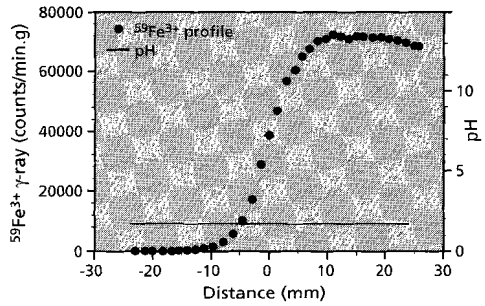

Fig. 4.11 $^{59}Fe^{3+}$ profile in jarosite

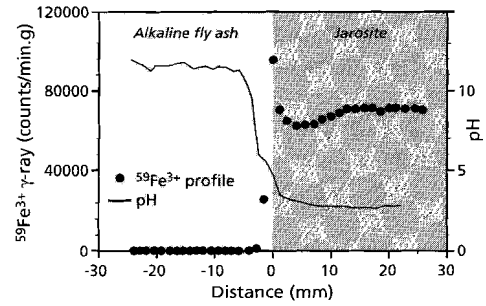

Fig. 4.12 $^{59}Fe^{3+}$ profile in jarosite/fly ash

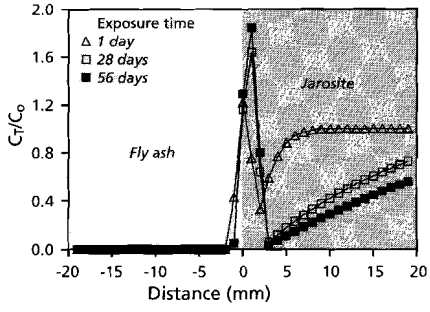

Fig. 4.13 Modeled Fe^{3+} profiles in jarosite/fly ash using the program DPLM.

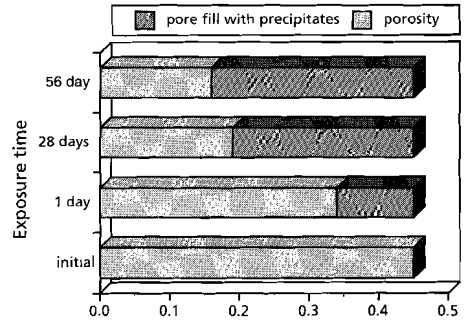

Fig. 4.14 Caculated porosity change at the interface of jarosite/fly ash using the program DPLM

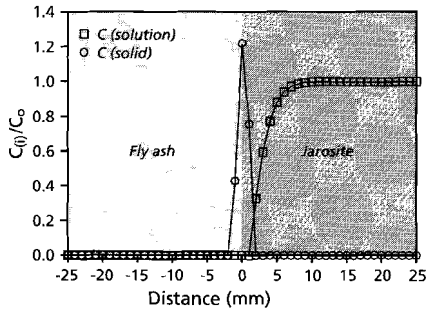

Fig. 4.15 Distribution of Fe^{3+} in solution and solid in jarosite/fly ash (exposure time = 1 day)

4.5.5 Model application: prediction of an disposal site of layered jarosite/fly ash

In an industrial disposal site of layered/fly ash, the boundary and initial conditions differ from those considered in our model which were based on specifically designed radio tracer experiments. The main differences are two-fold. One is that our diffusions experiments were conducted in a closed system with the diffusion tube length as limiting factor. There is no supply of outside sources of reacting solutes. Another is that the initial concentration of $^{59}Fe^{3+}$ radio tracers is much lower than the actual initial concentration of reacting solutes of Fe^{3+} in the emanating pore fluids. This causes the reaction front to develop at a substantially lower pH predicated by the magnitude of the solubility product of ferric oxyhydroxide as a function of pH.

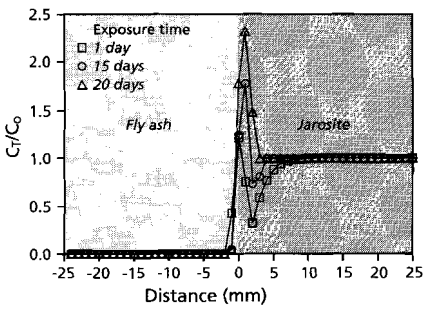

Fig. 4.16 Modeled Fe^{3+} profiles in a open system, with a continous supply of 0.01M Fe^{3+}

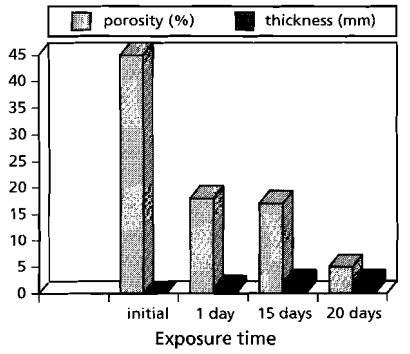

Fig. 4. 17 Development of porosity and thickness of self forming layer in the hypothetical system.

The modeled Fe^{3+} profiles in such an open system are depicted in Figure 4.16 showing the time dependent increase in Fe^{3+} accumulation at the interface. The porosity decrease at the interface due to pore filling precipitates is illustrated in Figure 4.17. As

long as sufficient Fe^{3+} is available, precipitation of FeOOH will continue until a sealing layer is formed in the interfacial region between acidic jarosite and alkaline fly ash, hence a steady state is reached, as indicated by the two horizontal straight lines appearing in each of the two media. For this particular case, we have assumed that the supply of OH^- from alkaline fly ash is steady and continuous. Figure 4.16 and 4.17 also show that we would expect a very low about 0.05 porosity layer of about 2 mm thick to be formed less than 20 days after contacting acidic jarosite with alkaline fly ash. Note that the porosity change in this model is contributed solely by FeOOH, one of the two newly formed minerals at the interface. Therefore, in practice we would expect a faster speed of sealing layer formation in such system.

Our modeling results of the layered jarosite/fly ash system provide the crucial information concerning waste isolation. Thus, such system and our model may have wide applications in waste management.

4.6 Conclusions

Considering discontinuities caused by physical or chemical gradients in porous media is crucial for understanding reactive transport in natural processes. Generation of an additional third zone, which possesses different transport and thermodynamic properties from either of the adjacent homogeneous ones, as occur in natural environments affirms the effect of discontinuities in porous media on transport processes and the mobility of chemical constituents.

The effect of discontinuities caused by physical gradients in porous media can be described mathematically with a model which has analytical solutions under constrained initial and boundary conditions. The results of such model simulation indicate that physical restrictions are of minor significance relative to those caused by chemical contrasts on the transport of chemical components.

The models used to describe the effect of discontinuities caused by chemical contrast are variable and depend on the characteristics of chemical reactions. If the chemical reaction rate is sufficiently fast with respect to the rate of transport, chemical equilibria are accommodated, whereas if the chemical reaction reaction rate is comparable with that of transport, chemical kinetics must be taken into account. Commonly, one needs to determine the chemical kinetics independently to distinguish and adopt one of these two possible models. In most cases, the model which involves chemical reaction will not have an analytical solution. Numerical solutions have to be established. Our model suggests that discontinuities caused by chemical gradients will not only affect the transport but also the mobility of constituents. As a consequence, it may locally affect the transport properties and develop a new reaction zone which has properties differing in

transport and thermodynamics relative to the original two source media, eventually in turn influencing the overall transport process enormously. In a particular case, where precipitation occurs, a new reaction zone with lower permeability may form due to pore filling by precipitates. Without considering the change in porosity caused by precipitation, our model will not be able to mimic the actual transport properly. For instance, the model results of pH evolution in jarosite/fly ash do not agree well with the measured one, as illustrated in Fig. 4.6 and Fig. 4.9, because in the modeling we assume the physical properties, e.g. porosity and diffusivity in the system to remain constant, which is not the case in practice. Conversely this indicates the necessity of developing models which consider such highly dynamic coupled effects as change in transport properties with precipitation.

It is important to conduct experiments under boundary conditions which are consistent with boundary conditions required by our mathematical model. Without this strict constraint, it becomes impossible to determine experimentally the parameters required by the model and to verify the model experimentally. Radio tracer diffusion experiments are the most simple, precise, and accurate experimental approach despite their limitation caused by its exchange.

Our modeled profiles of $^{59}Fe^{3+}$ agree well with our measured one in the layered jarosite/fly ash system. The model takes into account local porosity change due to precipitation and its calculation was accomplished by operating our newly developed FORTRAN program DPLM based on the classic implicit fourth-order Runge-Kutta numerical method.

The application of our model to industrial layered acidic jarosite/alkaline fly ash deposition suggests that there is a potential benefit to layered disposal of these two chemically contrasting wastes. By making use of the chemical reactions between them to neutralize (acid and base reaction), to isolate (sealing layer formation due to pores filling by precipitates), and to immobilize (reduce mobility of chemical constituents due to precipitation) the wastes. Our model DPLM enables quantitative exploration of self-forming processes in chemically discontinuous porous media.

List of symbols

Symbol	Definition	Dimension
C^i	concentration of constituent i in the medium	$g \cdot (cm^3)^{-1}$
θ	porosity of the medium	dimensionless
t	time	s
x	distance	cm
q	velocity of pore fluid	$cm \cdot s^{-1}$
D^i_e	effective diffusion coefficient of constituent i	$cm^2 \cdot s^{-1}$
D^i_o	molecular diffusion coefficient of constituent i	$cm^2 \cdot s^{-1}$
R^i	chemical or biological reaction rate involving constituent i	$g \cdot (cm^3 \cdot s)^{-1}$
T	tortuosity of the medium	dimensionless
ρ_{medium}	bulk density of the medium	$g \cdot (cm^3)^{-1}$
SS^i	concentration of constituent i in the medium	$g \cdot g^{-1}$
L	total transport distance	cm
K_w	ionization constant of water	at 25 °C equals 10^{-14}
β_1	concentration of proton ion substrate concentration of hydroxide ion in pore fluid	$g \cdot (cm^3)^{-1}$
β_2	concentration of hydroxide ion substrate concentration of proton ion in pore fluid	$g \cdot (cm^3)^{-1}$
K_d	partitioning coefficient of component between aqueous and solid phase	$cm^3 \cdot g^{-1}$
R_T	retardation factor	dimensionless
C_T	sum of concentration in solid and aqueous phase	$g \cdot (cm^3)^{-1}$
M_{medium}	mass of the medium	g
V_{medium}	volume of the medium	cm^3
M^i	mass of constituent i in medium	g
C^i_{medium}	concentration of constituent i in medium	$g \cdot (cm^3)^{-1}$
$C^{i/min}_{medium}$	mass of constituent i in the form of mineral per volume of the medium	$g \cdot (cm^3)^{-1}$

$M^{i/min}$	mass of constituent i in the form of mineral	g
A	area	cm^2
W^i_m	molecular weight of component i	g
$W^{p/min}_m$	molecular weight of the mineral involving involving component i	g
M_{min}	mass of the mineral	g
V_{min}	volume of the mineral	cm^3
V^i_{min}	mole number of i in one mole of the mineral	dimensionless
ω^i_{min}	ratio of the molecular weight of i to that of the mineral	dimensionless
ρ_{min}	density of the mineral	$g{\cdot}(cm^3)^{-1}$
$\theta_{initial}$	initial porosity of the medium	dimensionless
h	time interval h=Dt	s
Δx	distance interval	cm
N	a constant equals	$g{\cdot}(cm^3)^{-1}$
F^n_m	finite difference scheme of components, F represents i concentration C ii porosity θ iii effective diffusion coefficient D subscript m denotes distance and subscript n denotes time	

Acknowledgements

Dr H. van der Sloot provided access to the facilities of the Energy Research Foundation (ECN) the Netherlands, Professor Dr. M. Hassanizade made me aware of the connection between experimental execution and modelling. Dr. H. J. S. Dorren helped me to select the proper numerical method for model calculation. Professor Dr B.H.W.S. de Jong edited and corrected the numerous draughts of this manuscript.

Chapter 5

Chemical nature of sealing layer in jarosite/fly ash

Chapter 5.1

Characterization of amorphous black ferric oxyhydroxide: photoelectron spectroscopy, conversion electron Mössbauer spectroscopy, and adsorbtion chemistry

Abstract

A novel form of amorphous ferric black iron oxyhydroxide has been synthesized by hydrolysis of ferric nitrate with ammonia. The material is hard and has the local structure of akageneite according to conversion electron Mössbauer results, fractures conchoidally, has a surface area around 300 m^2/gram and a point of zero charge at a pH between 7 and 8. The adsorption isotherms of three oxyanions, chromate, phosphate, and arsenate and two cations lead and zinc have been determined indicating that the absolute adsorption characteristics are about three times higher than those of conventional ferric oxyhydroxides. Competive experiments between phosphate and arsenate indicate that the phosphate-FeOOH substrate interaction is energetically favored over the arsenate one.

5.1.1 Introduction.

We have argued in previous studies (Ding *et al.*, 1996, 1997, 1998a) that the formation of impermeable layers in natural and artificial systems, is commonly due to the formation of sparingly soluble salts at the interface between two strata which differ in chemical properties. We have illustrated this process in detail on a system consisting of jarosite and fly ash, in which the precipitation of gypsum and a brown ferric oxyhydroxide zone created an impermeable layer due to pore filling. The question which arises and which we want to address here concerns the nature of the chemical reactivity of such layer in particular the role played by FeOOH. This last substance has been the subject of a very large number of studies ably reviewed in some recent books (Cornell and Schwertman (1996), Dzombak and Morel (1990)).

Iron and manganese exhibit among the largest number of oxidation states of any of the elements in the periodic table, offering an easy rationalization for the observation that their oxyhydroxides form the prime substrates for removal of a large variety of cations or anions from surface waters. Despite the well-known utility of such substrates much theoretical and experimental work remains to be done in terms of detailed chemical mechanisms involving characterizable elementary steps in the adsorption. Recent developments in analytical technique have started to provide detailed structural and chemical observations of adsorbates and provided more direct quantitative information on the sorbed complex as among others summarized by Brown(1990) in his spectroscopic studies of chemisorption reaction mechanisms at oxide water interfaces. Among these techniques, EXAFS has been widely adopted to probe surface structure (Waychunas et al, 1995, 1996) primarily delineating the various geometries of adsorption complexes such as inner or outer sphere, mono *versus* bidentate complexes and so on.

From a quantum mechanical perspective the state of describing the interaction between adsorbate, i.e. the adions or admolecules and substrate remains by and large wanting. Getting to this next stage requires the exploration of the nature of the chemical reaction between solid and solute for which we need to know firstly the direction of electron transfer from substrate to adduct and secondly the relative position of empty and occupied energy states of substrate and adduct to asses their mutual affinity. Such shallow surface states are most adequately sampled by photoelectron spectroscopy.

Though conceptually easy there are in practice some severe constraints in carrying out a experimental program focussed at the electronic states of surfaces. Among these are that the substrate has to have a sufficiently high surface area in order for there to be a chance to distinguish between surface and bulk atoms in the substrate. Secondly the material should be preferably amorphous and hence not contain any preferred crystal planes. Thirdly the surface concentration of admolecules or adatoms should be sufficiently high to distinguish between bulk, surface, and perturbed surface atoms of the substrate.

To carry out this program we have synthesized a form of amorphous ferric oxyhydroxides which has not been mentioned in the open litterature (Blumer, 1980), but which is in its local structure and chemical composition is identical to the brown colored one observed in our self sealing layer in the jarosite/fly ash system. This material is brittle with conchoidal fracture planes, has a surface area around 300 m^2/gram (Juergens 1995), has the characteristic shiny black color of specular hematite, consists of ferric ions, and is x-ray amorphous. Our choice of ferric oxyhydroxides rather than manganese oxyhydroxides was predicated by the utility of Mössbauer spectroscopy for iron containing substances which enables characterization of the amorphous ferric oxyhydroxide phase.

Next to characterizing this novel black ferric oxyhydroxide spectroscopically, we inves-

tigated the sorption of cations (Pb^{2+} and Zn^{2+}) and oxyanions(AsO_4^{3-}, PO_4^{3-}, CrO_4^{2-}) as a function of solution pH and determined their adsorption isotherms. The reason for our choice of $Pb^{2+}$and Zn^{2+} as cations is that they occur in jarosite, which also contains a fair amount of arsenic (0.28 wt%). We did choose phosphate and chromate next to arsenate to test how different anions interact with an FeOOH surface and in particular the extent to which the point of zero charge affects the sorption of these species. Finally we carried out competitive experiments between phosphate and arsenate to test which anionic species has the largest affinity for a FeOOH surface.

Our principal findings are that the local environment of this material consists of β-FeOOH, akaganeite. Phosphate and arsenate sorption onto FeOOH are not PZC dependent in contrast to that of chromate lead and zinc. We shall also show that in competitive experiments phosphate wins out over arsenate. Finally we shall show that the unique sorption characteristic of black iron oxyhydroxide manifests itself in its up to three times larger adsorbtion capacity vis a vis conventional ferric oxyhydroxides.

5.1.2 Experimental

Amorphous ferric oxyhydroxide was prepared in a flask by hydrolysis of a stirred 0.1M $Fe(NO_3)_3$ solution with 0.1M $NH_3.H_2O$. The temperature was kept at 50°C with a recirculating water bath. The base was introduced by automatic titration at a constant rate of about 2 drops/s, up to a solution pH of 7.5, after which the solution was stirred for another half hour. The resulting suspension was filtered, washed firstly with distilled water, next three times with a pH 7 washing solution. After drying, the filter cake was placed in a drying oven at 105°C. The brown variety of amorphous ferric oxyhydroxide is the normal precipitate formed whenever nitrogen-free reagents are used such as ferric sulphate and sodium or potassium hydroxide.

Adsorption experiments were carried out at a constant suspension concentration of 1.35×10^{-3} M and an ionic strength of 0.01 N $NaNO_3$ at room temperature. The suspension was equilibrated before introducing the adions at designated pH between 4 and 10, adjusted by either adding 1M HNO_3 or 1M NaOH for one hour in a sealed reaction flask with continuous N_2 sparge to create a carbonate free environment. After adding the adions into the equilibrated suspension, the initial pH of the solution was measured, followed by shaking continuously for 24 hours. The final pH was measured at the end of the reaction period and the suspension was filtered with 0.20 μm filter paper. The supernantant solution was analyzed by ICP. Blank experiments without iron oxyhydroxide were run to test if any chemical were adsorbed onto the walls of the flask.

XPS measurements were carried out on OCTOPUS, a multichamber UHV preparation and analysis system connected to a 3MV single-ended and a 6 Mv tandem van der Graaff generator, using a Clam-2 hemispherical sector analyzer and a VG XR2F2 twin

anode x-ray source with standard Al/Mg anodes. Spectra were recorded using the AlKα source operated at a power of 120W and a constant pass energy of 20 eV for the analyzer, using the C (1s) spectral line as reference.

Conversion electron Mössbauer experiments were carried out using a ^{57}Co in Rh source.

5.1.3 Results

Adsorption of cations and oxyanions

Figure 5.1.1 shows adsorption of oxyanions with respect to pH, indicating that sorption of all oxyanions is largest at low pH and decreases with increasing pH. Figure 5.1.1 also shows that the adsorption behavior of arsenate as a function of pH is similar to that of phosphate. This is because both are triacidic and have similar proton dissociation constants, suggesting at a specific pH, a similar species distribution for arsenate and

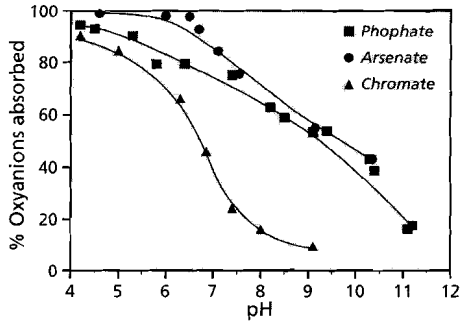

Fig. 5.1.1 Adsorption of oxyanions as a function of pH

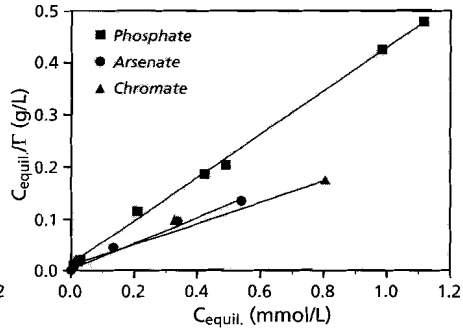

Fig. 5.1.2 Oxyanions adsorption isotherm

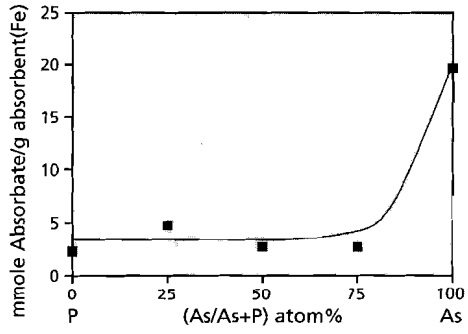

Fig. 5.1.3 Competitive adsorption between arsenate and phosphate on black iron oxyhydroxide. The datapoints represent the sum of anions adsorbed

phosphate. Thus, oxyanions of arsenate and phosphate, as ligand substituents reacting with sorbent, possess the same chemical structure. Sorption of chromate on the other hand decreases rapidly with increasing pH. At a pH of about 8, virtually no adsorption takes place. The results of constant pH isotherms of oxyanions are shown in Figure 5.1.2, indicating that adsorption of arsenate, phosphate, and chromate follow a Langmuir adsorption isotherm. Mixtures of arsenate and phosphate were used to study the mixed oxyanion effect. Our results shown in Figure 5.1.3 indicate that that arsenate adsorption is significantly reduced in the presence of phosphate.

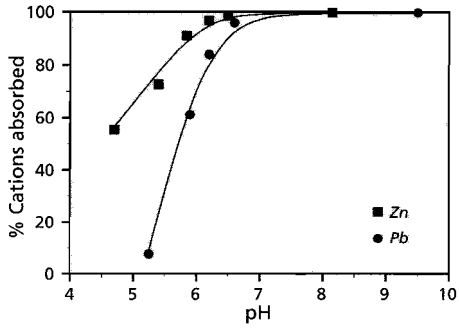

Fig. 5.1.4 Adsorption of cations as a function of pH

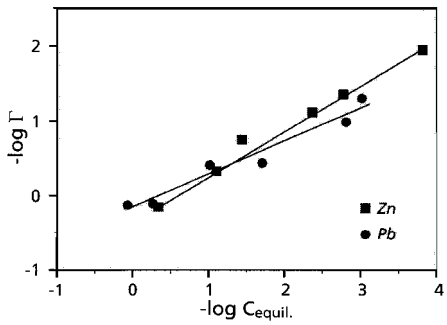

Fig. 5.1.5 Cations adsorption isotherm

Table 5.1.1. lists of cations and oxyanions adsorption isotherm constants and their isotherm characteristics.

	pH	Range of Γ studied	Langmuir Equation * $C_{equil}/\Gamma=K_L/\Gamma_{max}+(1/\Gamma_{max})C_{equil}$		
Oxyanions			K_L (mmol/L)	Γmax (mmol/g)	r^2 ***
AsO_4^{3-}	5.5	1.10 ~ 3.97	0.016	3.92	0.99
PO_4^{3-}	4.5	0.84 ~ 2.32	0.026	2.39	0.99
CrO_4^{2-}	5.5	0.14 ~ 4.58	0.074	4.82	0.98
AsO_4^{3-} *ref#.*	5.0~6.0		3.96E-04 ~ 3.09E-04	1.1 ~ 0.85	0.99
			Freundlich Equations** $\Gamma = K_F \bullet C_{equiln}$		
Cations			K_F	n	r^2
Pb^{2+}	4.5	0.04 ~ 1.34	1.42	0.44	0.96
Zn^{2+}	5.5	0.01 ~ 1.40	1.85	0.59	0.99
Pb^{2+} *ref##.*	4.1~5.0	5.66E-04 ~ 1.42		0.5	

*** C_{equil} is the equilibrium concentration of ions in solution (mmol/L), Γ is the adsorption per unit mass adsorbent (mmol/g), K_L is the Langmuir constant(mmol/L), Γ_{max} is the maximum adsorption per unit mass adsorbent (mmol/g).**

**** K_F is the Freundlich constant, all the other terms are defined above.**

***** r is the correlation coefficient**

***ref#* (Pierce and Moore, 1982)**

***ref##* (Benjamin and Leckie, 1981)**

The results of lead and zinc cation adsorption as a functon of pH are shown in Figure 5.1.4. Their adsorption increases rapidly with rising pH despite precipitation due to hydrolysis which occurs at high pH. Figure 5.1.5 shows a constant pH isotherm of cations adsorption. In contrast to oxyanions, the cations show the characteristic shape of a Freundlich sorption isotherm. The adsorption isotherm constants and the isotherm characteristics for all oxyanions and cations are collected in Table 5.1.1.

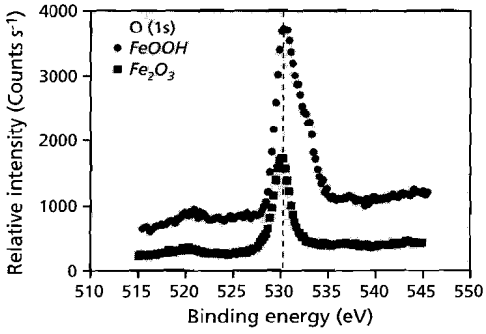

Fig. 5.1.6 O(1s) spectra of Fe_2O_3 and black FeOOH

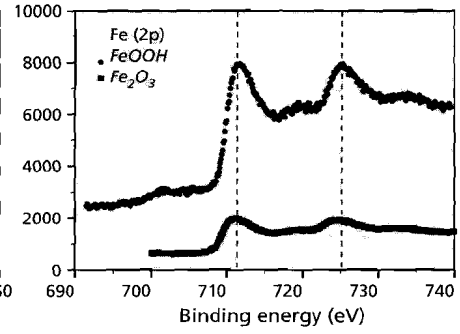

Fig. 5.1.7 Fe(2p) spectra of Fe_2O_3 and black FeOOH

Table 5.1.2. Summary of FeOOH and Fe_2O_3 core XPS spectra

FeOOH	Measured binding energy (eV)	Reference * binding energy (eV)
O(1s) O^{2-}	530.1, FWHM = 2.5	530.3 ± 0.2
O(1s)OH^-	531.2, FWHM = 3.0	531.4 ± 0.2
Fe(2p1/2)	725.0, FWHM = 5.0	724.9 ± 0.2
Fe(2p3/2)	711.7, FWHM = 4.2	711.9 ± 0.2
Fe(3s)	94.3, FWHM = 3.9	94.2 ± 0.2
Fe(3p)	56.3, FWHM = 3.8	56.6 ± 0.2
Fe_2O_3	Measured binding energy (eV)	Reference binding energy (eV)
O(1s)O^{2-}	530.2, FWHM = 2.61	
Fe(2p1/2)	725.5, n.d.	
Fe(2p3/2)	711.3 n.d.	710.7, FWHM = 4.8

* McIntyre and Zetaruk (1977)

X-Ray Photoelectron Spectroscopy of Amorphous FeOOH and Fe_2O_3

Figure 5.1.6 shows the O(1s) XPS spectra of synthesized amorphous black ferric oxyhydroxide and hematite. Clearly, the spectrum of O(1s) of ferric oxyhydroxide contains two peaks. One centered at 530.1(eV), with a FWHM of 2.52(1.64) (eV) is due to oxygen, the other centered at 531.2 (eV), with a FWHM of 2.95(2.80) (eV) to hydroxyl. The spectrum of O(1s) of hematite has only one very sharp peak centered at 530.2 (eV), with a FWHM of 2.61(eV). These results suggest that a clear difference of Fe(III) oxide and oxyhydroxide reflects on the difference of their O(1s) XPS spectra.

The Fe(2p1/2, 2p3/2) XPS spectra of FeOOH and Fe_2O_3 are shown in Figure 5.1.7. All the XPS results of our synthesized FeOOH and Fe_2O_3 agree well with the reference data, as summarized in Table 5.1.2.

Conversion electron Mössbauer spectrosocpy (CEMS)

Conversion electron Mössbauer spectra of black iron oxyhydroxide, brown iron oxyhydroxide, and hematite are shown in Figure 5.1.8. The black and brown variety of FeOOH are indistinguishable from one another in the surface layer sensitive to CEMS (100 nm). None of the samples is magnetically ordered at room temperature. The quadrupole splitting of both samples agrees with that of β-FeOOH (akageneite) in which normally two doublets are visible with splittings of 0.55 and 0.95 mm/s (Murad and Johnston, 1987). Black iron oxyhydroxide transforms to specular hematite upon heating, the transformation being near completion after 4 hours at 250°C with a concomittant density increase from 3.04 to 4.91 gr/cc. Spectrum 3 shows the result with as major component hematite(55%), and a second component which in all likelyhood also consists of hematite in which the grains are sufficiently small that the Fe spins exhibit superparamagnetic behavior. The third component in this spectrum looks very similar to that of the starting material indicating that the sintering from FeOOH to Fe_2O_3 has not gone to completion.

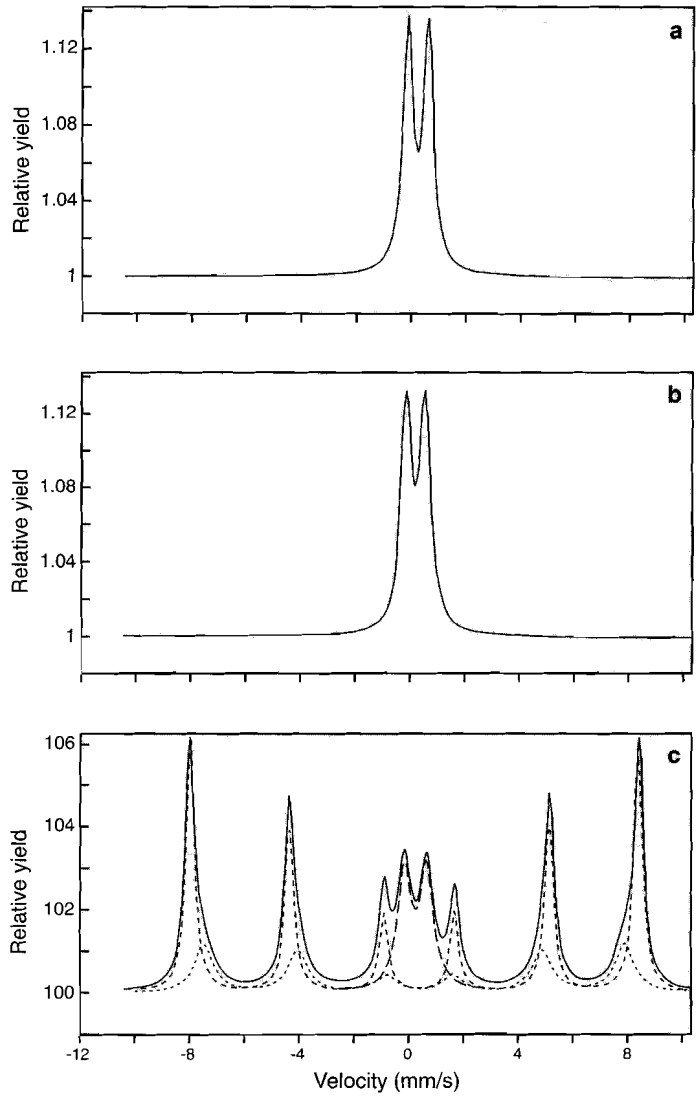

Fig. 5.1.8 Conversion electron Mössbauer spectra of brown FeOOH(a), black FeOOH(b), and heated treated black FeOOH(c). The quadrupole splitting and isomer shift of the doublets are characteristic of akaganeite. The sextet in (c) is in actuality due to two forms of hematite, one of which, due to its small crystallite size exhibits superparamagnetism. The central doublet in (c) shows that not all FeOOH is crystallized.

5.1.4. Discussion

We focussed our study on a novel form of iron oxyhydroxide, a black variety similar to specular hematite. The reason for using this material rather than the identical brown variety which is the result of precipitation from sulfate containing solutions, is the high surface area and friability of the black variety. These physical advantageous characteristics magnify the phenomena associated with surface adsorbtion enabling a subtantially more detailed assesment of its principles and characteristics. We shall start this discussion with the nature of black iron oxyhroxide, followed by the cause for its color, the characteristics of the adsorbtion of cations and anions, and finish with a discussion of its adsorbtion isotherms.

The nature of amorphous black ferric oxyhydroxide

Black ferric oxyhydroxide is an x-ray amorphous, friable material with conchoidal fracture and a density around 3.1 gr/cc (de Jong, 1982). Multi point BET (Juergens, 1995) analysis shows that the surface area of this material lies around 300 m^2/gram depending on the preparative conditions, the highest value found in our experiments being 333 m^2/gram. Hysteris loops of the adsorbtion-desorbtion isotherms show that most samples have an type E hysteresis loop (Juergens, 1995). This type of hysteresis loop can be attributed to ink-bottle pores, i.e. pores with a small neck. The pore size distribution of black FeOOH is also variable, the sample with a surface area of 333 m^2/gram having a narrow distribution with an average pore diameter of 3.2 nm. It is likely that the hydrolysis/precipitation with $Fe(NO_3)_3$ and NH_4OH gives this material its unique pore structure.

The color of black iron oxyhydroxide

Black iron oxyhydroxide has a dark red brown color in grains smaller than 40 μm. This puzzling large increase in visible light absorption as a function of particle size has been the subject of numerous studies (Schugar *et al.,* 1967, 1972, Rossman, 1975, 1976a,b, Manning, 1973, Strens & Wood, 1979) and reviewed in Cornell and Schwertmann (1996). The general conclusion reached is that the anomalously high extinction coefficient of specular hematite is caused by antiferromagnetic coupling of spins on neighboring sites. As argument against this conclusion can be stated that d(Fe-Fe) in hematite is 0.289 nm versus 0.304, 0.306, 0.301-0.328 in akageniete, lepidocrocite, and goethite respectively. Considering that spin coupling decreases at some large power n of $(1/r)^n$ (cnf Mydosh, 1993), one would not expect specular hematite and black ferric oxyhdroxide to have similar extinction coefficients. Against this interpretation argues additionally that whereas black ferric oxyhydroxide with an akageneite-like edge sharing array of ferric octahedra shows specular reflectance, lepidocrocite and goethite do not, nor does the akageneite-like amorphous red ferric oxyhydroxide which we synthesized.

PZC dependent adsorption

One of the important properties of ferric oxyhydroxide is its Point of Zero Charge (PZC) generally laying in the range between pH 7-8. Thus for a solution pH below 7, the surface charge of ferric oxyhydroxide will be positive and anions, sensitive to this charge will be adsorbed below this pH and desorbed above it. Similarly at a solution pH above 8, cations will be adsorbed on the, at that pH, negatively charged surface of ferric oxydroxide. However ions which form sufficiently strong chemical bonds with the ferric oxyhydroxide surface will affect the PZC substantially. Adsorption of such ions will not follow surface charge density versus pH, and thus adsorption will not be affected by the PZC.

Figure 5.1.1 and Figure 5.1.4 indicate clearly that sorption of chromate, lead, and zinc depend on the PZC of the substrate. At a pH below 7, CrO_4^{2-} is substantially sorbed as mentioned by Benjamin and Leckie (1981), and at a pH above 8, Pb^{2+} and Zn^{2+}. However neither phosphate nor arsenate, show in their adsorption behavior a clear change when crossing the PZC. These results suggest that the chemical bond between ferric oxyhydroxide and arsenate or phosphate is much stronger and not influenced by van der Waals type interactions due to surface charge. Furthermore, the binding energy between phosphate and ferric oxyhydroxide is larger than that of arsenate.

Adsorption isotherms

In aquatic system, adsorption between ions and adsorbent is not only influenced by solution pH, but also type of ion, their concentration and the nature of the adsorbent. Adsorption mechanisms and isotherms are not unique but depend on experimental conditions. We have carried out a study on adsorption mechanisms of the five selected ions by testing the substrates before and after adsorption using XPS, the results of which we shall present elsewhere (Ding *et al.*, 1998c). Here, we shall focus on the adsorption isotherms of these ions.

For every ion studied, its adsorption isotherm was obtained by measuring the ion partitioning between ferric oxyhydroxide and the solution phase over a specified range of total ion concentration, the amount of adsorbent, and pH. The themodynamic constant in either the Langmuir equation, K_L or in the Freundlich equation, K_F gives such partitioning potential and is a measure of bond strength (Benjamin 1983) in specific situation.

For example, as seen from Table 5.1.1, the value of phosphate $K_{L\,(P)}$=0.026 is larger than that of arsenate $K_{L(As)}$=0.016. We expect therefore theoretically that chemical bonding between phosphate and ferric oxyhydroxide will be stronger than between arsenate and the substrate. Two of our experimental results support this contention. One comes from the adsorption of oxyanions as a function of pH. The PZC of ferric oxyhydroxide

affects phosphate absorption less than arsenate, suggesting that the adsorption between phosphate and ferric oxyhydroxide involves chemical bonding rather than surface charge balancing. Secondary evidence comes from our mixed oxyanion experimental result. As illustrated in Figure 3, the presence of PO_4^{3-} reduces AsO_4^{3-} adsorption significantly but the presence of arsenate has no effect on phosphate adsorbtion. The non-linearity in absorbance of a system containing two oxyanions is a manifestation of the mixed anions effect wich in solid electrolytes manifests itself as a non-linear increase in electrical conductivity of intermediate compounds vis a vis theirend members (Mizzoni *et al.*, 1988; Kudo and Fueki 1990).

However, in comparing the value of phosphate $K_{L(P)}$=0.026 with that of chromate $K_{L(Cr)}$=0.074, we might conclude that chemical bonding between chromate and ferric oxyhydroxide is stronger than that between phosphate and the adsorbent. This conflicts with our results on the adsorption of chromate as a function of pH, which indicates that CrO_4^{2-} adsorption depends strongly on the PZC. Therefore, for PZC dependent adsorption, it seems more reasonable to consider K_L as a measure of partitioning potential rather than a measure of bond strength.

As last point we want to point out that, Γ_{max} of our arsenate adsorption is about 3 times larger relative to values reported elsewhere for conventional ferric oxyhydroxides. Besides its obvious industrial utility it is important in our surface studies because it enables characterization of the ferric oxydroxide surface states and their variation upon sorption using XPS, which generally as detection limit requires more than 4 wt% (element/substrate).

5.1.5 Summary and conclusion

In the course of a study on self sealing/healing layers in chemically contrasting solid wastes, we have synthesized and characterized a novel form of ferric oxyhydroxide. This material gets its unique properties by hydrolysis of ferric nitrate with ammonia. It is black, amorphous with a local structure similar to akaganeite (β-FeOOH), fractures conchoidally, has a Point of Zero Charge at pH between 7 and 8, a surface area around 300 m^2/gram and ink bottle shaped pores with pore diameter around 4 nm. Its adsorbtion characteristics have been determined using three oxyanions, chromate, arsenate, and phosphate, and two cations lead and zinc. Of the oxyanions, arsenate and phosphate, and, as demonstrated elsewhere, molybdate and tungstate adsorbtion are not PZC dependent, whereas chromate, and lead, and zinc are. This possibility for regeneration of an adsorbing substrate by pH switching around the PZC is an important industrial asset. The absolute adsorbtion characteristics of this material as inferred from their Langmuir and Freundlich adsorbtion isotherms are three times higher than that of conventional ferric oxyhydroxides.

Chapter 5.2

XPS studies on the electronic structure of bonding between solid and solutes: adsorption of arsenate, chromate, phosphate, Pb^{2+}, and Zn^{2+} Ions on amorphous black ferric oxyhydroxide

Abstract

We characterized in a previous paper (Ding *et al.*, 1998b) the adsorbtion of three anions and two cations on a novel form of amorphous black ferric oxyhydroxide which resembles in local structure β-FeOOH, akaganeite. Here we characterize the nature of the interaction between FeOOH substrate and admolecules with photoelectron spectroscopy on the core and valence band levels of trivalent iron and oxygen using frontier molecular orbital theory as theoretical framework. Our findings indicate that substantial and variable charge transfer occurs in which the FeOOH substrate can function either as a Lewis acid or base. Our findings also indicate that large variations in valence band XPS spectra are observed for the least strongly bound surface ions in accordance with expectations from frontier molecular orbital theory.

5.2.1 *Introduction*

Hydrous ferric oxide has been the subject of a large number of studies ably reviewed in some recent chemical, geochemical, and hydrometallurigical books such as Cornell and Schwertman (1996), Dzombak and Morel (1990), Voigt *et al.*, (1997), and Dutrizac and Harris (1996). In the course of a study on self-sealing/healing layer formation in porous media (Ding *et al.*, 1996, 1997, 1998a), we have reported previously (Ding *et al.*, 1998b) the synthesis of a new black form of amorphous ferric oxyhydroxide resembling in local structure akaganeite and characterized it with X-ray photoelectron spectroscopy (XPS), conversion electron mössbaur spectroscopy, and classical aquatic adsorption experiments.

Despite much theoretical and experimental work on cation and anion absorption on ferric oxyhydroxides focussing primarily on solutes in aquatic systems, much remains to be done in terms of detailed chemical reaction mechanisms involving characterizable elementary chemical steps. Recent developments in analytical technique have started to provide detailed structural and chemical observations of adsorbates (Becker *et al.*, 1997) and provided more direct and quantitative information of the sorbed complex, as for instance summarized by Brown (1990) in his spectroscopic studies of chemisorption reaction mechanism at oxide-water interfaces. Among these techniques, EXAFS has been widely adopted to probe the surface structure (Waychunas *et al.*, 1995, 1996) primarily delineating the various geometries of adsorption complexes such as inner-sphere, outer-sphere, mono-dentate, bi-dentate and so on. From a quantum mechanical perspective the state of describing the interaction between adsorbate, the adions or admolecules, and substrate remains by and large wanting. To get to this next stage requires exploration of the nature of the chemical reaction between solid and solute. To do so we need to know first of all how and if electrons transfer from substrate to adducts i.e. the direction of charge transfer. Secondly we need to know the relative position of empty and occupied energy states of substrate and adduct to asses their mutual affinity. X-ray photoelectron spectroscopy (XPS), as a surface analytical technique, provides the proper level of information to answer these questions or at least provide internally consistent rationalizations between spectroscopic and solution chemical observations.

XPS is a surface analytical technique devised at the end of sixties to provide chemical analyses of surfaces (Siegbahn *et al.* 1967). Since the early seventies studies on FeOOH have been carried out focussing primarily on testing core levels spectra of pure materials. In the course of these studies it became clear that chemical shielding affects the position of these core levels. To quantify the nature of these shifts Bagus and Bauschlicher (1980) carried out Hartree Fock calculations on an oxygen atom with varying charge showing that variations in valence state occupancy can cause a chemical shift of about 20 eV for the O(1s) core level. A simple formula based on these calculations relating O(1s) binding energy with oxygen valence charge was subsequently devised to get an internally consistent oxygen charges for oxide materials (de Jong, 1989, de Jong *et al.*, 1994). The issue here is if and how the O and Fe charge will vary when FeOOH reacts with adducts enabling an assessment of the magnitude and direction of electron transfer between substrate and adduct. In addition we wanted to rationalize how the valence band structure of FeOOH changes as a function of different adducts using a frontier orbital perspective as laid down by Fukui *et al.*, (1954), Klopman(1968, 1974), and Hoffman(1988).

The purpose of this research is then twofold: to determine the charge transfer between the FeOOH surface and the adducts adsorbed on it, and to study the nature of the interaction between FeOOH substrate and admolecules and ions from a frontier orbital perspective.

To accomplish these goals we have carried out XPS measurements on the pristine FeOOH substrate and its surface complexes. By tracking Oxygen (1s) and Fe core levels, e.g., the Fe (2p), Fe (3p), and Fe(3s) binding energy shifts relative to those of FeOOH itself, we determined the direction of charge transfer between substrate and adduct. The shifts in valence band XPS spectra of the surface complexes provide a quantitative measure of the resulting charge transfer between highest occupied and lowest unoccupied molecular orbital (HOMO-LUMO) and the character of bonding on surface complexes.

Our most interesting XPS results show that the FeOOH surface can act as a Lewis acid or base in its interaction with different adatoms and admolecules. Thus phosphate and arsenate oxyanions donate electrons to the substrate that acts therefore as a Lewis acid. The FeOOH surface functions as Lewis base in its interaction with chromate. The adsorption between the FeOOH surface and zinc or lead cations does not involve noticeable electron transfer as might be anticipated for an outer sphere complex. Our valence band XPS spectral results enable us to rationalize the relative affinity of absorption on FeOOH substrate which in decreasing order goes from P, As, Cr, Zn, to Pb. Our research indicates the feasibility to probe with XPS the solid-solute interface and to reveal the nature of chemical reactions in terms of charge and energy transfer between frontier orbitals.

5.2.2 Experimental

Synthesis of amorphous iron oxyhydroxide

Amorphous iron oxyhydroxide was prepared in a flask by hydrolysis of a stirred 0.1M $Fe(NO_3)_3$ solution with 0.1M $NH_3 \cdot H_2O$. The temperature was kept constant (at 50 °C) with a recirculating water bath. Base was introduced by automatic titration at a constant rate of about 2 drops/s, up to a solution pH of 7.5 after which the solution was stirred for another half hour. The resulting suspension was filtered, washed firstly with distilled water; next three times with a pH 7 washing solution, and diluted with distilled water.

XPS specimen preparation

The experimental XPS measurements and their energy calibration have been mentioned elsewhere (Ding *et al.*, 1998b). Sample prepation for our XPS measurements, involved running individual adsorption experiments at a constant pH of 4.5 (for arsenate and phosphate), pH 5.0 (chromate), pH 5.5 (for zinc), and pH 4.5(for lead). The selected pH values for oxyanions reflect their maximum adsorption capacity and to avoid zinc and lead surface precipitation during adsorption. 10 ml of 0.1 M arsenate (in the form of H_3AsO_4), phosphate (in the form of NaH_2PO_4), chromate (in the form of K_2CrO_4), lead (in the form of $Pb(NO_3)_2$) and Zinc (in

the form of $Zn(NO_3)_2$) were mixed with a 200 ml $Fe(OH)_3$ suspension containing 0.056 gram ferric iron. The ionic strength of the solutions was controlled with 0.1N $NaNO_3$. The experiment was conducted in a sealed reaction flask with continuous N2 sparge, keeping the temperature constant at 25°C. The suspension was kept stirring for 24 hours. After filtration, the residue was dried overnight in an oven at 105°C. The resulting black specimen consisted of x-ray amorphous FeOOH only. The dried material was powdered and pelletized under vacuum, following the common procedure used in preparing KBr pellets for IR spectroscopy.

XPS measurements

XPS measurements were carried out on OCTOPUS, a multichamber UHV preparation and analysis system connected to a 3MV single-ended and a 6 Mv tandem van der Graaff generator, using a Clam-2 hemispherical sector analyzer and a VG XR2F2 twin anode x-ray source with standard Al/Mg anodes. Spectra were recorded using the AlKα source operated at a power of 120W and a constant pass energy of 20 eV for the analyzer, using the C (1s) spectral line as reference.

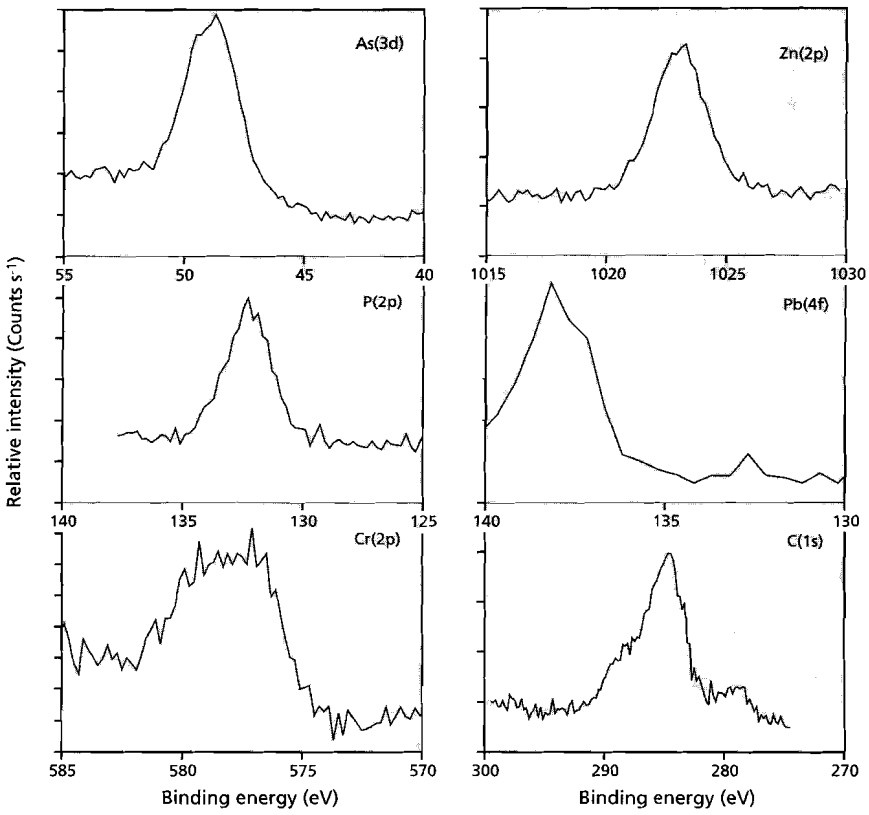

Fig. 5.2.1 Photoelectron spectra of anions and cations on black iron oxyhydroxide.

5.2.3 Results

Cations and oxyanions identification using XPS spectra

The cations Zn^{2+} and Pb^{2+}, oxyanions AsO_4^{3-}, PO_4^{3-} and CrO_4^{2-} in their FeO(OH) surface complexes are individually detectable with XPS, as shown in Figure 5.2.1. Our measured binding energies of each element agree well with reference XPS data (Wagner *et al.*, 1978). Our chemical analyses show about 8 wt% , 7 wt%, 6 wt% , 10wt%, and 9 wt% of As, P, Cr, Zn, and Pb respectively as being present in surface complexes.

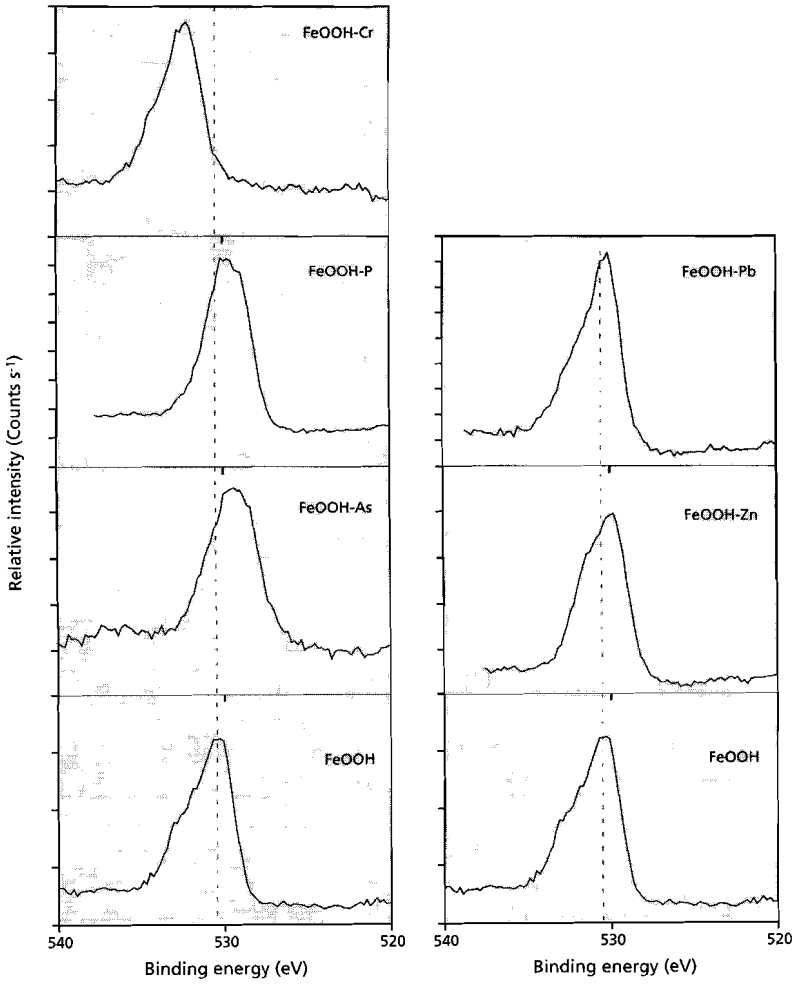

Fig. 5.2.2 O(1s) core level photoelectron spectra of anions and cations adsorbed on black iron oxyhydroxide and of pristine FeOOH.

O (1s) spectra of FeOOH surface complexes

After exposing the FeOOH substrate to solutions containing arsenate, phosphate, and chromate oxyanions, changes in intensity as well as peak position occur in the spectrum of O(1s) in comparison to that of pure FeOOH as indicated in Figure 5.2.2. Our results show that due to the chemical adsorption between substrate and adducts, the peak of O(1s) spectra of surface complexes has shifted to less negative binding energy for arse-

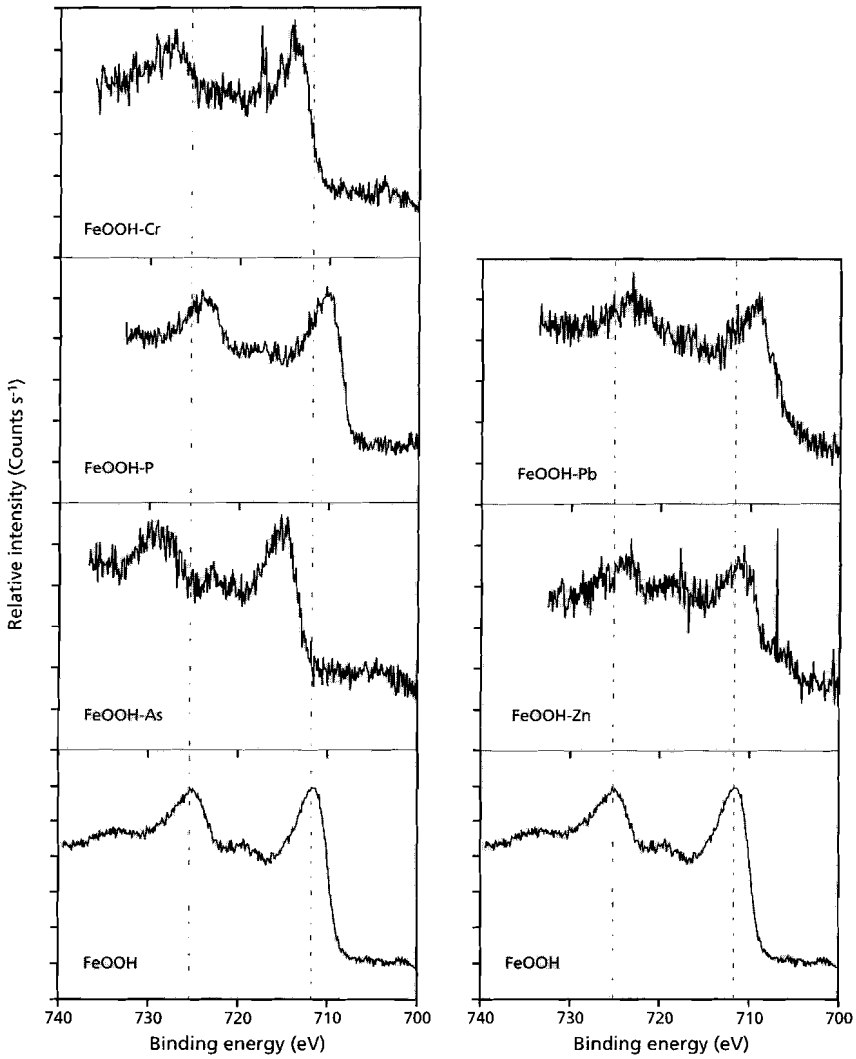

Fig. 5.2.3 Fe (2p) core level photoelectron spectra of anions and cations adsorbed on black iron oxyhydroxide and of pristine FeOOH

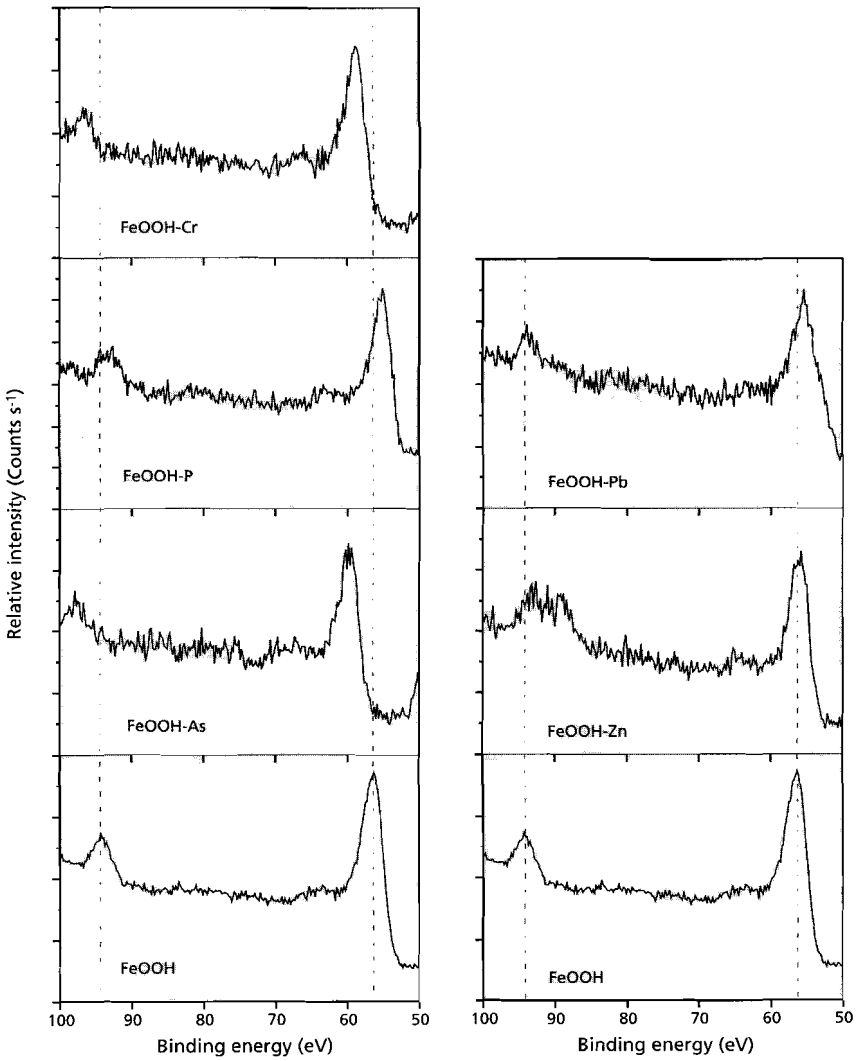

Fig. 5.2.4 Fe(3s) and (3p) core level photoelectron spectra of anions and cations adsorbed on black iron oxyhydroxide and of pristine FeOOH

nate and phosphate relative to that of FeOOH, and more negative binding energy for chromate. In contrast the peak shift is negligible for substrates on which the cations lead and zinc are adsorbed as illustrated in Figure 5.2.2.

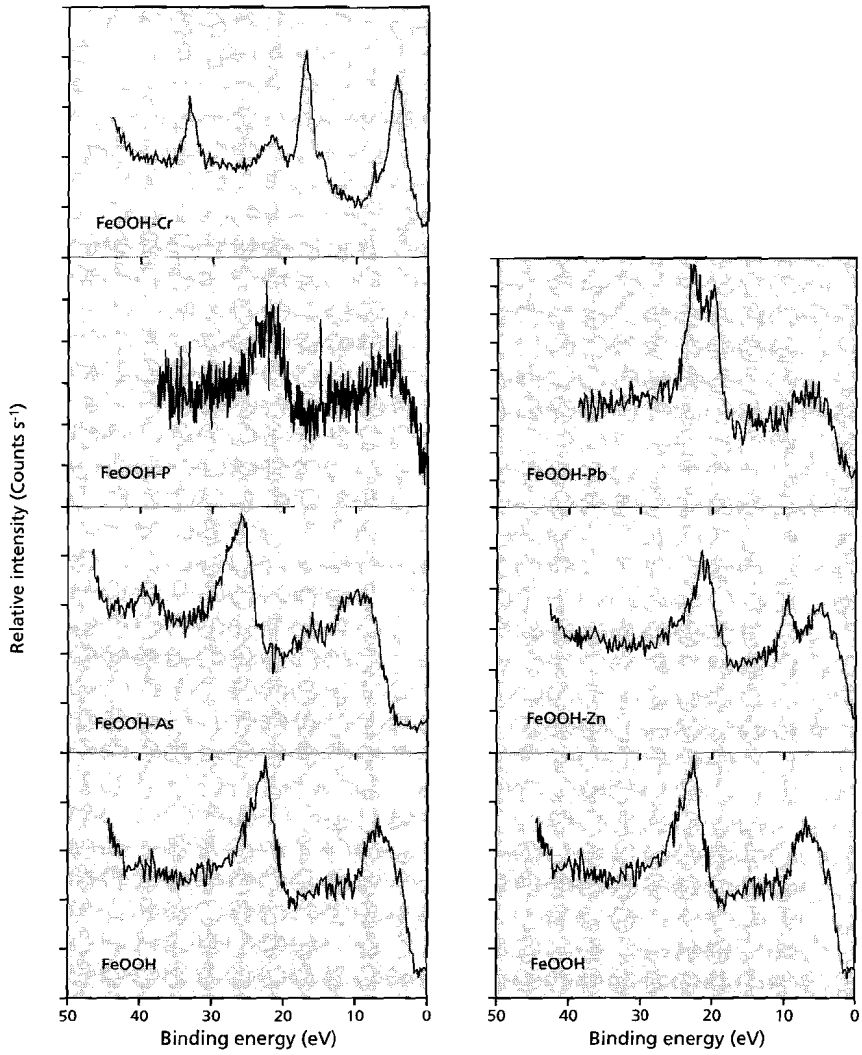

Fig. 5.2.5 Valence band spectra of FeOOH and FeOOH with adsorbed cations and anions

Fe (2p) and Fe (3s, 3p) spectra of FeOOH surface complexes

Similarily, core level Fe(2p) spectra of adsorbates show different degrees of shift relative to the pure substrate, as demonstrated in Figure 5.2.3. In comparison with FeOOH, the Fe(2p) XPS spectra of adsorbates of arsenate, chromate shift to more negative binding energy, whereas that of phosphate, zinc and lead shift to only slightly less negative

binding energy. Similar trends to those in Fe(2p) XPS spectra, are detected in Fe(3s, 3p) spectra of FeOOH adsorbates as shown in Figure 5.2.4.

Valence band spectra of FeO(OH) surface complexes

Figure 5.2.5 present the valence band spectra of surface complexes and substrate. As can be seen, the valence band spectra of FeOOH-As and FeOOH-P complexes are almost identical to that of FeOOH, whereas those of FeOOH-Cr, FeOOH-Zn, and FeOOH-Pb are distinctly different from that of FeOOH.

5.2.4 Discussion

In the following we shall address two issues. The first one is the nature of the overall charge transfer as deduced from core level XPS shifts of iron and oxygen, in short the chemistry of complex formation. The second one is the nature of this charge transfer, the relation between HOMO and LUMO of substrate and admolecules or atoms, as deduced from XPS variations of the valence band.

Effect of charge transfer on the binding energy of the core levels

As observed in our O(1s), Fe(2p),and Fe(3s,3p) spectra of FeOOH surface complexes, core level binding energy shifts occur relative to those for the FeOOH substrate. These core level shifts reflect electron transfer in the valence band, where the actual charge transfer due to chemical reactions has to take place. Therefore, by tracking the change in core level peak position of the substrate with and without formation of surface complexes, it is possible to deduce the direction of electron transfer during adsorption.

The relation between oxygen (1s) binding energy and the direction of charge transfer in the valence states

The oxygen (1s) binding energy and intensity shift depend on the concentration of different oxygen atoms in particular on the surface of a material. These core level shifts can be correlated with variations in charge density of oxygen in the valence band as shown by Bagus and Bauschlicher (1980). A simple formula connecting O(1s) chemical shift and charge can be constructed having as principal advantage that all charges derived in this manner are internally consistent (de Jong, 1989, de Jong *et al.* 1994)

$$Qo = -4.372 + [385.023 - 8.976\,(545.509 - O1sBE)\,]^{1/2}/4\,.\,488 \qquad (5.2.1)$$

Here Q_o is the actual oxygen charge in a material and O1sBE is the O(1s) binding energy as determined from XPS. It should of course be kept in mind that charges as such never represent absolute values but depend on the way electron density is partitioned over the different atoms making up a molecular frame. However the values calculated according to the above formula tend to be close to those deduced from *ab initio*

Hartree Fock calculations on oxygen containing molecules using a Mulliken population analysis, *e.g.* -0.74 for O in SiO_2 vs -0.81 calculated for the bridging oxygen atom in $H_6Si_2O_7$ (de Jong, 1989, Burhardt *et al.*, 1991) , so some fair consistency prevails.

Applying the above equation to our particular experiments, the actual oxygen charge of FeOOH and its variation on surface complexation can be calculated as summarized in Table 5.2.1. Inspection of this table indicates that oxygen can either become more or less negative relative to the oxygen charge on FeOOH which we took as point of reference.

Thus, the oxygen charge of the FeOOH-Cr surface complex is less negative than that of FeOOH itself, indicating that during the chemisorption of Cr on FeOOH electron transfer occurred from substrate to adduct. In contrast, the oxygen charges in surface complexes of FeOOH-As and FeOOH-P are more negative than that of FeOOH, indicating that during chemisorption of As and P on FeOOH electron transfer from adduct to substrate occurs. In other words, the surface of FeOOH acts as Lewis base, an electron donor, to chromate admolecules, and as Lewis acid, an electron acceptor to arsenate and phosphate admolecules. The magnitude of the oxygen (1s) chemical shift indicates the strength of the surface-oxyanion interaction without giving explicit information of the nature of this interaction.

The oxygen charges in both zinc and lead FeOOH surface complexes are similar to those of the pristine substrate, indicating that adsorption of lead and zinc on FeOOH does not involve noticeable electron transfer between surface and adsorbate and suggesting that these cations form weak bonds with the FeOOH substrate.

Table 5.2.1. Oxygen (1s) binding energies and oxygen charges for FeOOH and its surface complexes

compounds	binding energy (eV)		oxygen charge		charge transfer relative to O in FeOOH
	O	OH	O	OH	
FeOOH	530.3	531.7	-0.859	-0.772	
FeOOH-As	528.4	529.3	-0.982	-0.924	accepts electrons
FeOOH-P	528.9	529.3	-0.949	-0.924	accepts electrons
FeOOH-Cr	532.1	532.7	-0.747	-0.710	donates electrons
FeOOH-Pb	530.4		-0.853	-	no transfer
FeOOH-Zn	529.9	531.3	-0.885	-0.797	no transfer

The relation between Fe core level binding energy and the direction of electron transfer in valence states

The relation between oxygen (1s) binding energy and its actual charge in a compound should of course be consistent with shifts and charges for Fe core level binding energies. Experimentally these shifts are on the order of 5 eV thus substantially smaller than the approximately 20 eV which covers the range from 0 to -2 for oxygen. By correlating the oxygen charge with that for iron in iron oxides, and connecting these charges with observed, core level Fe XPS results provide an internally consistent assessment of the direction of charge transfer between the FeOOH substrate and adsorbates.

There exists indeed a linear relation between Fe core level binding energies and their actual charge when plotted against one another for metallic iron and iron oxides. The results of this procedure are summarized in Table 5.2.2 where the quantitative relation between Fe core level binding energies for Fe(2p), Fe(3s), and Fe(3p) are shown as well as the linear formula connecting charge, Q, with binding energy, X. All the binding energy data come from reference (McIntyre and Zeatruk, 1977). The oxygen charge is calculated according to Eq. 5.2.1.

Table 5.2.2 The relation between Fe core level binding energy and its charge

compound	binding energy (eV)				calculated charge		equations*
	Fe(2p)	Fe(3)	Fe(3)	O(1s)	iron	Oxygen	
Fe	706.9	53.0	90.9		0		Q Fe(2p) = 0.3233X-228.51, r2 = 0.999
FeO	709.5	54.9	92.5	530	+0.8786	-0.8786	Q Fe(3p) = 0.4835X-25.632, r2 = 0.998
Fe_2O_3	711.0	55.7	93.6	530	+1.3179	-0.8786	Q Fe(3s) = 0.4925X-44.744, r2 = 0.993

* Q Fe(i) is the charge of Fe with respect to (i) core level, X is the binding energy of Fe(i) core level, r is the correlation coefficient.

Table 5.2.3 Fe core level binding energies and Fe charges for FeOOH and its surface complexes

compounds	Fe core level energy (eV)			Fe charge				charge transfer relative to Fe in FeOOH
	Fe(2p)	Fe (3p)	Fe (3s)	Fe(2p)	Fe(3p)	Fe(3s)	aver.	
FeOOH	711.7	56.3	94.3	1.58	1.59	1.70	**1.62**	
FeOOH-As	716.9	59.7	97.9	3.26	3.23	3.47	3.32	Fe donates electrons
FeOOH-P	710.3	55.2	93.2	1.13	1.06	1.16	1.12	Fe accepts electrons
FeOOH-Cr	713.6	58.8	96.6	2.20	2.80	2.83	2.61	Fe donates electrons
FeOOH-Zn	710.6	55.8	93.0	1.23	1.35	1.06	1.21	Fe accepts electrons
FeOOH-Pb	709.6	55.5	93.9	0.90	1.20	1.50	1.20	Fe accepts electrons

With the formulas in Table 5.2.2 we can relate the observed Fe core level binding energies for FeOOH and its surface complexes to their iron charge as summarized in Table 5.2.3. Our results in Table 5.2.3 suggest that the adsorption of arsenate and chromate on FeOOH affects the charge on the iron atom much more strongly than that of phosphate, zinc, and lead. In particular the adsorption of zinc and lead on FeOOH has virtually no effect on the charge density on Fe .

Combining the results from Table 5.2.1 and Table 5.2.3, as illustrated in Figure 5.2.6, reveals that the FeOOH substrate surface acts as a Lewis acid on adsorption of phosphate: iron becomes less positive and oxygen more negative relative to iron and oxygen in FeOOH. It also reveals that the FeOOH substrate surface acts as a Lewis base on adsorption of chromate: iron becomes more positive and oxygen less negative relative to iron and oxygen in FeOOH, and that the adsorption of zinc and lead on FeOOH, involves virtually no charge transfer. However our results also reveal mixed behavior as indicated by the adsorption of arsenate on FeOOH in which the oxygen atom becomes more negative and the iron atom more positive *vis a vis* those for FeOOH or in other words the oxygen atom acts as a Lewis acid and the Fe atom as Lewis base. It of course remains puzzling why the chemical interaction between FeOOH and phosphate is stronger than that of FeOOH and arsenate, as we observed in our competitive aquatic chemical experiments presented previously (Ding *et al.*, 1998b). To rationalize this we need to consider the frontier orbitals between substrate and admolecules.

Interaction of orbitals on FeOOH surface

Frontier orbitals are important in the study of interactions between two molecules because they determine the character of charge transfer and thus the nature of the bonding. Two factors characterize this interaction: the difference in energy between the highest occupied and lowest unoccupied state between subtrate and adduct and the overlap between the molecular orbitals on substrate and adduct as shown in Figure 5.2.7 according to Hoffmann (1988).

In our particular case, according to our oxygen (1s) and Fe core levels photoelectron spectra, the overall effect is that the surface of FeOOH serves as Lewis base or Lewis acid to oxyanions adsorbates. Alternatively, we can state that the interaction of HOMO/LUMO in FeOOH with those of the adsorbates results in bonding formation between substrate and adsorbates.

Further qualitative analysis of the orbitals and their interaction can be done by simple perturbation MO theory. This theory predicts that for two interacting orbitals of suitable symmetry and overlap, the smaller the difference in orbital energies, the greater the mutual perturbation or interaction. Thus the interaction between two systems invoved in MO interaction is described by the expression (Hoffmann 1988):

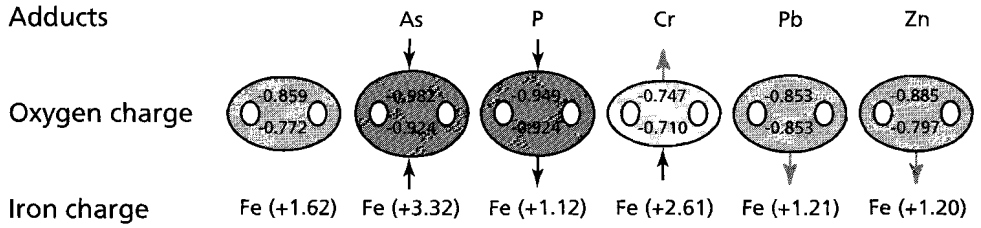

Fig. 5.2.6 Synopsis of charge transfer across the oxide surface in FeOOH for the different cations and anions

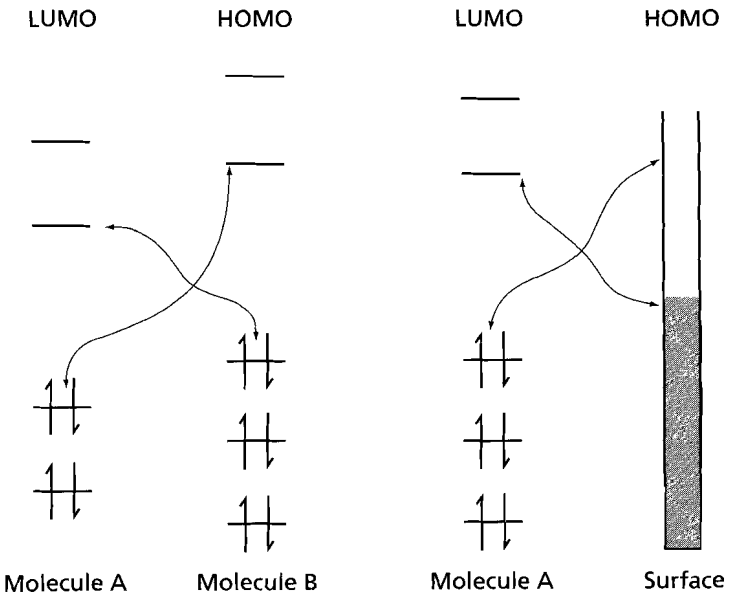

Fig. 5.2.7 Principles of HOMO-LUMO interaction according to Hoffmann (1988)

$$\Delta E = \frac{|H_{eg}|^2}{E_e - E_g}$$

where, ΔE is potential energy of the combined system, E_e and E_g are the excited (empty) acceptor state and filled ground donor state energy respectively, and H_{eg} is the strength of the pertubation. Clearly, for a specific perturbation strength, the greater the energy separation of the two systems, the lower the potential energy of the compound. Conversely, the less the energy level separation, the larger the potential energy of the compound.

The highest occupied MO's in FeOOH are primarily non-bonding O 2p-like states (Sherman, 1985) and thus differ from the full 2t2g iron 3d crystal field orbitals which most likely make up the valence band edge of hematite (Zhang *et al.*, 1993). Inspection of the valence band photoelectron spectra (Figure 5.2.5) of FeOOH before and after adsorption, shows that the pattens of FeOOH-As and FeOOH-P are similar to that of FeO(OH), in contrast to marked differences between FeOOH and FeOOH-Cr, FeOOH-Zn and FeOOH-Pb. Employing perturbation theory in these cases, we conclude that the energy level separations between HOMO/LUMO in FeOOH and phosphate and arsenate are rather small so that after orbital interaction no large spectral variation occurs. Consequently, we expect the potential energy of FeOOH-P and FeOOH-As compound to be high and therefore chemically difficult to dissociate. In contrast to phosphate and arsenate, the energy level separations between HOMO and LUMO in FeOOH-Cr, FeOOH-Pb and FeOOH-Zn cases are large, as reflected in the large spectral variation. Following the same argument, we therefore predict that chemical dissociation of FeOOH-Cr, FeOOH-Pb and FeOOH-Zn is easier than that of FeOOH-P and FeOOH-As. These results agree well with our aquatic chemical experiments, where FeOOH-As and FeOOH-P complexes remain stable at pH values far above the point of zero charge, whereas the release or adsorption of cation or anion on FeOOH-Cr, FeOOH-Zn and FeOOH-Pb is directly related to the point of zero charge.

5.2.5 Summary and Conclusions

Our X-ray photoelectron spectroscopy measurements on black iron oxyhydroxide FeOOH and its surface complexes FeOOH-As, FeOOH-P, FeOOH-Cr, FeOOH-Pb and FeOOH-Zn indicate that chemisorption occurres between substrate and oxyanions admolecules. In chromate adsorption, electrons are transferred from substrate to adduct in which the surface of FeOOH functions as Lewis base. Contrary, in the adsorption of arsenate and phosphate, electrons transfer from adduct to substrate. In these cases, the surface of FeOOH functions as a Lewis acid. Adsorption of zinc and lead cations on FeOOH provides no clear evidence of chemisorption, i.e., there is neg-

ligible electron transfer between substrate FeOOH and adducts. Therefore, one can consider the adsorption between FeOOH and zinc and lead closer to physisorption in which hydrated clusters form outer sphere complexes.

Finally, we estimated qualitatively the energy level separation between HOMO and LUMO of the frontier orbitals for surface complexes. The energy difference between the HOMO and LUMO in FeOOH-P complex and FeOOH-As complex are small resulting in a substantial potential molecular energy. This implies strong chemical bonding between FeOOH and phosphate and arsenate. However, the energy differences between HOMO and LUMO in FeOOH-Cr, FeOOH-Pb and FeOOH-Zn are large. Therefore, the potential molecular energies of complexes FeOOH-Cr and FeOOH-Zn and FeOOH-Pb are small. We would expect weaker chemical bonding formation in FeOOH-Cr compound and almost no chemical bond formation in FeOOH-Pb and FeOOH-Zn. Our aquatic chemistry experiments (Ding *et al.*, 1998b) provide evidence consistent with these theoretical consideration.

Acknowledgements

I would like to thank the Faculty of Earth Sciences at Utrecht University for providing an "AIO" fellowship to carry out my Ph.D. study. Special thank goes to Professor Dr. R.D. Schuiling for supporting this research.

Chapter 6

General Conclusions

In this thesis the mechanism of formation of self-sealing layers in porous media and the impact of such self-forming layer on the transport and mobility of chemical constituents is studied systematically. Particular emphasis has been given to the layered acidic jarosite/alkaline coal fly ash system, because of the need to search for an alternative option to solve on the one hand the waste acidic jarosite leaching problem and on the other to keep jarosite as a resource for future use. This study is divided into four main themes.

I. Investigation of the feasibility of sealing layer formation in jarosite/fly ash with focus on the nature of the two parent materials, including their leaching behavior and acid-base properties.

II. Characterisation of the newly formed sealing layer and exploration of its effect on transport resistance and chemical retention of constituents.

III. Investigation of the effects of discontinuities in porous media on reactive transport in general, modelling sealing layer formation in layered materials, and experimental verification using radio tracer diffusion in the jarosite/fly ash system. Two computer programs DNLM and DPLM were developed for this purpose.

IV. Exploration of the nature of chemical reactivity of the sealing layer in jarosite/fly ash, i.e. chemical interaction between the FeOOH substrate, which is one of the newly formed phases in the sealing layer, and solutes such as arsenate, phosphate, chromate, Pb^{2+} and Zn^{2+}.

6.1 Starting materials, sealing layer formation, and feasibility

XRD results indicate that ammoniumjarosite $(NH_4)Fe_3(SO_4)_2(OH)_6$ and glassy amorphous phases dominate in waste jarosite and coal fly ash respectively. Chemical analysis of waste jarosite shows a fairly high amount of heavy and toxic elements such as Pb, Zn, and As. The acid-base titration results reveal that jarosite is acidic with a solution pH around 2 at a liquid to solid ratio of 10. The coal fly ash used in this study is alkaline with a solution pH around 12 at the same liquid to solid ratio. The results from the leaching tests indicate that the principal elements released from jarosite are Fe, Al, Zn, Ca, Pb, S, As and from fly ash Al, Ca, S. The release of Fe, Al, Zn, Pb, and As is strongly pH dependent and largely controlled by the solubility of the min-

erals. The release of sulphate is independent of pH and mainly controlled by its availability. The release of Ca is decreases at high pH, in all likelihood due to solubility control exerted by Ca containing minerals, such as $CaCO_3$, CaO, or calcium aluminum silicates.

According to their leaching behavior and acid-base properties, we can expect that as a result of the large pH gradient between the wastes, precipitation reactions will occur at the interface between jarosite and fly ash when the two are put adjacent to one another. These interface precipitation reactions will result in immobilization of most constituents released from both wastes due to low solubility or sorption. Based on preliminary calculation, the potential for precipitate formation in the system of jarosite/fly ash will be sufficient for sealing layer formation. Therefore, using self-sealing layers as a barrier for waste jarosite isolation and immobilization is certainly an option from a theoretical perspective. Another, alternative option to dispose of acidic jarosite in an environmentally sound manner is to simply mix acidic jarosite and alkaline coal fly ash. According to our acid-base titration experiments, only 25 wt% of fly ash will bring the solution pH of jarosite and fly ash at liquid to solid ratio of 100 up to about 5. Nevertheless, self-sealing isolation and immobilization is the recommended option because it enables jarosite to be recycled, in contrast to neutralization by mixing with alkaline coal fly ash which will prevent jarosite from being used as a future resource.

6.2 Characteristics and impact of the sealing layer in jarosite/fly ash

The interface of the jarosite/fly ash system has been studied by X-ray Diffraction (XRD), Optical microscopy, X-ray Photoelectron Spectroscopy (XPS), and Conversion Electron Mössbauer Spectroscopy (CEMS). Optical microscopy of thin sections of layered jarosite/fly ash showed clearly the formation of a new mineral layer between jarosite and fly ash. Interface XRD results indicated that gypsum $CaSO_4 \cdot 2H_2O$ as crystalline phase was formed as anticipated from our chemical reaction mechanism. As x-ray amorphous phase ferric oxyhydroxide FeOOH was formed as identified not only by its brownish color in thin section but also by XPS and CEMS.

The overall resistance to transport in the layered jarosite/fly ash system increased by about two orders of magnitude after only 3 days. This increase in overall resistance is primarily due to an increase in resistance of the interface self-forming layer. A quantitative assessment on how a change in resistance of a porous medium affects transport was made by simulating breakthrough curves of an inert constituent at various resistances. Comparing a $^{59}Fe^{3+}$ tracer diffusion experiment in jarosite only, with that in the layered jarosite/fly ash system, suggests that Fe^{3+} mobility is significantly affected by interface reactions. The reduction in Fe^{3+} mobility in the layered jarosite/fly ash

system is due to the extremely low solubility of ferric oxyhydroxide at the interface between these two materials, where a very sharp change in pH occurs. Along the same line of argument we predict the chemical retention of the cations such as Al^{3+} and Pb^{2+} in such a mixed system.

6.3 Mathematical description of reactive transport in layered materials

Considering discontinuities caused by physical or chemical gradients in porous media is paramount for an understanding of reactive transport under natural conditions. Generation of a reactive third zone, which possesses different transport and thermodynamic properties from either of the adjacent homogeneous layers, confirms the significant effect that such discontinuities in a porous medium have on the transport of dissolved constituents. In addition, the nature of the precipitates formed may also lead to secondary chemical interactions of dissolved constituents with the newly formed phases.

The effect of discontinuities caused by physical gradients in porous media can be described mathematically with a model which has analytical solutions under constrained initial and boundary conditions. The results of such model simulation indicate that physical gradients between layered materials are, relative to chemical gradients, of minor significance in the transport of constituents.

Mathematical modelling of the effects of discontinuities in porous media caused by chemical gradients has been carried out by simulating three typical cases: pH interface, linear adsorption (Kd) interface, and precipitation interface. The simulation results indicate that discontinuities caused by chemical gradients will not only affect the transport but also the mobility of constituents. As a consequence, interface reactions may locally affect the transport properties and develop a new reaction zone. Such zone has properties differing in transport and thermodynamics from the parental media and the potential to influence the overall transport process enormously. In the modelled jarosite/fly ash system, a new reaction zone of about 1 mm thick and reduced porosity (from an initial value of 0.45 to about 0.20) formed after 56 days due to pore filling by precipitates. When the change in porosity caused by precipitation is not taken into account, the model which simulates pH profiles in the jarosite/fly ash system does not mimic the actual transport properly. Conversely this indicates the necessity of developing models which consider such highly dynamic coupled effects as variation in transport properties with precipitation.

It is important to conduct the experiments under boundary conditions which are consistent with the boundary conditions required by our mathematical model. Without this strict constraint, it becomes impossible to determine experimentally the parameters required by the model and to verify the model experimentally. Radio tracer dif-

fusion experiments are the most simple, precise and accurate experimental approach, despite their limitations due to isotopic exchange.

The modelled profiles of $^{59}Fe^{3+}$ agree well with the measured one in the layered jarosite/fly ash system. The model takes into account local porosity changes due to precipitation. Its calculation was accomplished by operating our newly developed FORTRAN program DPLM based on the classical implicit fourth-order Runge-Kutta numerical method.

The application of the model to industrial layered acidic jarosite/alkaline fly ash deposition suggests that there is a potential benefit to layered disposal of these two chemically contrasting wastes. Thus, when the Fe^{3+} concentration in pore fluid is 0.01 M, the self-forming layer at the interface jarosite/fly ash will be about 2 mm thick with a porosity of about 5% in less than 20 days. By making use of chemical reactions the wastes will be neutralized (acid and base reaction), isolated (sealing layer formation due to pores filling by precipitates), and immobilized (reduced mobility of chemical constituents due to precipitation).

The DPLM program enables quantitative exploration of self-forming processes in chemically discontinuous porous media under the following limitations. Firstly, the self-forming layer is caused by pore filling precipitates. Secondly, the precipitation reaction has to be fast enough that the transport term in the reaction zone can be neglected implying that the removal of a constituent will only be affected by chemical reaction. Thirdly, the current version of the model can only simulate the behavior of a constituent involving a single reaction. Future work might focus on the simulation of other principal constituents such as Al^{3+}, Zn^{2+}, Pb^{2+}, Ca^{2+} and SO_4^{2-} and determine their spatial and temporal variation in the layered jarosite/fly ash system. Fourthly the current model is one dimensional. This is proper for the jarosite/fly ash system because radioactive cross sections of the tube when placed on a photographic plate showed homogeneous blackening, in accordance with longitudinal petrographic thins sections which showed a very sharp flat reaction zone. These results indicate that no fingering occurs in jarositye/fly ash, but do not preclude that it might occur in other systems.

6.4 Chemical reactivity of sealing layer in jarosite/fly ash: the nature of FeOOH adsorption

The amorphous ferric oxyhydroxide scale at the interface between jarosite and fly ash functions not only as a component of the sealing layer but also as an anion and cation trap. To elucidate the nature of this x-ray amorphous material as well as the nature of the adsorption process we have carried out XPS and conversion electron Mössbauer

spectroscopy. Our results indicate that the substrate, though x-ray amorphous amorphous, resembles β-FeOOH, akaganeite, in its local structure. The adsorption of chromate, lead and zinc on FeOOH are strongly pH and PZC dependent, whereas the adsorption of arsenate and phosphate on FeOOH is PZC independent implying a high chemical affinity for FeOOH. These results are consistent with our interpretation of XPS measurements using frontier molecular orbital theory. In addition, we found that adsorption isotherms of arsenate, phosphate and chromate obey the Langmuir equation and those of lead and zinc ions the Freundlich equation. Our mixed oxyanion experimental results suggested that the presence of PO_4^{3-} reduces AsO_4^{3-} adsorption significantly but the presence of arsenate does not reduce phosphate adsorption.

Our X-ray photoelectron spectroscopy measurements on the core levels of iron and oxygen in FeOOH and its surface complexes: FeOOH-As, FeOOH-P, FeOOH-Cr, FeOOH-Pb and FeOOH-Zn indicate that chemisorption occurred between substrate and oxyanions admolecules. In chromate adsorption, electrons transfer from substrate to adduct in which the surface of FeOOH acts as Lewis base. In contrast adsorption of arsenate and phosphate, involves electron transfer from adduct to substrate. In these last two cases, the surface substrate acts as Lewis acid. Adsorption of zinc and lead cations on FeOOH do not show clear evidence of chemisorption, as we did not notice any electron transfer between substrate FeOOH and these two adions. We infer therefore that adsorption between FeOOH and zinc and lead cations involves physisorption in which hydrated clusters form outer-sphere complexes.

Our XPS measurements of the valence band of the FeOOH substrate and its variation with surface complexes enable us to estimate quantitatively the energy level separation between highest occupied molecular orbital(HOMO) and lowest unoccupied molecular orbitals (LUMO) of the surface complexes and to assess the affinity between FeOOH and these adducts. From a frontier orbital perspective, the energy difference between the HOMO and LUMO in FeOOH-As and FeOOH-P, with a similar valence band XPS spectrum of the substrate before and after complexation, is small resulting in a substantial potential molecular energy. This implies strong chemical bonding between FeOOH and phosphate and arsenate. However, the energy differences between HOMO and LUMO in FeOOH-Cr, FeOOH-Pb and FeOOH-Zn are large, as reflected by a clear difference in their valence band XPS spectra. Therefore, the potential molecular energies of the FeOOH-Cr, FeOOH-Zn and FeOOH-Pb are small, implying weaker chemical bonding in FeOOH-Cr compound and virtually none in FeOOH-Pb and FeOOH-Zn. These results are consistent with our aquatic chemical observation.

6.5 Waste management issues

As demonstrated, using self-sealing layers as a barrier for waste jarosite isolation and immobilization is certainly an option from a theoretical and experimental perspective.

The purpose of the development of the model has been to predict the formation of seals in environments and on a scale not amenable to laboratory verification. An alternative option to the disposition of acidic jarosite in an environmentally sound manner would be to simply mix acidic jarosite and alkaline coal fly ash as proposed in Chapter 2. According to our acid-base titration experiments, about 70 wt% fly ash will increase the solution pH to about 7. This reduces the mobility of environmentally critical elements by up to 11 orders of magnitude. The mobility of several anionic species in this pH domain is not significantly reduced, being primarily dependent on the surface adsorption of ferric oxyhydroxides which change their PZC around this pH. Self sealing isolation and immobilization remains the recommended option because it enables jarosite to be recycled, in contrast to neutralization by mixing it with alkaline fly ash preventing its future use as a resource.

References

Artiola, J.F. (1996) Waste disposal, In: Pepper, I.L., Gerba, C.P., Mark, L. (Eds.) *Pollution Science*, Academic Press, Inc., pp 135-149.

Albarède, F. (1995a) Transport, advection and diffusion, *Introduction to Geochemical Modeling*, Cambridge University Press, pp 401-476.

Albarède, F. (1995b) Useful numerical analysis, *Introduction to Geochemical Modeling*, Cambridge University Press, pp 111-165.

Baes, C.F. and Mesmer, R.E. (1976) The hydrolysis of cations, John Wiley, NY. pp 489.

Baes, C.F. and Mesmer, R.E. (1981) The thermodynamics of cation hydrolysis, *American Journal of Science*, Vol. 281, pp 935-962.

Bagus, P.S. and Bauschlicher, C.W. (1980) Core binding energy for free negative ions of oxygen O^0 to O^{2-}, *J. Electron Spectrosc. Relat. Phenom.* Vol. 20, pp 183-190.

Bear, J (1972) Dynamics of fluids in porous media, Elsevier, Amsterdam. pp 764.

Becker, U., Hochella, M.F. Jr., and David, J.V. (1997) The adsorption of gold to galena surfaces: Calculation of adsorption/reduction energies, reaction mechanisms, XPS spectra, and STM images, *Geochim. Cosmochim. Acta*, Vol. 61, No. 17, pp 3565-3585.

Benjamin, M.M. and Leckie, J.O. (1981) Multiple-site adsorption of Cd, Cu, Zn, and Pb on amorphous iron oxyhydroxide, *Journal of Colloid and Interface Science*, Vol. 79, No. 1, pp 209-221.

Benjamin, M.M. (1983) Adsorption and surface precipitation of metals on amorphous iron oxyhydroxide, *Environ. Sci. Technol.*, Vol. 17, pp 686-692.

Blumer, D. (1980) Extraction of tungsten from brines, Occidental Research Report 80-037B, pp 136.

Brown, G.E., Jr. (1990) Spectroscopic studies of chemisorption reaction mechanisms at oxide-water interface, In Hochella M.F., Jr. and White A.F. (editors), *Mineral-water Interface Geochemistry*, Reviews in Mineralogy, Vol.23, pp 309-364.

Burkhard, D.J.M., De Jong, B.H.W.S., Meyer, A.J.H.M., and Van Lenthe, J.H. (1991) $H_6Si_2O_7$: *ab initio* molecular orbital calculations show two geometric conformations. *Geochim. Cosmochim. Acta* Vol. 55, pp 3453-3458.

Carnahan, C.L. (1990) Coupling of precipitation-dissolution reactions to mass diffusion via porosity changes, In: Melchior, D.C. and Bassett, R.L. (Editors), *Chemical Modeling of Aqueous System II*, American Chemical Society Symposium Series, pp 234-242.

Carlson, C.L. and Adriano, D.C. (1993) Environmental impacts of coal combustion residues, *J. Environ. Qual.*, Vol. 22, pp 227-247.

Conry, M.J. , De Coninck, F. and Stoop, S G. (1996) The properties, genesis and significance of a man-made iron pan podzol near Castletownbere, Ireland, *European Journal of Soil Science*, Vol. 47, pp 279-284.

Cornell, R.M. and Schwertmann, U. (1996) The iron oxides, structure, properties, reactions, Occurrence and uses, VCH Verlagsgesellschaft mbH, D-6845, Weinheim, pp 573.

Côté, P.L. and van der Sloot, Process and barrier for the contaminants of wastes, Canadian Patent application (1989), *European Patent Approved*, 20 June, 1994.

Crampton, C.B. (1963) The development and morphology of iron pan podzols in mid and south wales, *Journal of Soil Science*, Vol.14, No.2, pp 282-302.

Crank, J. (1975) The mathematics of diffusion, Clarendon Press, Oxford, pp 414

Cussler, E.L. (1984) Diffusion: Mass transfer in fluid system. Cambridge University Press, pp 525

Das, H.A., van der Sloot, H.A., and de Groot, G.J. (1989) Determination of the apparent diffusion constants in water containing granular solid, *Appl. Radiat. Isot.* Vol. 40, No. 7, pp 615-619.

Das, H.A. (1992) Applications of isotopes and radiation in conservation of the environment, Proceedings of Symposium on application of isotopes and Radiation in Conservation of the Environment, International Atomic Energy Agency, IAEA-SM-325/117, Karlsruhe, Vienna, 1992, pp 583-597.

Das, H.A. (1993) Influence of the water-content on the effective diffusion coefficient in granular solid material and its measurement by miniaturized radio-tracer experiments, *Appl. Radiat. Isot.*, Vol. 44, No. 9, pp 1245-1247.

Das, H.A. (1994) Radiotracer investigates of wet granular waste contaminant, *Appl. Radiat. Isot.*, Vol. 45, No. 5, pp 627-630.

Das, H.A. and van der Weyden, R.D. (1995) Isotopic exchange measurements in batch adsorption and desorption experiments, *Journal of Radioanalytical and Nuclear Chemistry*, Vol. 191, No.2, pp 229-238.

Das, H.A. and van der Weijden, R.D. (1996) Radiotracer measurement of isomorphic substitution, accompanied by surface adsorption of a trace cation into a crystalline host matrix, *Journal of Radioanalytical and Nuclear Chemistry*, Vol. 204, No.1, pp 205-211.

Davis, A., Link, T.E., Baugh, K., and Witham, R. (1996) Stabilization of lead in acidic mine filtercake by addition of alkaline tailings, *J. Environ. Qual.*, Vol. 25, pp 1077-1082.

de Groot, G.J. and Hoede, D. (1994) Validation of dutch standard leaching tests using NEN-ISO 5725, In: Goumans, J.J.J.M., van der Sloot, H.A., and Aalbers, Th. G. (Editors), *Environmental Aspects of Construction with Waste Materials*, Elsevier Science B.V. pp 305-314.

de Jong, B.H.W.S. (1982) Characterization and anion adsorption capacities of the black iron oxide, *ORC Status Report*, ORC 82-006, pp 46.

de Jong, B.H.W.S. (1989) Glass: *Ullmann's Encycl. Ind. Chem. A*, Vol. 12, pp 365-432.

de Jong, B.H.W.S. (1994) Low-temperature structure of lithium nesosilicate, Li_4SiO_4, and its Li_{1s} and O_{1s} X-ray photoelectron spectrum, *Acta Cryst., B,* Vol. 50, pp 511-518.

Ding, M. (1994) Immobilization of contaminants at the interface between jarosite and alkaline fly ash, *MSc Thesis*, International Institute for Hydraulic and Environmental Engineering, Delft, the Netherlands, pp 55.

Ding, M. (1996) Effect of interface precipitation on the bulk diffusivity in jarosite and alkaline coal fly ash, *Progress Report*, ECN & Utrecht University, the Netherlands, pp 85.

Ding, M., van der Sloot, H.A., and Geusebroek, M. (1996) Interface reaction affects Fe^{3+} mobility in jarosite and alkaline coal fly ash, *Ceramic Transactions,* Vol. 72, *Environmental Issues and Waste Management Technologies in Ceramic and Nuclear Industries II*, V. Jain and D. Peeler Eds. pp 475-484.

Ding, M., van der Sloot, H.A., and Geusebroek, M. (1997) Interaction of Fe^{3+}, Ca^{2+}, and SO_4^{2-} at the jarosite/alkaline coal fly ash interface, Geochemistry, Xie, X. J. Ed. *Proceedings 30th International Geological Congress,* Vol. 19, pp 207-222, VSP.

Ding, M., Geusebroek, M., and van der Sloot, H.A (1998a) Interface precipitation affects the resistance to transport in layered jarosite/fly ash, *J. of Geochemical Exploration* (in press)

Ding, M., de Jong, B.H.W.S., Niessen, B., van der Meer, J.P.M., and van Hinsberg, V.J. (1998b) Characterization of amorphous black ferric oxyhydroxide: X-ray photoelectron spectroscopy, conversion electron mssbaur spectroscopy, and chemical adsorption, *Geochim. Cosmochim. Acta* (submitted)

Ding, M., de Jong, B.H.W.S., Roosendaal, S.J., and Vredenberg, A. (1998c) XPS studies on the electronic structure of bonding between solid and solutes: adsorption of arsenate, phosphate, chromate, Pb^{2+} and Zn^{2+} ions on amorphous black ferric oxyhydroxide, *Geochim. Cosmochim. Acta* (submitted)

Ding, M. (1998d) Discontinuities in porous media affect the transport and mobility of chemical constituents, *Water Resource Research* (to be submitted).

Dutrizac, J.E. and Harris, G.B., editors, (1996) Iron control and disposal: Part 8 - Disposal practices for iron residues, *Proceedings 2nd Intern. Symp. on Iron Control in Hydrometallurgy, Can. Inst. of Mining, Metallurgy and Petroleum*, Quebec, 1996, pp 682.

Dzombak, D.A. and Morel, F.M.M. (1990) Surface complexation modeling: hydrous ferric oxide, John Wiley & Sons. Inc. pp 393.

Elgersma, F. (1992) Integrated hydrometallurgical jarosite treatment, *PhD Thesis*, ISBN 90-370-0073-8 Delft University of Technology, Delft, the Netherlands, pp 288.

Fleischer, M. (1983) Glossary of mineral species, *the Mineralogical Record Inc.*, pp 202.

Freeze, R.A., Cherry, J.A. (1979) Groundwater, Prentice-Hall, Englewood Cliffs, N.J., pp 604.

Fukui, K., Yonezawa, T., and Shingu, H. (1954) Molecular orbital theory of orientation in aromatic, heteroaromatic, and other conjugated molecules, *J. Chem. Phys.*, Vol. 22, pp 1433-1442.

Fuller, C.C., Davis, J.A., and Waychunas, G.A. (1993) Surface chemistry of ferrihydrite: Part 2. Kinetics of arsenate adsorption and coprecipitation, *Geochim. Cosmochim. Acta*, Vol. 57, pp 2271-2282.

Handbook of Chemistry and Physics, 61st edition (1980-1981), CRC Press.

Hage, J.L.T., Schuiling, R.D. (1996) An integrated jarosite and sludge treatment process, In: Dutrizac, J.E. and Harris, G.B. (Eds.), *Iron Control and Disposal, Proceedings 2nd Intern. Symp. On Iron Control in Hydrometallurgy*, pp 581-596, Canadian Institute of Mining, Metallurgy and Petroleum.

Hassanizadeh, S.M. and Gray, W.G. (1989a) Derivation of conditions describing transport across zones of reduced dynamics within multiphase systems, *Water Resources Research*. Vol. 25, pp 529-539.

Hassanizadeh, S.M. and Gray, W.G. (1989b) Boundary and interface conditions in porous media, *Water Resources Research*. Vol. 25, pp 1705-1715.

Hassett, W.R.R.J.J. and Griffin, R.A. (1986) Competitive coefficients for the adsorption of arsenate, molybdate, and phosphate mixtures by soil, *Soil Sci. Soc. Am, J.*, Vol. 50, pp 1176-1182.

Hockley, D. E., van der Sloot, H.A. (1991a) Long-term processes in a stabilized waste block exposed to seawater, *Environ. Sci. & Technol.*, Vol. 25, pp 1408-1414.

Hockley, D.E., and van der Sloot, H.A. (1991b) Modeling of interactions at waste-soil interfaces, In: J.J.J.M. Goumans, H.A. van der Sloot, and Th. G. Aalbers, (Eds.), *Waste Materials in Construction*, Elsevier Science Publishers B.V., pp 341-352.

Hockley, D.E., van der Sloot, H.A. and Wijkstra, J. (1992) Waste-soil interface, ECN-R-92-003, pp 61.

Hockley, D.E., and van der Sloot, H.A. (1993) Processes affecting contaminate release from waste-soil interfaces, In: Arnould, M., Barrs, M., Cme, B., Eds. *Proceedings Geoconfine' 93*, Vol. 1, *Geology and Confinement of Toxic Wastes*, Balkema Rotterdam, pp 265-271.

Hoffmann, R. (1988) Solid and surfaces: a chemist's view of bonding in extended structures, VCH Publishers, Inc. pp 142.

Juergens, L.P.H. (1995) " Black" iron (oxy)hydroxide. I. Synthesis and characterization; II Tungstate and chromate adsorption, *MSc thesis*, Utrecht University, Utrecht, the Netherlands, pp 77.

Jurjovec, J., Blowes, D.W., and Ptacek, C.J. (1995) Acid-neutralization and effect of jarosite co-disposal with mine tailings, Sudbury '95 Conference, *Mining and Environment*, Vol. 1, pp 29-38, May 28-June 1, 1995, Sudbury, Ontario.

Klopman, G. (1968) Chemical reactivity and the concept of charge and frontier controlled reactions, *J. Am. Chem. Soc.*, Vol. 90, pp 223-234.

Klopman, G. (1974) The generalized perturbation theory of chemical reactivity and its applications, *Chemical Reactivity and Reaction Paths*, edited by Klopman G., Wiley, pp 369.

Koffman, E.B. and Friedman, F.L. (1997) FORTRAN, Addison Wesley Longman, Inc., pp 653.

Kosson, D.S., Van Der Sloot, H.A., and Eighmy, T.T. (1996) An approach for estimation of contaminant release during utilization and disposal of municipal waste combustion residues, *Journal of Hazardous Materials*, Vol. 47, pp 43-75.

Kudo, T., and Fueki, K. (1990) Solid State Ionics, VCH, publishers, Inc. pp 241.

Langmuir, D. (1997) Aqueous environmental geochemistry, Prentice-Hally, Inc. pp 600.

Lichtner, P.C., Steefel, C.I. and Oelkers, E.H., Editors, (1996) Reactive transport in porous media, *Reviews in Mineralogy* Volume 34, Ribbe, P.H., Series Editor, Mineralogical Society of America, Washington DC, pp 438.

Lützenkirchen, J. and Behra, P. (1996) On the surface precipitation model for cation sorption at the (hydr)oxide water interface, *Aquatic Geochemistry*, Vol. 1, pp 375-397.

Manceau, A. (1995) The mechanism of anion adsorption on iron oxides: Evidence for the bonding of arsenate tetrahedra on free $Fe(O, OH)_6$ edges, *Geochim. Cosmochim. Acta*, Vol. 59, No. 17, pp 3647-3653.

Mangold, D.C. and Tsang, C.F. (1991) A summary of subsurface hydrological and hydrochemical models, *Reviews of Geophysics*, Vol. 29, pp 51-79.

Manning, P.G. (1973) Extinction coefficients of Fe^{3+} spectral bands as indicators of local crystal composition, *Can. Min.*, Vol. 12, pp 120-123.

McIntyre, N.S. and Zeatruk, D.G. (1977) X-ray photoelectron spectroscopic studies of iron oxides, *Anal. Chem.*, Vol. 49, No. 11, pp 1521-1529.

Menchetti, S. and Sabelli, C. (1976) Crystal chemistry of the alunite series: crystal structure refinement of alunite and synthetic jarosite, *-N. Jb. Miner. Mh.*, 1976, H. 9, pp 406-417, Stuttgart 1976.

Mizzoni, M.S., Dumbaugh, W.H., and Tyndell, B.P. (1988) Mixed halide effect in lead silicate glasses, *Am. Ceram. Soc. Bull*, Vol. 9, pp 1494-1498.

Murad, E. and Johnston, J.H. (1987) Iron oxides and hydroxides, In: Long, G. edited *Mössbauer Spectroscopy Applied to Inorganic Chemistry*, Plenum, NY, 2: pp 507-582.

Mydosh, J.A. (1993) Spin glasses: an experimental introduction, Taylor & Francis, London, pp 256.

Nakashima, S. (1995) Diffusivity of ions in pore water as a quantitative basis for rock deformation rate estimates, *Tectonophysics*, Vol. 245, pp 185-203.

NEN 7341 Leaching characteristics of building and solid waste materials - leaching tests - Determination of the availability of inorganic components for leaching, Sept. 1993, Netherlands Normalization Institute, the Netherlands.

NEN 7349 Leaching characteristics of building and solid waste materials - leaching tests - Determination of the leaching of inorganic components from granular materials with the cascade test, draft 1993, Netherlands Normalization Institute, the Netherlands.

NEN 7343 Leaching characteristics of building and solid waste materials - leaching test - Determination of the leaching of inorganic components from granular materials with the column test, June 1994, Netherlands Normalization Institute, the Netherlands.

Norton, G.A., Richardson, and R.G., Markuszewski, R. (1991) Precipitation of jarosite compounds as a method for removing impurities from acidic wastes from chemical coal cleaning, *Environ. Sci. Technol.*, Vol. 25, pp 449-455.

Paterson, M.S. (1995) A Theory for Granular Flow Accommodated by Material Transfer via an Intergranular Fluid, *Tectonophysics*, Vol.245, pp 135-151.

Pierce, M.L. and Moore, C.B. (1982) Adsorption of arsenite and arsenate on amorphous iron hydroxide, *Water Res.* Vol. 16, pp 1247-1253.

Poirier, J.P. (1991) Introduction to the physics of the earth's interior. Cambridge University Press, pp 264.

Press, W.H., Flannery, B.P., Teukolsky, S.A., and Vetterling, W.T. (1987) Numerical recipes: The art of Scientific Computing, Cambridge University Press, pp 818

Rossman, G.R. (1975) Spectroscopic and magnetic studies of ferric oxyhydroxide sulfates: Intensification of color in ferric iron clusters bridged by a single hydroxide ion, *Am. Min.*, Vol. 60, pp 698-704.

Rossman, G.R. (1976a) Spectroscopic and magnetic studies of ferric oxyhydroxide sulfates: The series $Fe(OH)SO_4nH_2O$ and the jarosites, *Am. Min.*, Vol. 61, pp 398-404.

Rossman, G.R. (1976b) The optical spectroscopic comparison of the ferric iron tetrameric clusters in amarantite and leucophosphite, *Am. Min.*, Vol. 61, 933-938.

Rubin, Jacob (1983) Transport of reacting solutes in porous media: relation between mathematical nature of problem formation and chemical nature of reactions, *Water Resources Research*, Vol.19, No.5, pp 1231-1252.

Sahimi, M. (1995) Flow and transport in porous media and fractured rock: from classical methods to modern approaches, VCH, pp 482.

Scaini, M.J., Bancroft, G.M., and Knipe, S.W. (1997) An XPS, AES, and SEM study of the interactions of gold and silver chloride species with PbS and FeS_2: Comparison to natural samples, *Geochim. Cosmochim. Acta*, Vol. 61, No. 6, pp 1223-1231.

Schaefer, C.E., Arands, R.R., Van Der Sloot, H.A., and Kosson, D.S. (1995) Prediction and experimental validation of liquid-phase diffusion resistance in unsat-

urated soils, *Journal of Contaminant Hydrology*, Vol. 20, pp 145-166.

Schnoor, J.L. (1996) Environmental modeling: fate and transport of pollutants in water, air, and soil, Wiley, New York, pp 682.

Schuiling, R.D. (1989) Environmental technologies based on geochemical processes, *Geologie en Mijnbouw*, Vol. 68, pp 271-275.

Schuiling, R.D. (1990) Geochemical engineering: some thoughts on a new research field, *Applied Geochemistry*, Vol. 5, pp 251-262.

Schuiling, R.D. and Van Gaans, P.F.M. (1994) Self-sealing of the waste sulfuric acid lake of the TiO_2 plant at Armyansk, Crimea, Ukraine, *Abstr. 16th General Meeting of the Int. Miner.* Ass., Pisa.

Schuiling, R.D. (1996) Geochemical engineering: principles and case studies, In: Reuther, R. (Ed.), *Geochemical Approaches to Environmental Engineering of Metals*, Springer, Heidelberg, pp 3-12.

Schuiling, R.D. and Van Gaans, P.F.M. (1997) The waste sulfuric acid lake of the TiO_2-plant at Armyansk, Crimea, Ukraine. Part I. Self-sealing as an environmental protection mechanism, *Applied Geochemistry*, Vol. 12, pp 181-186.

Sherman, D.M. (1985) SCF-X-SW MO study of Fe^{3+} coordination sites in iron oxides: applications to spectra, bonding and magnetism, *Phys. Chem. Min*, Vol. 12, pp 311-314.

Schugar, H., Walling, C., Jones, R.B., and Gray, H.B. (1967) The structure of iron (III) in aqueous solution, *J. Am. Soc.*, Vol. 89, pp 3712-3720.

Schugar, H.J., Rossman, G.R., Barraclough, C.G., and Gray, H.B. (1972) Electronic structure of oxo-bridged iron (III) dimers, *J. Am. Chem. Soc.*, Vol. 94, pp 2683-2690.

Siegbahn, K., Nordling, C.N., Fahlman, A., Nordberg, R., Hamrin, K., Nedman, J., Johnsson, G., Bermark, T., Karlsson, S.E., Lindberg, B. (1967) ESCA: Atomic, molecular and solid state structure studied by means of electron spectroscopy. *Almqvist and Wiksells*: Uppsala, Sweden.

Steefel, C.I. and Lasaga, A.C. (1990) Evolution of dissolution patterns: permeability change due to coupled flow and reaction, In: Melchior, D.C. and Bassett, R.L. (Editors) *Chemical Modeling of Aqueous System II*, American Chemical Society Symposium Series, pp 212-225.

Steefel, C.I. and Lasaga, A.C. (1994) A coupled model for transport of multiple chemical species and kinetic precipitation/dissolution reactions with application to reactive flow in single phase hydrothermal systems, *American Journal of Science*, vol. 294, pp 529-592.

Stoffregen, R.E. (1993) Stability relations of jarosite and natrojarosite at 150-250 °C, *Geochim. Cosmochim. Acta*, Vol. 57, pp 2417-2429.

Strens, R. G. J. and Wood, B. J. (1979) Diffuse reflectance spectra and optical properties of some iron and titanium oxides and oxyhydroxides, *Min. Mag.*, Vol. 43, pp 347-354.

Stumm, W. (1992) Chemistry of the solid-water interface: processes at the mineral-water and particle-water interface in nature system, John Wiley & Sons, Inc. pp 428.

van Cappellen, P. and Gaillard, J. F. (1996) Biogeochemical dynamics in Aquatic sediments, in Lichtner, P.C., Steefel, C.I., Oelkers, E.H., Editors, *Reactive Transport in Porous Media*, Ribbe, P.H., Ed., Reviews in Mineralogy Vol. 34 pp 335-376.

van der Sloot, H.A. and Côté, P. (1989) Modelling chemical interactions at a waste/waste interface, *Environ. Technol. Letters*, Vol. 10, pp 969-976.

van der Sloot, H.A., de Groot, G.J., and Hoede, D. (1991) Mobility of trace elements derived from combusion residues and products containing these residues in soil and groundwater, ECN-C-91-059, pp 190.

van der Sloot, H.A., Hockley, D.E., Wijkstra, J., and Stegemann, J.A. (1993a) Self-forming and self-repairing seals for waste isolation, ECN-RX-93-021. pp 7.

van der Sloot, H.A., Hockley, D.E., Wijkstra, J. and Stegemann, J.A. (1993b) Self-sealing and self-repairing seals for waste isolation, In: Arnould, M., Barrs, M., Côme, B. (Eds) *Proceedings Geoconfine' 93, Vol. 1, Geology and Confinement of Toxic Wastes*,

Balkema Rotterdam, pp 73-79.

van der Sloot, H.A., Kosson, D.S., Eighmy, T.T, Comans, R.N.J., and Hjelmar, O. (1994) Approach towards international standardization: a concise scheme for testing of granular waste leachability, In: Goumans, J.J.J.M., van der Sloot, H.A., and Aalbers, Th. G. (Editors) *Environmental Aspects of Construction with Waste Materials*, Elsevier Science B.V. pp 453-466.

van der Sloot, H.A., Pereboom, D., McGregor, R., Stegemann, J. and Taat, J. (1995a) Properties of self-forming and self-repairing seals, In: Christensen, T.H., Cossu, R., Stegmann, R. (Eds.), *Proceedings 5th Landfill Symposium*, Vol. II, *Siting, Lining, Draining and Landfill Mechanics*, Sardinia, 1995, pp 131-141.

van der Sloot, H.A. (1995b) Development in evaluating environmental impact from utilization of bulk inert wastes using laboratory leaching tests and field verification, ECN-RX-95-056.

van der Sloot, H.A., Cnubben, P.A.J.P, Geusebroek, M.G., Naus, R., Jansen-Venneboer, J.W., Bosman, P., Krom, A., and Sollman, C. (1997a) The self-forming and self-repairing sealing method: development of concept towards full scale application, *Landfill Symposium*, Sardinia, 1997.

van der Sloot, H.A. (1997b) Leaching characteristics of lead-zinc primary smelters slags, ECN-C-97-098, pp 48.

van Gaans, P.F.M. and Schuiling, R.D. (1997) The waste sulfuric acid lake of the TiO_2-plant at ArmyansK, Crimea, Ukraine. Part II: Modeling the chemical evolution with PHRQPITZ, *Applied Geochemistry*, Vol. 12, pp 187-201.

Voigt, J.A., Wood, T.E., Bunker, B.C., Casey, W.H., and Crossey, L.J. editors. (1997) Aqueous chemistry and geochemistry of oxides, oxyhydroxides, and related materials, *Materials Research Symposium Proceedings*, Vol. 432, pp 372.

Voronkevich, S.D. (1994) Engineering geochemistry: problems and applications, *Applied Geochemistry*, Vol.9, pp 553-559.

Wagner, C.D., Davis, L.F., Riggs, W.M., Moulder, J.F and Muilenberg (Eds.) (1978) Handbook of X-ray Photoelectron Spectroscopy, Perkin Elmer Corporation, Eden Prairy, Minnesota.

Wang, R., Bradley, W.F., and Steinfink, H. (1965) The crystal structure of alunite, *Acta Cryst.*, Vol 18, pp 249-252.

Warren, C.J. and Dudas, M.J. (1984) Weathering processes in relation to leachate properties of alkaline fly ash, *J. Environ. Qual.*, Vol. 13, No. 4, pp 530-538.

Waychunas, G.A., Rea, B.A., Fuller, C.C, and Davis, J.A. (1993) Surface chemistry of ferrihydrite: Part 1. EXAFS studies of the geometry of coprecipitatated and adsorbed arsenate, *Geochim. Cosmochim. Acta*, Vol. 57, pp 2251-2269.

Waychunas, G.A., Davis, J.A., and Fuller, C.C. (1995) Geometry of sorbed arsenate on ferrihydrite and crystalline FeOOH: Re-evaluation of EXAFS results and topological factors in predicting sorbate geometry, and evidence for monodentate complexes, *Geochim. Cosmochim. Acta*, Vol. 59, No. 17, pp 3655-3661.

Waychunas, G.A., Fuller, C.C., Rea, B.A., Davis, J.A. (1996) Wide angle X-ray scttering (WAXS) study of "two-line" ferrihydrite structure: Effect od arsenate sorption and counterion variation and comparison with EXAFS results, *Geochim. Cosmochim. Acta*, Vol. 60, No. 10 pp1765-1781.

Zachara, J.M., Girvin, D.C., Schmidt, R.L., and Resch, T.C. (1987) Chromate adsorption on amorphous iron oxyhydroxide in the presence of major groundwater ions, *Environ. Sci. Technol.*, Vol. 21, pp 589-594.

Zhang, Z., Boxall, C. and Kelsall, G.H. (1993) Photoelectrophoresis of colloidal iron oxides 1. Hematite (α-Fe_2O_3). *Colloids Surf. A*, Vol. 73, pp 145-163.

142

Samenvatting

Reactief transport in poreuze media kan leiden tot het ontstaan van natuurlijke of kunstmatige zelf-vormende lagen. Deze vaak harde banken met geringe permeabiliteit, functioneren gewoonlijk als een vergaarbak voor een grote verscheidenheid aan anorganische en organische stoffen. Hun ontstaan is het gevolg van een transport fase waarbij stoffen migreren langs chemische gradiënten. Dit proces wordt gevolgd door precipitatie in een concentratie fase op plaatsen waar verschillen in redox of base-zuur eigenschappen domineren. Deze neerslagen vullen poriën en vormen een laag die in fysisch en chemisch karakter verschilt van die der oorspronkelijke moeder materialen.

Discontinuïteiten in chemische eigenschappen op het grensvlak tussen materialen is de drijvende kracht achter spontane laag vorming. Op hun beurt hebben zulke zelf-vormende lagen een grote invloed op het transport en de mobiliteit van stoffen. Dat zelf-vormende lagen stoffen ondoorlaatbaar kunnen afsluiten wordt bijvoorbeeld geïllustreerd door veen moerassen. Deze eigenschap opent de mogelijkheid om industriële afvalprodukten af te sluiten van hun omgeving. Een dergelijke barrière zou, afgezien van het afsluitende karakter, ook zelf helend zijn in die zin dat het afsluit mechanisme er voor zorgt dat een breuk erin weer gedicht wordt. Kortom, elke mechanische beschadiging in een afsluitende laag zou nieuwe migratie en neerslag tot gevolg hebben, althans zolang de reagentia voorraad strekt. Daarenboven zouden een groot aantal chemische componenten waaronder organische via co-precipitatie of oppervlakte adsorptie geïncorporeerd kunnen worden gedurende de vorming van zulk een afsluitende laag.

Dit proefschrift behandelt het vormingsmechanisme van zelf- afsluitende/helende isolatie en immobilisatie in gelaagde materialen en de invloed van zulke zelf-vormende lagen op het transport en de mobiliteit van stoffen, waarbij de nadruk ligt op het gelaagde zure jarosiet/basische vliegas systeem. De strategie tot oplossing van dit probleem begint met een onderzoek naar de ontstaans mogelijkheid van zelf-afsluitende lagen in het gelaagde jarosiet/vliegas systeem. Hierna worden experimenteel de karakteristieken bestudeerd van afsluitende lagen en hun invloed op transport en mobiliteit van stoffen, waarna een wiskundige beschrijving van de laag ontwikkeling wordt gegeven. Tenslotte wordt de chemische reactiviteit van zelf-afsluitende lagen in jarosiet/vliegas onderzocht. Zelf-afsluitende isolatie en immobilisatie in plaats van neutralizatie wordt aanbevolen voor het verwerken van het zure jarosiet afval, waartoe een laag van zure jarosiet moet worden geplaatst tegen een basische vliegas laag.

In Hoofdstuk 1 worden de vorming van natuurlijke zelf-vormende lagen en eerdere studies over dit onderwerp samengevat en worden de praktische voortvloeisels van zelf-vormende lagen bediscussieerd. Facetten van zelf- afsluitende isolatie en immobilisatie worden geïdentificeerd waarbij de problematiek in het jarosiet/vliegas systeem centraal staat. In dit Hoofdstuk worden de doelstellingen en werkzaamheden van de huidige studie gedefinie-

rd.
In Hoofdstuk 2 wordt de aard van de twee moeder materialen, jarosiet en vliegas, bestudeerd waaronder hun chemische samenstelling, de aanwezige mineralen, hun basische, zure en uitloog eigenschappen. Deze verkennende experimenten verschaffen niet alleen achtergrond over de materialen, maar, vanuit praktisch oogpunt gezien, ook belangrijke informatie over hun gedrag in het milieu en mogelijke milieu technische gevolgen

In Hoofdstuk 3 wordt de aard van de zelf vormende laag aan het grensvlak in het gelagde jarosiet/vliegas systeem bestudeerd en tevens het effect ervan op de totale weerstand tegen transport en chemische vastlegging. Met behulp van standaard karakterisatie technieken wordt aangetoond dat driewaardig ijzer oxyhydroxyden en gips de belangrijkste neerslagen vormen in de laag. Transport eigenschappen en mobiliteit van stoffen in gelaagde materialen worden bepaald met radiotracer, $^{3}H^{+}$, $^{22}Na^{+}$, $^{59}Fe^{3+}$, diffusie experimenten en de hydraulische geleidbaarheid door stromings metingen in een kolom. Er wordt aangetoond dat een zelf-vormende laag het transport proces door een gelaagd systeem totaal veranderd.

Hoofdstuk 4 richt zich op het modelleren van het algemene effect van Discontinuïteit in poreuze media op het transport en de mobiliteit van stoffen. De nadruk ligt op de model simulatie van reactief transport in gelaagde materialen, het ontstaan van een zelfvormende laag op het tussenvlak, de numerieke oplossing van dit model en de ontwikkeling van een computer programma. De kalibratie en verificatie van het model zijn uitgevoerd met behulp van radio tracer, $^{3}H^{+}$, $^{22}Na^{+}$, $^{59}Fe^{3+}$, diffusie experimenten in reageer buizen in het gelaagde jarosiet/vliegas systeem. Onze simulatie geeft aan dat op het laagvlak tussen gelaagde materialen, de bestaande verschillen in tortuositeit de transport processen nauwelijks beïnvloeden. Dit in tegenstelling tot bestaande chemische gradiënten, zoals pH of oxidatie graad, die niet alleen het transport beïnvloeden maar ook de mobiliteit van de stoffen.

Hoofdstuk 5 beschrijft de chemische reactiviteit van zelf-vormende lagen in het gelagde jarosiet/vliegas systeem door het afzonderlijke bestuderen van driewaardig ijzer oxyhydroxide FeOOH, een van de twee neerslagen die de afsluitende laag vormen. Hierbij wordt de aard van de chemische ad-sorptie van arsenaat, phosphaat, en chromaat anionen, en zink en lood kationen erop beschreven. Afgezien van een klassiek chemisch oogpunt, wordt ook vanuit het frontier orbital concept de elektronische bindings struktuur tussen het FeOOH substraat en toegevoegde moleculen bestudeerd. X-ray photoelectron spectroscopie wordt gebruikt ter verificatie van de op oppervlakte gevormde arsenaat, phosphaat. chromaat, lood en zink complexen. Deze studie op het gebied van de oppervlakte chemie in contact met waterige oplossingen representeert een nieuw benadering van vaste stof-water interactie.

In Hoofdstuk 6 worden algemene conclusies getrokken gebaseerd op de resultaten ver-

meld in de Hoofdstukken 2 tot en met 5. Samenvattend behelzen deze conclusies dat zelf-afsluitende/helende isolatie een relatief goedkope, betrouwbare, veilige milieukundige optie is en als toepassing van belang is bij het besturen van jarosiet afval. De vorming van zulk een isolerende laag vereist de migratie van stoffen vanuit twee verschillende moeder materialen, die te samen reageren en precipiteren op het grensvlak. De zelf-vormende laag in het gelaagde zure jarosiet/basische vliegas bestaat uit amorf driewaardige ijzeroxyhydroxide FeOOH en gips $CaSO_4.2H_2O$, en ontstaat door neerslag reacties tussen de belangrijkste component uit jarosiet (Fe^{3+}, SO_4^{2-}) en vliegas (Ca^{2+}, OH^-). Zulk een laag heeft een belangrijke invloed op de weerstand tot transport en het chemische vastleggen van componenten. Het wiskundige model beschrijft de transport eigenschappen in gelaagde materialen, waarbij rekening wordt gehouden met een verandering van poreusiteit door neerslag, en een numerieke oplossing is met succes neergelegd in het nieuw ontwikkelde program DPLM en toegepast op het gelaagde jarosiet/vliegas systeem. Chemische reactiviteit van de zelf-vormende lagen in het gelaagde jarosiet/vliegas systeem is voornamelijk het gevolg van driewaardig ijzer oxyhydroxiden, welke een grote ad-sorptie capaciteit hebben voor een grote verscheidenheid aan kationen en anionen. XPS als oppervlakte techniek is toegepast om ad-sorptie tussen vaste stof en oplossing te bestuderen, en verschaft gedetailleerde bindings informatie van kern en valentie band verschuivingen. Deze dragen ertoe bij dat de aard van de chemische binding tussen vaste stof en vloeistof kan gerationaliseerd worden vanuit een frontier orbital gezichtspunt. Tenslotte worden openstaande vragen behandeld en enige suggesties gedaan voor werk in de toekomst.

博士论文概述

自然界或人为活动导致的自生层是由于反应物在两个相邻的可渗透介质中迁移，转化的结果．这样的自生层有时非常坚硬，具有较小的渗透性，并通常累积了大量的有机和无机化学物质．它的形成包括两个阶段．首先是发生介质间化学组成元素的迁移，迁移的动力来自于系统中所存在的势能差，比如浓度梯度的存在；随之，沉淀反应在这些化学组成元素间发生，沉淀物填充介质中的孔隙部分，直到形成一个新的，与起始两个介质在物理和化学特性上不同的中介层．显然，起始两介质间物理或／和化学性质的突跃即势能差的存在，是导致自生层的关键因素．反过来，这样的自生层又会对整个系统的传输性能及化学组成元素的迁移及其可迁移性产生相当大的影响．自生层可以是一个完全不渗透的自封隔绝层．正是由于这个原因，自封隔绝被认为是一个富有生命力的环境技术被用于在工业有毒废弃物和放置它的周围环境之间创造一个隔离层．自封层除了具有隔绝功能，在出现裂缝时还具有自愈合特性．这样，任何对自封层的机械损伤将会导致化学组成元素进一步的迁移和沉淀，只要系统具有充足的反应组成元素．通常，在自封层的形成过程中，由于共沉淀或表面吸附，同时还伴随着多种化学组分包括有机物的固化．

本文对多层可渗透介质中自封隔绝和固化的生成机理及其对化学组成元素迁移和可迁移性的影响从实验，理论和模型三方面进行了系统地研究，特别是针对黄钾铁矾／粉煤灰体系．实验方面，首先需要对自封层的组成和特征以各种检测手段加以鉴定，然后进行它对系统的迁移阻力和化学组成元素滞留的定量测定．模型方面，需要建立一个用于描述和预测一般性可渗透介质中反应物的传递特征的模型，该模型应能模拟自生层的发生及形成过程．为此，开发了计算机程序DPLM (Diffusion Preciptation in Layered Materials)．在这一部分工作中不仅描述了怎样推导模型和建立它的数值解，还探讨了怎样设计适当的实验为模型中所需参数及模型的校正和验证提供数据．此外，对黄钾铁矾／粉煤灰体系中自生层的化学反应性能从以下二个方面进行了研究：一是从溶液化学角度例如溶液 值，离子强度，被吸附物及吸附剂的浓度，测定了非晶形三价铁的羟基氧化物FeOOH对AsO_4^{3-}，PO_4^{3-}，CrO_4^{2-}，Pb^{2+}，Zn^{2+}的吸附性．FeOOH是黄钾铁矾／粉煤灰体系中组成自生层的两个沉淀物之一．二是利用基质 和它的吸附配合物FeOOH－As，FeOOH－P，FeOOH－Cr，FeOOH－Pb，FeOOH－Zn的 光电光谱结果，从量子力学的角度探索固体与溶质间化学吸附本质－既化学键的特征，它是本论文最重要的贡献之．作为实际应用，提出了一个综合治理黄钾铁矾，粉煤碳这两个具有相反化学性质的废弃物的方案以期达到隔绝，中和及固化的整体效果．

第一章对自然界中的自生层以及前人在这一领域的研究进行了总结，并提出了它的实际意义．从各方面对可渗透介质中自封隔绝和固化特别是针对黄钾铁矾／粉煤灰体系确定了研究方向及目的．并简要地陈述了每一个方面的研究结果及结论．

第二章探讨了二个母体介质黄钾铁矾和粉煤碳的特性，包括其化学成份及矿物组成，酸碱性，主要释放元素及释放机理．

第三章除了对黄钾铁矾／粉煤灰体系中的自生层进行了鉴定外，还测定了该自生层对系统总体传输阻力和化学滞留的影响．各种标准检测手段的结果表明，三价铁的羟基氧化物FeOOH和石膏$CaSO_4 \cdot H_2O$是组成自生层的两个新生矿物．黄钾铁矾／粉煤灰体系的传输性能是采用放射性示踪弥散和流动态柱状水力输导方法测定的．其结果表明，由于自生层的存在，黄钾铁矾／粉煤灰体系的传输性能完全不同于单一的黄钾铁矾或粉煤碳体系的传输性能．

第四章主要是建立数学模型，用以模拟并展示可渗透介质中由于物理或／和化学突跃对化学组成元素的迁移及其可迁移性的影响．其中，用于模拟两个相邻的可渗透介质界面间自生层的演化过程的模型只存在数值解，为此，编制了计算机程序DPLM．该模型的校正和验证是在黄钾铁矾／粉煤灰体系中采用放射性示踪弥散实验完成的．模拟结果表明，在两个相邻的可渗透介质间，存在的物理突跃仅仅对化学组成元素的传输过程产生影响．与此不同，存在的化学突跃不仅对化学组成元素的传输过程而且对其可迁移性都会有很大的影响．

第五章探讨了黄钾铁矾／粉煤灰体系中自封层的化学反应性能．首先分离出非晶形三价铁的羟基氧化物FeOOH，它是组成自封层的两个沉淀物之一．然后，研究它对砷酸盐，磷酸盐，络酸盐，铅离子和锌离子的化学吸附本质．除了从溶液化学角度，更强调了基质FeOOH和各溶质间的化学键的研究，结合理论上的前沿分子轨道概念与所测定的基质FeOOH和它与各溶质的表面配合物的X-射线光电光谱．此研究结果为水体表面化学提供了一个量子力学的途径．

第六章罗例了基于从第二章至第五章中的发现所得到的一般性结论．

总体来说，自封隔绝是相对廉价，可靠，安全的环境技术，在废物管理方面有深远的意义．它的形成需要来自于化学性质相反并相邻的两个母体介质中化学组成元素的迁移及它们在两母体介质界面间的沉淀反应．黄钾铁矾／粉煤灰体系中的自生层是由非晶形三价铁的羟基氧化物FeOOH和石膏$CaSO_4 \cdot H_2O$组成．它们的产生是由于来源于黄钾铁矾的主要化学组成元素Fe，和来源于粉煤碳的主要化学组成元素Ca相互发生沉淀反应的结果．该自生层在很大程度上影响了系统的传输阻力和组成元素的化学滞留．通过建立数学模型，系统地研究了两个相邻可渗透介质中，物理及化学突跃的存在对系统传输性能的影响．特别强调了自生层现象的体系，它的数值解及计算机程序DPLM，对它的模拟考虑到了由于沉淀反应所产生的孔隙度变化．该模型成功地被应用到黄钾铁矾／粉煤灰体系中．这一体系中自生层的化学反应性能主要是非晶形三价铁的羟基氧化物的贡献．因为它具有很强的对多种阴阳离子及有机物的吸附能力．XPS，作为表面测定技术，被应用到固体与溶质间的吸附研究中．在XPS谱图中所能观察到的原子的核电子带及价电子带的移位，为我们提供了详细的化学键的信息，使对固体与溶质间化学键本质的了解深入到量子力学的角度．

Acknowledgements

The research for my PhD and writing of this thesis would not have been accomplished without the encouragement, help, support, and advice of numerous people.

During my stay at IHE Delft I encountered professor Schuiling who provide a research opportunity for me at Utrecht University as part of my MSc degree on self sealing isolation and immobilization phenomena, a subject which I continued to study subsequently for my PhD. I am grateful for the opportunity he provided, the trust and support he put into me, and the generosity with which he allowed me to attend a large number of conferences. My co-promotor Dr. van der Sloot provided access to his research facility at ECN to carry out radiotracer experiments and generously shared his extensive expertise on the environmental consequences of layer formation in porous media, and leaching behavior of solid material. I appreciate all the advice and help he has given me.

I would also like to thank professor B. de Jong for his constant encouragement, being available when problems arose, and for his patient reading and correcting of the numerous draughts of my papers, and translated the summary into Dutch. He helped me with the quantum mechanical and spectroscopic aspects of surface adsorption. I shall always remember that he said the best return for him is to pass it on.

Experimental details concerning radio tracer analysis were provided by Marco Geusenbroek and made it possible to acquire superb data sets. Professor Slanina at ECN followed my progress and councilled me whenever problems arose, whereas professor Das provided me with references and suggestions. I am also grateful for the warm hospitality received in the Northern part of Holland by Mmes van der Sloot and Slanina.

For the modeling part of my thesis I found solid advice and expertise by Professor Hassanizadeh who directed me towards the proper experimental design needed for modeling purposes. For expertise on numerical modeling I have depended on Dr. Harm Dorren who pointed out the advantages of the Runge-Kutta numerical methods for me. Sander Roosendaal of Debye Institute, Section Interface Physics, Utrecht University showed me how to carry out photoelectron spectroscopy on ferric oxyhydroxides as did professor Niessen from Groningen University with respect to conversion electron Mössbauer spectroscopy.

The members of the geochemistry department including my fellow graduate students provided council, expertise or good cheer whenever necessary. These include profes-

sor van der Weijden and Dr. Loch, Dr. Vriend, Dr. Zijlstra, Dr. Jongbloed, Gijs Nobbe, Arianne Steenbrugge, Guido Holman, Jeroen de Graaf, Patrick Spek, Hans Haage and the two sophomores Juliëtte van der Meer and Vincent van Hinsberg who carried out some of the experiments on ferric oxyhydroxides. Besides geochemistry other people who helped in various ways were Dr. de Boorder, Dr. McDonald, Dr. Peach, professor Spiers, Dr. van Roermond, professor Verhulst, Dr. Woensdregt, Hans Meeldijk, Rianne Super, Ir Djie Kwee, Thea Broers, and Helen de Waard, the people from the grinding shop, Inge Nussgen and Otto Stiekema, from the machine shop Tony van de Gon Netscher and Hans Bliek, and those from the audio visual service Paul van Oudenallen, Jaco Bergenhenegouwen, Brigit Benders, and Fred Trappenburg. In the course of this all Mr. F. van Nierop battled with the foreign police to keep my visum status proper and ensured that my parents and son could be present at my defense.

Outside the university many Dutch and Chinese families and friends made my stay easy such as the van Sloten's in Rijswijk, the Duineveld's in Bergen, Qin Liu and Xili Wang in de Bilt, Jianzhong Zhang and Hong Yang in Enschede, Yangxiao Zhou and Lei Zhang in Delft, Xichuan Wang now in Quebec, Yixian Zhao in Utrecht, Chao Xu now in Shenyang, China, Zepeng Xiao now in Toronto, Helen and Pauline van Veen, and Virginia Heidweilldr.

I have always received support and council from my great friends and colleagues back in China especially professor Changming Ye, professor Jingyi Lui, professor Chaoqiu Chen, Lihong Fan, Yanfang Ge, Dr. Bojie Fu, Xingjun Ying, and Liding Cheng.

During this academic pursuit my parents, Benchao Li and Xuan Ding, and my brother and his wife, Qizhi Ding and Yatao Bi, uncomplainingly and gracefully took care of the education and welfare of my son Yuewen and provided council and moral support to their daughter, sister, and mother during her stay in this for them so far away and strange land.

Despite all the help this thesis remains the fruit of my brain and is my sole responsibility. Hence any mistakes, inaccuracies or omissions do not reflect on the quality of my supporters but on those I posses myself.

Thanks to all of you!

Curriculum Vitae

Date of birth: 15-01-1963
Place of birth: Beijing

High school education:

1978 – 1980 Guiyang Number 2 School, Guiyang, Guizhou, China.

University education:

1980 – 1984 Analytical Chemistry, BSc Degree, Department of Chemistry, Center South University of Technology, Changsha, China.

1984 – 1987 Coordination Chemistry, MSc Degree, Department of Chemistry, Center South University of Technology, Changsha, China.

1992 – 1994 Water Quality Management, MSc Degree, Department of Environmental Engineering, International Institute for Hydraulic and Environmental Engineering, Delft, the Netherlands.

1994 – 1998 (AIO) PhD research studentship, Department of Geochemistry, Utrecht University, Utrecht, The Netherlands.

Working experience:

1987 – 1992 Research associate, Research Center for Eco-Environmental Sciences, Academia Sinica, Beijing, China.

Colophon

Publication by Mei Ding
Lay-out and design: Audio visual Services Faculty of Earth Sciences
Print: Ponsen en Looijen bv. Wageningen

Typefaces: PBembo, Frutiger, Symbol, Delta Symbol, Times.

Paper: Cover 240 grs/m^2